# NEUTRON MEASUREMENT AND TRANSIENT ANALYSIS IN A SOURCE DRIVEN SUBCRITICAL ASSEMBLY FOR ACTIVE INTERROGATION AND RADIOISOTOPE APPLICATIONS

by

**ABBAS JOHAR JINIA**

**A Thesis**

*Submitted to the Faculty of Purdue University*
*In Partial Fulfillment of the Requirements for the degree of*

**Master of Science**
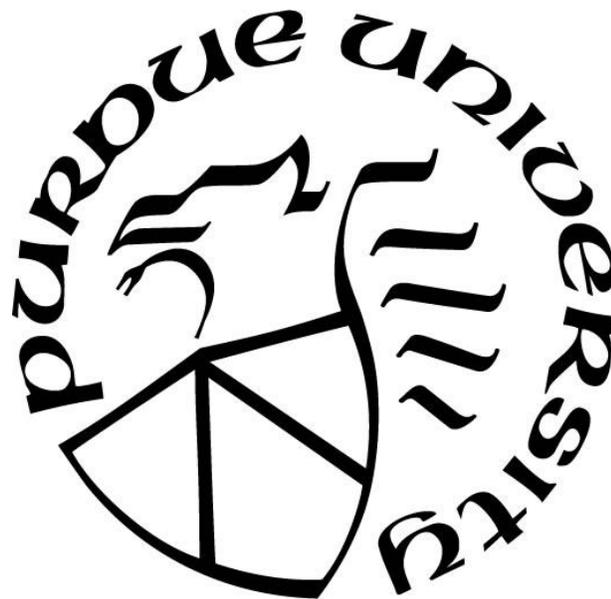
School of Nuclear Engineering
West Lafayette, Indiana
December 2018

# THE PURDUE UNIVERSITY GRADUATE SCHOOL
## STATEMENT OF COMMITTEE APPROVAL

Dr. Robert S. Bean, Chair

    School of Nuclear Engineering

Dr. Allen L. Garner

    School of Nuclear Engineering

Dr. Shripad Revankar

    School of Nuclear Engineering

Dr. Terry Grimm

    School of Nuclear Engineering

Dr. Maria A. Okuniewski

    School of Materials Engineering

**Approved by:**

    Dr. Shripad Revankar

        Head of the Graduate Program

# ACKNOWLEDGMENTS

# TABLE OF CONTENTS

# LIST OF TABLES

# LIST OF FIGURES

# ABSTRACT

Author: Jinia, Abbas, J. MSNE
Institution: Purdue University
Degree Received: December 2018
Title: Neutron Measurement and Transient Analysis in a Source Driven Subcritical
      Assembly for Active Interrogation and Radioisotope Applications
Major Professor: Dr. Robert Bean

Detecting hidden/smuggled special nuclear materials (SNM) is one of the unsolved problems in the safeguards industry. The biggest challenge is to quantify and track SNM and prevent the use of these materials for illicit purposes. The goal is to detect smallest quantity of SNM in large cargo containers, at the ports of entry, in the shortest amount of measurement time. Currently passive detection techniques, which is based on long-lived isotopes, are used to detect hidden SNM. This technique is not very reliable, as appropriate shielding of the SNM can reduce detection signals from these long-lived isotopes. Accelerator based active interrogation methods are proposed to solve the SNM problem. Besides SNM, another challenge in the nuclear industry is to meet the demand and supply of medical radioisotopes, particularly Tc-99m (half-life 6 hours). Mo-99, which decays to Tc-99m, is one of the fission products found in nuclear reactors. Because of short half-life of 66 hours, Mo-99 cannot be stockpiled. The shutdown of various research reactors globally disrupted the supply of Mo-99. Because of the financial and regulatory burden on the nuclear reactors, accelerator-based systems can be used to produce Mo-99.

With the aim to solve these two major challenges, a preliminary study is done to understand the neutrons behavior on milliseconds (or shorter) time steps in an accelerator driven subcritical system. A pulsed external neutron source, i.e. Deuterium-Deuterium (DD) generator, drives the assembly. Using first principles, the transient equations are derived and the neutron population at different time stamps is calculated. The Li-6 detector's response to the neutron population is predicted. Experiments are performed to compare the predicted behavior with the observed behavior. The model is extended further to investigate the case of no uranium fuel inside the system. Transient measurements, in the absence of the uranium fuel, are made and the neutron die-away time is determined. This die-away time is compared with the predicted time.

# 1. INTRODUCTION

Special nuclear material (SNM), primarily enriched uranium and plutonium, is easily shielded from passive detection systems at ports of entry. This is one of the greatest national security challenges plaguing countries around the world. An individual could intentionally smuggle SNM, raising questions to national safeguards and material accountancy measurements. To overcome this hindrance, official bodies and companies have increased investments in active interrogation (AI), making AI of SNM a dynamic area of research and development. Active interrogation may be defined as the "use of ionizing radiation to induce nuclear reactions that uniquely identify or quantify special nuclear material through fission or isotopic identification"[1]. Passive detection systems tend to fail in detecting moderately shielded enriched uranium and plutonium. The capability of ionizing radiation to penetrate through the attenuating medium makes AI more reliable and trustworthy than passive detection. Active and passive detection techniques, to interrogate matter, exist in literature for diverse applications [2]–[5].

According to The Royal Society, "Robust nuclear security requires the prevention of, detection of, and response to, theft, sabotage, unauthorized access, illegal transfer or other malicious acts involving nuclear and radiological material and their associated facilities" [6]. Prevention, detection and response are the key to combat potential threats. Recent technological advances in electron accelerators and nuclear radiation detectors make active interrogation systems for detection of shielded SNM technically and economically feasible. The superconducting electron linear accelerator (linac) can perform standard x-ray radiography to image cargo for illegal imports in a similar manner as luggage at the airport. While the radiograph is being collected, the same x-ray beam used to image the cargo will induce some fission if there is any shielded SNM present. Additional radiation detectors are used to detect the neutrons and gammas released during fission and subsequent decay of the fission fragments, thereby giving an unambiguous positive identification of shielded SNM. Apart from X-ray radiography, portable fast neutron radiography techniques and neutron imaging techniques currently exist [7], [8].

Subatomic particles or ions are accelerated to high velocities using linac, producing a beam of accelerated particles. These particles pass through an appropriate converter and

gets converted to energetic photons/X-rays. These photons obtained from the accelerated particles in the linac, can be used to produce neutrons through photonuclear reactions with suitable targets. The produced neutron actively interrogates any SNM present in the cargo container. The detection of prompt and delayed γ-rays, and prompt and delayed neutrons during the fission process play a vital role in the AI process. During AI, the behavior of neutrons in transient scenarios is crucial in verifying the presence of SNM. These transients depend on the quantity of SNM (i.e. multiplication factor), type of SNM (i.e. U-235 vs Pu-239), and composition of the system (i.e. surrounding moderator, shielding, etc.). Both prompt and delayed neutrons' temporal behavior will provide valuable information on the sample under interrogation.

In medicine, meeting worldwide demand for medical radioisotope production is a serious dilemma. The most commonly used medical radioisotope is Technetium-99m. Radiopharmaceuticals containing Tc-99m are used for diagnostic nuclear medical imaging applications. Tc-99m is one of the very few medical isotopes that can produce high quality images with low radiation doses to patients. One way to obtain Tc-99m is through the decay of Molybdenum-99. Mo-99 is produced by fission of uranium in nuclear reactors; however very few nuclear reactors in the world produce Mo-99. Due to shutdowns of several reactors and extended outages, the production and supply of Mo-99 is facing global shortages. This has led to significant efforts to obtain Mo-99 without a nuclear reactor, which reduces the regulatory burden and financial risk; and without using highly enriched uranium (HEU), which reduces non-proliferation issues.

A uranium target assembly (UTA) containing low enriched uranium (LEU) driven by a superconducting electron linac can produce Mo-99 and other life-saving medical radioisotopes such as Xe-133, and I-131. The system is a light water cooled, pool-type subcritical assembly consisting of LEU and coupled to an external neutron source based on a superconducting electron linac and lead-bismuth eutectic (LBE) neutron converter. To ensure subcriticality of UTA at all times and safe operation of the subcritical assembly, neutron emission from the core has to be constantly monitored (during steady-state and transient scenarios). Since a superconducting electron linac is always accompanied by an intense gamma field, the neutron detectors must monitor neutron flux under an extreme

gamma environment. Neutron die-away signal detection is key to ensuring that the system is subcritical, hence, a major merit in nuclear criticality safety over nuclear reactors.

From meeting medical isotope needs to be establishing an active interrogation program, neutron detection is essential for success. Both AI systems and medical radioisotope production systems use the same basic idea of causing fission in a subcritical assembly through photonuclear reactions. Obtaining a strong neutron source for fission requires an appropriate neutron converter. Typically, neutron intensity less than $10^{10}$ n/s is desirable to obtain decent success in AI and radioisotope programs. The high energy photons produced by the accelerated particles in the linac can be used to obtain high neutron intensities, through photonuclear reactions. It was discovered that for a linac with less than 10 MeV energy, beryllium (Be) and $D_2O$ are the favored converters, capable of producing $10^{11}$ n/s [9]. Another promising neutron converter is Li-7, which can produce 60 keV neutrons through the (p, n) reaction [10]. The protons for this reaction are obtained through a radio-frequency quadrupole linac.

Because neutrons can penetrate through the shielding material, one can use them to determine elemental composition. Two different approaches to determine elemental composition from fast neutron radiography already exist [11], [12]: fast neutron/gamma ray radiography (FNGR) and fast neutron resonance radiography (FNRR). FNRR measures neutron attenuation at various neutron energies, while FNGR measures the ratio of fast neutron and γ-ray mass attenuation coefficients. One may actively interrogate SNM by studying neutron signatures emitted by SNM; however, this requires highly sensitive neutron detectors which can measure tiny neutron intensities.

A detailed study on the fundamental properties of neutrons emitted by SNM and various neutron detectors is carried out and available in literature [13]. Neutron detectors can mainly be classified into two categories: thermal neutron detectors and fast neutron detectors. The neutron capture reactions that take place in thermal neutron detectors have a high Q-value, emitting energetic charged particles. These charged particles are helpful because they have greater energy thereby depositing more energy in the detector. This presents the opportunity for excellent gamma-ray rejection efficiency, a key requirement in AI of SNM. In contrast, the direct detection of fast neutron presents an important technical challenge. Neutrons with 200-300 keV energy range are fast neutrons. The

capture reaction cross-section value in the MeV energy range is 2 to 3 orders of magnitude smaller than for the thermal energy range. Despite the technical challenge, several approaches exist to detect fast neutrons directly. The physics behind the operation of thermal and fast neutron detectors and their technical challenges are briefly discussed in chapter 2.

The Li-doped-glass-polymer composite neutron detector is a scintillation detector with very good neutron-gamma discrimination, particularly at low neutron energies. An AI system consisting of $^{11}B(d, n\gamma)^{12}C$ neutron converter and Li-doped scintillation detector has been developed [14]. This system detects delayed neutrons to confirm the presence of SNM. Neutrons were obtained by directing the beam, obtained from the 3 MeV radio-frequency quadrupole (RFQ) accelerator, to a natural boron target (natural boron consisting of 19.9% $^{10}B$ and 80.1% $^{11}B$ was used). Natural uranium and tungsten were used as test objects for testing this AI system. Two neutron detectors, the EJ-309 liquid scintillator detector and the custom-built Li-doped scintillating detector, produced the curve (see figure 1.1 that represents the transient behavior of delayed neutrons for natural uranium). However, no transient behavior of neutrons was observed in the case of tungsten.
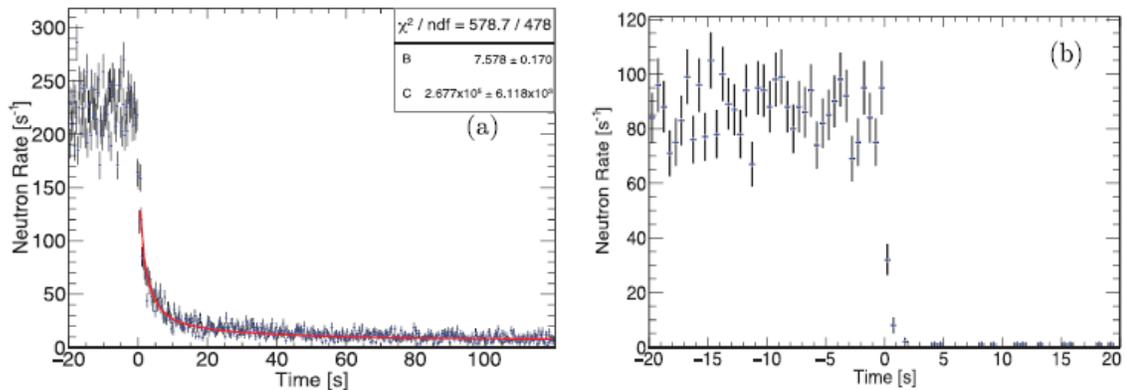


Figure 1.1 Delayed neutrons curve observed after the AI beam incident on (a) natural uranium and (b) tungsten is turned off for the EJ-309 liquid scintillation detector [14]

Taleyarkhan's group is developing a portable SNM system to detect 1kg of HEU in less than two minutes scan time [15]. This AI system consists of a deuterium-deuterium (DD) source and a tensioned metastable fluid detector (TMFD). The cargo container is actively interrogated using neutrons from the DD accelerator and a TMFD, either tensioned centrifugally or acoustically, is used to measure the resulting activity. A TMFD possesses

a unique capability of eliminating the majority of source DD neutrons when operated in threshold mode and are also blind to gamma photons. There exists evidence that a TMFD when tensioned centrifugally is 100% efficient in detecting alpha activity from uranium isotopes at 100 ppb concentrations [16].

Over the past decade, researchers have investigated various ways to produce Tc-99m. Tc-99m has a short half-life of 6 hours, one cannot produce Tc-99m directly and ship it to the hospitals for medical imaging applications. Mo-99 is a longer lived isotope ($T_{1/2}$ = 66 hours), which decays to Tc-99m, and is therefore used as a source of Tc-99m. Mo-99 production can be either reactor based or accelerator based [17]. Accelerator based production involves generating Mo-99 from other isotopes of Mo, such as Mo-100, through the $^{100}$Mo(n, 2n)$^{99}$Mo reaction, the $^{100}$Mo(p, pn)$^{99}$Mo reaction, or the $^{100}$Mo(γ, n)$^{99}$Mo reaction [18]. The Japan Atomic Energy Agency (JAEA) produced Mo-99, through the $^{100}$Mo(n, 2n)$^{99}$Mo reaction, by using 14 MeV neutrons from the D($^{3}$H, n)$^{4}$He reaction. [19]. Producing Mo-99 from Mo-100 is not economical because enriched Mo-100 is an expensive isotope. To obtain inexpensive and high activity Mo-99, researchers are investigating ways to induce fission of uranium, without a nuclear reactor and use of HEU, as Mo-99 is one of the fission fragments of uranium. Mo-99, with activity greater than 37 GBq, was obtained by fissioning LEU uranyl sulfate solution with neutrons produced by a linac [20]. Apart from a Mo-100 target, researchers have obtained Mo-99 by bombarding a 25 MeV proton beam, obtained from a 30 MeV cyclotron, onto a natural molybdenum target [21].

With the aim of producing medical radioisotopes without a nuclear reactor and developing AI techniques for detection of shielded SNM, neutron measurements and transient analysis in a linac-driven subcritical assembly is carried out in the present study. Both theoretical and experimental approaches will be used in this study.

## 2. RADIATION DETECTION AND MEASUREMENTS

The word radiation is generally used to denote the whole electromagnetic spectrum and all the atomic and subatomic particles that have been discovered. Radiation is broadly grouped into ionizing and nonionizing radiation. Ionizing radiation can ionize the atom or molecule of the medium through which it travels. X-rays, γ-rays, electrons, positrons, protons, alphas, neutrons, heavy ions and mesons are all included in ionizing radiation. On the other hand, nonionizing radiation is the electromagnetic radiation with wavelength of about 10 nm or longer. Radiowaves, microwaves, visible and ultraviolet light are included in this category of radiation. For radiation detection, it is the ionizing radiation that is of primary concern, because ionizing radiation results in partial or complete transfer of radiation energy to electrons.

### 2.1 Interaction of photons with matter

Photons are electromagnetic radiation that travel at the speed of light and they have zero rest mass energy. The classification of photons is based on their mode of origin. X-rays are photons that are emitted in atomic transition of bound electrons whereas γ-rays are the photons that are emitted following a nuclear transition. The term X-ray is generally used to denote photons with energy < 1 MeV and the term γ-ray is used to denote photons with energy > 1 MeV. In this text, the terms photon, γ and X-ray will be used interchangeably.

Usually the ionization and de-excitation of atoms from a higher energy level to a lower energy level leads to the emission of X-rays. Gamma rays are emitted when the nucleus de-excites to a lower energy level. Besides ionization and de-excitation processes, photons are also produced as bremsstrahlung. Bremsstrahlung results from the inelastic collision of atomic electrons with the nuclei. According to the classical theory, whenever an incident charged particle is deflected from its original path or experiences change in its velocity, the charged particle will emit electromagnetic radiation whose amplitude is proportional to the acceleration. Since any amount of energy, from zero up to total kinetic energy, can be radiated by the incident charged particle, a continuous X-ray spectrum is obtained.

Gamma rays may interact with matter through many possible interactions. Nonetheless, three interactions dominate in radiation measurements: photoelectric effect, Compton scattering and pair production. All these processes result in complete or partial transfer of energy of the γ-ray to the electron.

### 2.1.1 Photoelectric effect

The photoelectric effect is the interaction between an incoming photon and a bound atomic electron (figure 2.1). The incoming photon is absorbed by an atom, resulting in complete disappearance of the photon. Energy transfer takes places between the γ-ray and the bound electron. Because of this interaction, an energetic photoelectron is ejected by the atom from one of its bound shells. The kinetic energy of the ejected photoelectron is

$$E_{e^-} = h\upsilon - E_b \ \dots \dots (2.1)$$

where $h\upsilon$ represents the energy of the incoming γ-ray and $E_b$ is the binding energy of the photoelectron in its original shell. Along with the photoelectron, the photoelectric effect creates a positively ionized atom with a vacancy in one of its bound shells. The atom fills in this vacancy quickly by capturing a free electron from the medium and/or rearranging electrons within the atom itself.
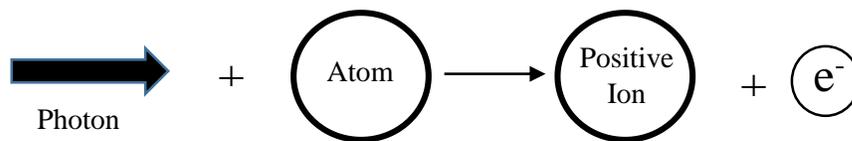


Figure 2.1 The photoelectric effect

X-rays or γ-rays with relatively low energy mainly interact with matter through the photoelectric effect. The probability for photoelectric absorption per atom over all ranges of gamma energy $E_\gamma$ and $Z$ is [22]

$$\tau = Constant * \frac{Z^n}{E_\gamma^3} \ \dots \dots (2.2)$$

where the exponent n varies between 4 and 5 depending on the value of $E_\gamma$. Eq. (2.2) is a rough approximation in which the probability for photoelectric effect has a severe dependence on the atomic number Z of the absorber atom. This is the very reason for using high Z materials, such as lead, in gamma ray shielding.

### 2.1.2 Compton scattering

Compton scattering, or the Compton effect is an interaction between the incident γ-ray and a free electron in the atom. When the energy of the incident photon is comparable to $mc^2$, the photon momentum cannot be neglected. This incident momentum must be conserved between the scattered photon and the electron with which the incident γ-ray interacts. Unlike photoelectric effect, the photon does not completely disappear after the Compton scattering. The photon is deflected through an angle θ with respect to its original direction. Following the Compton scattering, the photon travels with a lower energy and momentum, as part of its energy is transferred to the electron which then recoils. One must note that in Compton scattering, the incident photon does not transfer all its energy to the electron. Figure 2.2 illustrates the Compton scattering event.
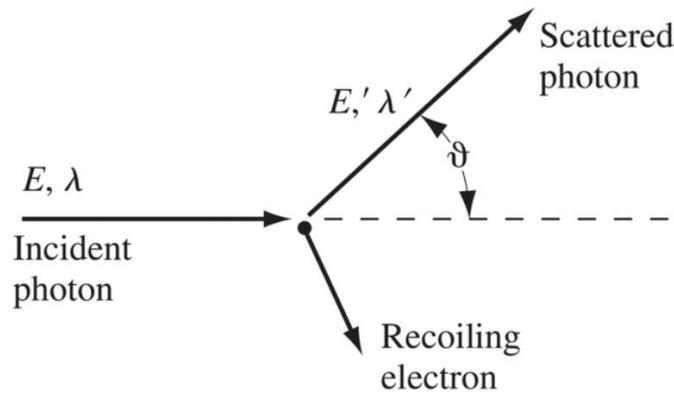


Figure 2.2 The Compton scattering [23]

Using the conservation laws for momentum and energy, the energy of the scattered photon and the recoil electron, in terms of scattering angle $\theta$, is

$$E_{\gamma'} = \frac{E_\gamma}{1 + \frac{(1 - cos\theta)E_\gamma}{mc^2}} \quad \dots\dots (\mathbf{2.3a})$$

$$T = \frac{\frac{(1 - cos\theta)E_\gamma}{mc^2}}{1 + \frac{(1 - cos\theta)E_\gamma}{mc^2}} * E_\gamma \dots\dots (\mathbf{2.3b})$$

where $mc^2$ represents the rest mass energy of the electron. The probability of Compton scattering is directly proportional to the number of electrons available as scattering targets

in the atom. Thus, this probability is linearly proportional to the atomic number Z of the material.

### 2.1.3 Pair production

Pair production is the interaction of an incident γ-ray that takes place in the Coulomb field of the nucleus. When the incident photon energy is above 1.02 MeV, interaction through pair production is energetically possible. In this interaction, the incident photon completely disappears and reappears again as positron-negatron pair whose total energy is simply equal to the incident photon energy.

$$hv = (T_- + mc^2) + (T_+ + mc^2) \dots \dots (2.4)$$

where $T_-$ and $T_+$ are the kinetic energies of the electron and positron respectively and $mc^2$ = 0.511 MeV, rest mass energy of the electrons. Following the pair production process, two annihilation photons are produced, as secondary products of this interaction, due to annihilation of positrons in the absorbing medium.

The expression for the probability of pair production is complicated. The exact expression for total pair production cross-section per nucleus can be found in [24]. This probability is found to be directly proportional to the square of the absorber atomic number Z.

The dependence of photon energy and absorber atomic number Z leading to photoelectric effect, Compton scattering, and pair production is illustrated in figure 2.3. A photon with relatively low energy (hυ) will interact through photoelectric effect. Pair production is the primary mode of interaction only for high photon energy (hυ). Compton scattering dominates in the entire range of intermediate hυ, for all Z.
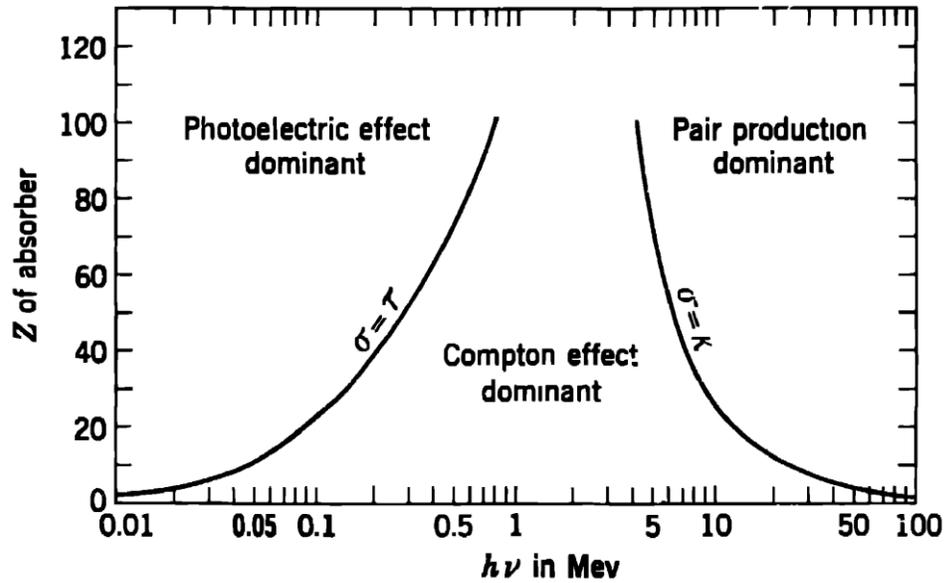
Figure 2.3 Relative importance of the three major types of γ-ray interaction. The lines show the values of Z and hυ for which the two neighboring effects are just equal [24].

### 2.1.4    Attenuation of Photons

To be able to detect γ-rays, the photon needs to travel through the matter without any kind of interaction. The probability of a photon crossing an absorber of thickness x, is simply equal to the product of the probabilities of survival for each particular type of interaction. The probability of a photon crossing a given absorber without interaction through photoelectric effect is $e^{-\tau x}$, where $\tau$ is the cross-section for photoelectric effect. Similarly the probability of gamma ray photon surviving Compton scattering and pair production is $e^{-\sigma x}$ and $e^{-\kappa x}$ respectively, with $\sigma$ and $\kappa$ being the cross-sections for Compton scattering and pair production, respectively. Thus, a collimated beam of γ-rays with initial intensity $I_{p0}$, crossing an absorber thickness x, will have residual intensity $I_p$ equal to

$$I_p = I_{p0}e^{-\tau x}e^{-\sigma x}e^{-\kappa x}$$
$$= I_{p0}e^{-(\tau+\sigma+\kappa)x}$$
$$= I_{p0}e^{-\mu x} \dots \dots (2.5)$$

where $\mu = \tau + \sigma + \kappa$ is called the total linear attenuation coefficient of γ-ray photons. Based on this probability, the average distance travelled by a γ-ray photon between two successive interactions is

$$\lambda_p = \frac{\int_0^\infty xe^{-\mu x}\, dx}{\int_0^\infty e^{-\mu x}\, dx} = \frac{1}{\mu} \ldots\ldots (2.6)$$

where $\lambda$ is called mean free path and it is simply the inverse of the linear attenuation coefficient.

The linear attenuation coefficient is highly dependent on the density ($\rho$) of the material and therefore, the mass attenuation coefficient is used for all practical purposes, and is defined as

$$Mass\ attenuation\ coefficient = \frac{\mu}{\rho} \ldots\ldots (2.7a)$$

For a compound or mixture, the mass attenuation coefficient is simply given as,

$$\left(\frac{\mu}{\rho}\right)_c = \sum_i w_i \left(\frac{\mu}{\rho}\right)_i \ldots\ldots (2.7b)$$

where $w_i$ is the weight fraction of element $i$ in the compound or mixture. Using eq. (2.7), eq. (2.5) can be rewritten as,

$$I_p = I_{p0} e^{-\left(\frac{\mu}{\rho}\right)\rho x} \ldots\ldots (2.8)$$

where $\rho x$ is called the mass thickness of the absorber and determines the degree of attenuation.

## 2.2    Interaction of neutrons with matter

Neutrons are neutral particles present in the nucleus of an atom. Since neutrons have no charge, they cannot interact in matter through Coulomb forces. The interaction of neutrons with matter occurs through nuclear forces. When a neutron interacts with matter, either the neutron totally disappears and is replaced by secondary radiation, or it scatters, or it gets absorbed.

The secondary radiation produced by neutron interactions are mainly heavy charged particles. These charged particles are the consequences of the neutron induced nuclear reactions. Besides neutron induced nuclear reactions, various neutron collision events also produce charged particles. The charged particles arising from neutron collision are the nuclei of the absorbing material itself which have gained energy during the collision event.

Most neutron detectors make use of this underlying idea of converting neutrons into some charged particle, which can then be detected directly.

Neutrons can also be detected through the radiative capture (n, γ) reaction. The radiative capture reaction results in complete absorption of the incident neutron and leads to the formation of a compound nucleus. The compound nucleus then decays to its ground state by emitting one or more γ-rays. Neutrons can be detected indirectly by detecting these emitted γ-rays. This neutron interaction is highly probable in most materials and plays an important role in the attenuation and shielding of neutrons.

This section will discuss the interaction of neutrons with matter. Based on the energy of the incoming neutron, the neutrons are classified as either slow/thermal neutrons and fast neutrons.

### 2.2.1   Interaction of slow/thermal neutron

Various neutron induced nuclear interactions and elastic scattering are the predominant interactions of slow/thermal neutrons. Because very little and or no energy is transferred to the nucleus in elastic scattering of slow neutrons, slow neutron detectors are not based on this type of interaction. The best possible way to detect thermal neutrons is through neutron induced nuclear reactions which can create secondary radiation of sufficient energy to be detected directly. For these nuclear reactions to be energetically possible, the Q-value of the neutron induced nuclear reaction should be positive, because incoming neutron energy is very low. Reactions such as radiative capture (n, γ), (n, α), (n, p) and (n, fission) are well suited for slow neutron detection.

### 2.2.2   Interaction of fast neutrons

The probabilities for neutron interaction decreases swiftly with increasing neutron energies. Inelastic scattering gains significance in the detection of fast neutrons, because neutrons can transfer a considerable amount of energy in one collision event, resulting in the slowing down of the neutrons. In an inelastic collision, part of the neutron's kinetic energy is transferred to the nucleus of the medium as an excitation energy. The secondary charged particle in this case is the excited nucleus, commonly referred to as the recoil nucleus. The excited nucleus de-excites to the ground state by emitting one or more

inelastic γ-rays. Inelastic scattering of neutrons and subsequent inelastic γ-rays play a vital role in the detection of fast neutrons. The presence of inelastic γ-rays constitutes a serious complication in the fast neutron detection, as the distinction of inelastic γ-rays from other γ-rays (other γ-rays may come from cosmic radiation or (n, γ) reactions) becomes difficult. Since a fast neutron have energy greater than 1 keV, it can transfer enough energy to a nucleus to cause the nucleus to become a heavy, charged particle. This heavy charged particle can be detected directly, since it will cause ionization of atomic molecules as it passes through the medium.

### 2.2.3 Attenuation of neutrons

Just like photons, neutrons also attenuate as they pass through an absorber material. The probability that a neutron will pass through the absorber material is equal to the product of the probabilities of survival for absorption and scattering interactions. A monodirectional beam of neutrons having initial intensity $I_{n0}$, crossing an absorbing medium of thickness $x$, will have residual intensity $I_n$ equal to

$$I_n = I_{n0}e^{-\Sigma_a x}e^{-\Sigma_s x}$$
$$= I_{n0}e^{-(\Sigma_a + \Sigma_s)x}$$
$$= I_{n0}e^{-\Sigma_t x} \ldots \ldots (2.9)$$

where $\Sigma_t = \Sigma_a + \Sigma_s$ is the total macroscopic cross-section and it greatly depends on neutron energy. The average distance travelled by a neutron between two successive interactions/collisions, called mean free path, is equal to

$$\lambda_n = \int_0^\infty x\Sigma_t e^{-\Sigma_t x}\, dx = \frac{1}{\Sigma_t} \ldots \ldots (2.10)$$

where $\Sigma_t e^{-\Sigma_t x}\, dx$ is the probability that a neutron will have its first collision in $dx$ in the neighborhood of $x$.

### 2.3 Current and Pulse modes of operation

Radiation detectors are operated either in current mode or pulse mode. In pulse mode operation (figure 2.4), the detector's output is typically connected to an RC circuit (preamplifier) which preserves information on the amplitude and timing of individual events. Pulse amplitude carries important information regarding the charge generated by a

particular radiation interaction in the detector. Every pulse will have different amplitude. Variation in the amplitude is either due to fluctuations in detector response to radiation or to the amount of energy deposited in the detector. In pulse mode operation, the dead time of the detector can result in loss of true event information because it occurred too quickly following the previous event. This may overwhelm the electronics setup of the detector.

In current mode operation (figure 2.5), a current measuring device is connected to the output of the detector. In this mode of operation, information about individual events is not preserved. The output of the current meter is the averaged dc current, over many interactions, produced in the detector. Radiation detectors operating in current mode are usually capable of withstanding high gamma doses/neutron fluxes. Because in current mode, the electrical signals from individual interactions are averaged together, the detector is not affected by dead time.
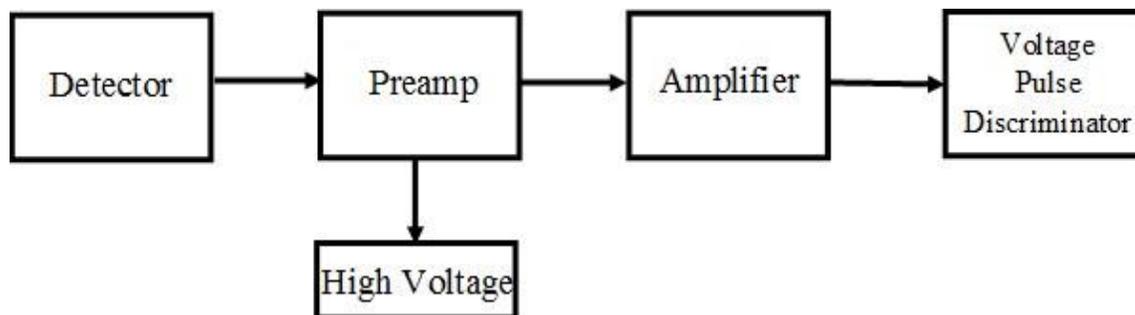
Figure 2.4 Typical block diagram for detectors operating in pulse mode
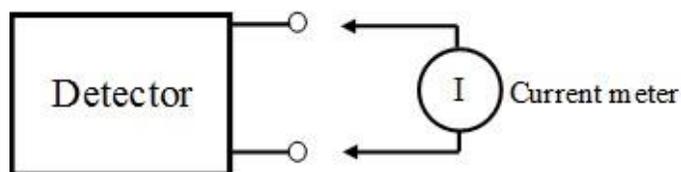
Figure 2.5 Typical block diagram for detectors operating in current mode

## 2.4 Radiation detectors

The various gamma detectors that will be used in this study are an HPGe detector, an ionization chamber and a NaI scintillation detector. A He-3 rem ball, a Li-6 detector and a compensated ionization chamber (CIC) are the different neutron detectors that be used to

detect delayed neutron intensities at different time stamps. These radiation detectors will be discussed briefly in this section. Note that this section does not intend to give detailed information about the operation of various gamma and neutron detectors. In depth explanation can be found in references [22], [25].

### 2.4.1 NaI scintillation detector

The NaI detector is an inorganic scintillation detector that can perform gamma ray spectroscopy. Scintillators are the materials that fluoresce when ionizing radiation interacts with them. Usually the light produced by scintillating crystals is very weak and hence it must be amplified. A photomultiplier tube amplifies the weak signal from the scintillating crystal and produces a strong pulse at its output.

NaI crystals possess excellent light yield, which makes it the best inorganic scintillating material for many applications. The hygroscopic nature of NaI crystal requires the crystal to be canned in an air tight container for normal use. Large detector volume, high density, and high atomic number make NaI a good gamma detector with decent efficiency. The NaI scintillation detector is operated in pulse mode and has typical decay time of the order of 230 ns.

### 2.4.2 Ionization chamber

The ionization chamber is the simplest gas-filled gamma detector. The operation of an ion chamber is based on the ionization of gas molecules. Gamma rays interact with the gas molecules through one of the many interactions discussed in section 2.1, resulting in the formation of an ion pair: free electron and positive ion. Through the application of appropriate electric field, these ion pairs are collected, which constitutes an electric signal. The total number of ion pairs created in the ionization chamber is directly proportional to the amount of energy deposited in the chamber. Ionization chamber can either be operated in current mode or pulse mode. For most applications ion chambers are operated in current mode.

### 2.4.3 HPGe detector

A high purity germanium detector (HPGe) is a semiconductor detector, having very good energy resolution. These detectors can resolve energy of the incident radiation out of

a polyenergetic energy spectrum. The ability to operate in vacuum, a linear relationship between pulse height and particle energy, insensitivity to magnetic fields and a fast pulse rise time are some other properties of semiconductor that makes HPGe detectors superior than the ion chamber and the NaI scintillation detector for high energy spectroscopy.

The function of a semiconductor detector is similar to the ionization chamber. In the ion chamber, an electric signal is produced by ionization of gas molecules and in the semiconductor detector, the electric signal is produced by the movement of electrons and holes across the p-n junction. For radiation detection applications, the p-n junction is to be connected in reverse bias. The incident radiation deposits energy into the detector, resulting in the formation of electron-hole pairs. By applying a suitable electric field, electrons and holes are collected and with appropriate electronics setup, a pulse, produced by these collected charges, is recorded.

The HPGe detector needs to be cooled by liquid nitrogen when in use. This cooling is required, because germanium has a relatively narrow energy gap, and at room temperature or higher temperature a leakage current due to thermally generated charge carriers induce very strong noise in the electronics setup. This noise can destroy the energy efficiency of the detector.

### 2.4.4   Compensated ionization chamber

A compensated ionization chamber (CIC) is a B-lined ionization chamber operating in current mode. The CIC consist of two chambers: one is a $^{10}$B-lined ion chamber and the second is a similar unlined chamber. Figure 2.6 shows a schematic of a typical CIC. Incoming neutrons interact with $^{10}$B in the B-lined chamber resulting in 2.31 MeV and 2.79 MeV charged particles. This interaction of boron with neutrons is as follows:

$$^{10}B + n = {}^{7}Li + \alpha + 2.31 MeV + \gamma(0.48 MeV) \ (94\%)$$

$$^{10}B + n = {}^{7}Li + \alpha + 2.79 MeV \ (6\%)$$
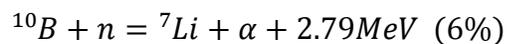
$^{7}Li$ and $\alpha$ are heavy charged particles. Heavy charged particles interact with matter through Coulomb forces. When Li and α comes in contact with chamber gas atoms, they instantaneously interact with gas atom electrons, causing ionization of gas atoms. On applying appropriate external bias voltage, the ion pairs are collected. These charges constitute current $I_{n\gamma}$. Any other gamma photons, besides those resulting from (n, γ)

reaction, incident on this B-lined chamber, will also contribute to $I_{n\gamma}$. Thus, total current produced in B-lined chamber is the sum of currents induced by neutrons and gammas. To compensate for gammas, there is a second chamber which is identical to the B-lined chamber, in terms of active volume, structural material and response to gamma flux, but without a $^{10}$B lining. This chamber is blind to neutrons and only responds to gammas. Current from the unlined chamber only reflects gamma interactions. By taking the difference between the two currents, a signal can be obtained that is purely from neutron reactions.
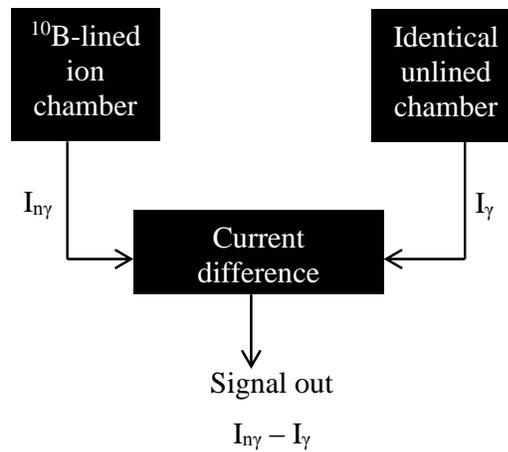


Figure 2.6 Schematic of B10 CIC [22]

### 2.4.5 Li-6 detector

The Li-6 detector is a thermal neutron detector based on the following (n, α) reaction.

$$^6_3Li + n = \alpha + ^3_1He + 4.78 MeV$$
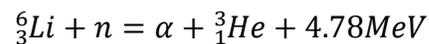
The cross-section value for this (n, α) reaction, at 0.025 eV neutron energy, is about 940 barns. In this type of neutron detector, Li-6 is usually surrounded by polyethylene to moderate fast neutrons to thermal energy levels. The heavy charged particles, $^3He$ and $\alpha$, interact with the gas atoms as they pass through the gaseous medium, resulting in ionization of atomic electrons. Unlike the CIC, the Li-6 detector is operated in pulse mode.

### 2.4.6  He-3 rem ball

The He-3 rem ball is another thermal neutron detector that consists of a He-3 proportional counter surrounded by a sphere of polyethylene. Neutrons are detected through the following (n, p) reaction:

$$^3_2He + n = \, ^3_1H + p + 0.765 \; MeV$$
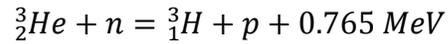
The thermal neutron cross-section value for this reaction is about 5330 barns, significantly higher than that for the boron and lithium reactions. He-3 counters can be operated at much higher pressures with adequate gas multiplication behavior and are therefore preferred for those applications in which maximum detection efficiency is required.

# 3.   EXPERIMENTAL EQUIPTMENT AND SETUP

## 3.1   Uranium Target Assembly

A pool type subcritical assembly, Uranium Target Assembly (UTA-1), has been developed, designed and constructed at Niowave Inc. headquarters in Lansing, Michigan. This assembly is used to perform the transient analysis of neutrons and measurements for active interrogation and radioisotope applications. Natural uranium and low enriched uranium (LEU) is used to fuel UTA-1. The assembly can be driven by an external neutron source. The UTA-1 is a standard 55 gallon stainless steel tank filled with light water which is used as a moderator, coolant and a shield for neutrons. Natural uranium and LEU targets are inserted into the fuel rods which are supported by an aluminum grid plate in the assembly. Provisions are made to insert various diagnostic tools into the assembly and extract volatile gases which build up during operations. Figure 3.1 shows a pictorial view of the UTA-1 subcritical assembly.
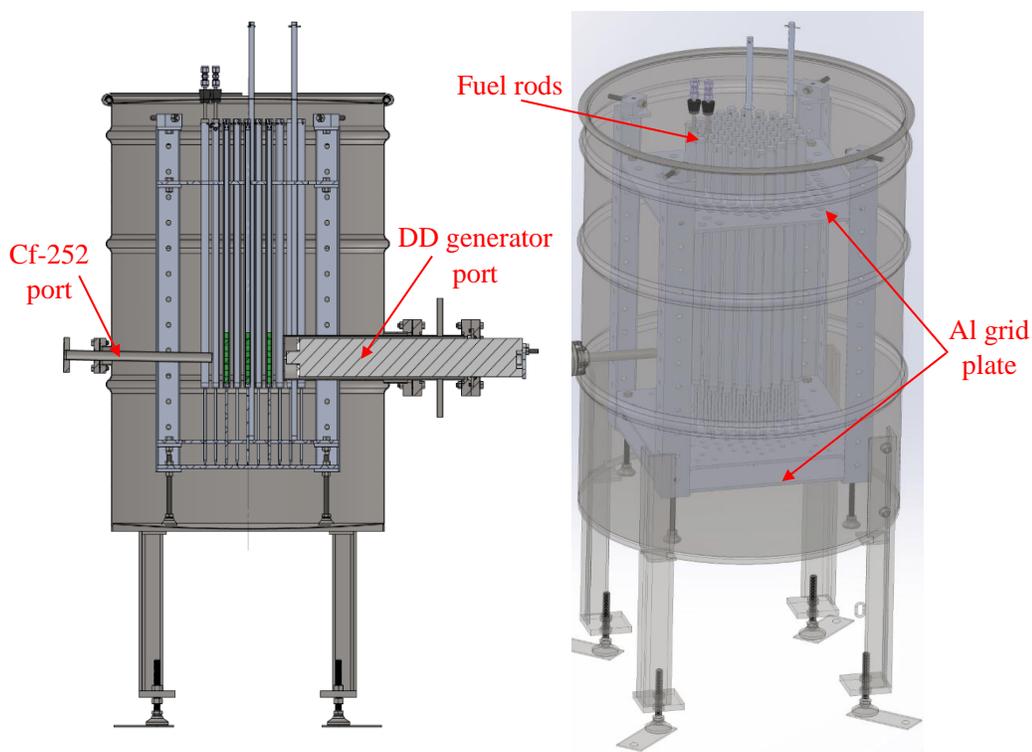


Figure 3.1 UTA-1 with Cf-252 port and DD generator port (left), 3D diagram of UTA-1 subcritical assembly (right)

### 3.1.1 UTA-1 design parameters and initial fuel loading

The UTA-1 has a total of 60 fuel rods, made from 6061 Al, of which 37 are loaded with LEU and 23 are loaded with natural uranium. The LEU is enriched to 6.4%. The LEU is in the form of $UO_2$ while the natural uranium is in metallic form. Eight pellets of LEU and two slugs of natural uranium are loaded into the fuel rods. The LEU pellets and the slugs of natural uranium result in around 100 mm active fuel height. The diameter of the LEU pellet is 8.19 mm while the diameter of the natural uranium pellet is 12.1 mm. The diameter of the LEU fuel rod is 7/16" while the diameter of the natural uranium fuel rod is 5/8". Figure 3.2 shows a typical fuel rod in the UTA-1 assembly.



688.4 mm

100 mm

164.1 mm
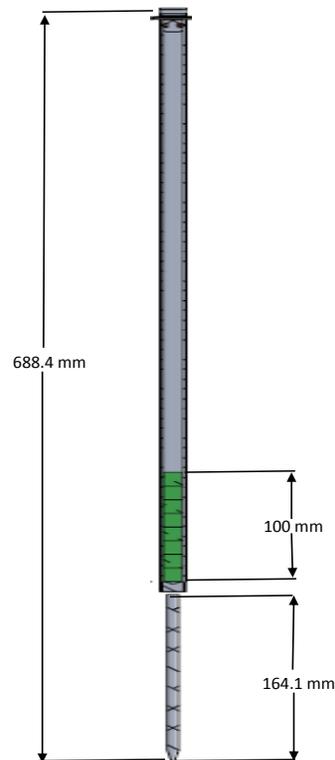
Figure 3.2 Fuel rod in UTA-1 assembly

The UTA-1 design parameters were calculated using MCNP6. The assembly is a deeply subcritical system with an effective multiplication factor of $k_{eff} = 0.412$. The UTA-1 can operate at a fission power of up to 24 milliWatts. Table 3.1 summarizes the important design parameters for UTA-1.

Table 3.1 UTA-1 Design Parameters

| Parameters | Values |
|---|---|
| k$_{eff}$ for UTA-1 | 0.412 |
| Cladding type | 6061 Al |
| **Fuel Rod (x37)** | |
| $^{235}$U enrichment (wt%) | 6.4 |
| Chemical Form | UO$_2$ |
| Pellet Mass (g) | 7 |
| Pellets per Rod | 8 |
| **Natural Uranium Rod (x22)** | |
| $^{235}$U enrichment (wt%) | 0.71 (natural) |
| Chemical Form | U (metal) |
| Slug Mass (g) | 100 |
| Slugs per Rod | 2 |
| **Natural Uranium Radiochemistry Rod (x1)** | |
| $^{235}$U enrichment (wt%) | 0.71 (natural) |
| Chemical Form | U (metal) |
| Pellet Mass (g) | 20 |
| Pellets per Rod | 5 |
| Slug mass (g) | 100 |
| Slugs per Rod | 1 |
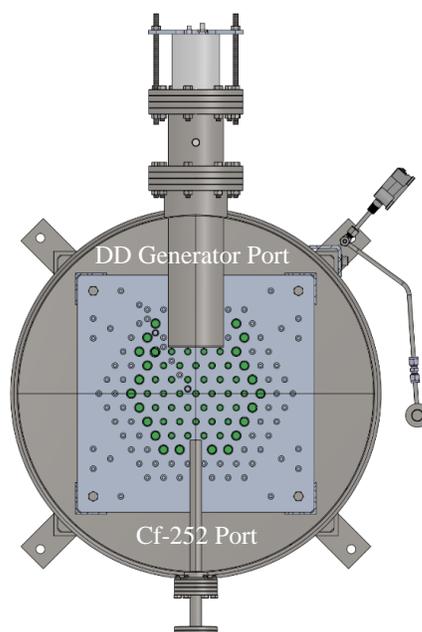


Figure 3.3 Cutaway of UTA-1 system with Cf-252 port and DD generator port. Uranium pellets are marked in green.

### 3.2    Silverside Li-6 neutron detector

A Li-6 neutron detector, developed by Silverside Detectors Inc., Cambridge, Massachusetts, is used to measure the neutron counts. The neutrons are detected in a thin, thermal neutron detection module, called Base Unit chamber. The base units are integrated into support frames, with a moderating material at the surface, for optimized neutron sensitivity. The base unit chamber is a Li-6 proportional chamber, in which neutrons enter after multiple collisions with the moderating material near the chamber surface. High density polyethylene is used as a moderating material. Alpha and He-3 particles created by the reaction between incident neutrons and Li-6 foil deposit energy in the chamber causing ionization in the gas medium. The ionized electrons are attracted to an array of wires biased at high voltage, constituting an electric signal. This electric signal is amplified and processed into neutron count rate data. Figure 3.4 shows a two base unit Li-6 detector.

The gamma absolute rejection ratio in the presence of neutrons (GARRn), for a two base unit Li-6 detector, is 1.015 in the presence of a 10 mR/hr gamma field and 1.008 in the presence of a 20 mR/hr gamma field. The Li-6 detector has a neutron detection efficiency of 1.87 cps/ng (moderated Cf-252 neutrons) and 1.27 cps/ng (bare Cf-252 neutrons) [26]. A built-in software, Silverside View, gives a plot of count rate versus time.

The detector can distinguish neutrons and gammas, based on what is called Time-over-Threshold. The Time-over-Threshold (TOT) is the amount of time the event pulse is above a voltage threshold; it is related to the pulse height. A typical single base unit histogram of counts versus TOT is shown in figure 3.5. Clearly, signals below 12 microseconds are gamma signals and all the signals above 12 microseconds come from neutron interactions. A neutron event deposits more energy in the gas medium than a gamma ray. Consequently, a neutron event causes more ionization of the gas molecules. This results in greater pulse amplitude at the output of the detector. So the detector will take longer time to recover from the last neutron event signal before it processes the new signal. In other words, the neutron event pulse amplitude will be greater than the set threshold amplitude for a longer period of time (as opposed to gamma pulse amplitude, which is always less than the neutron event pulse amplitude).

Table 3.2 Specifications of Silverside Li-6 Detector

| Dimensions | 47.6" x 13.2" x 6.9" |
|---|---|
| Operating voltage | 1050 volts |
| Battery operation time | Up to 12 hours |
| High voltage | |
| Detector Efficiency | 1.87 cps/ng (moderated CF-252 neutrons)<br>1.27 cps/ng (bare Cf-252 neutrons) |
| GARRn | 1.015 (at 10 mR/hr gamma field)<br>1.008 (at 20 mR/hr gamma field) |
| Pulse height spectroscopy software | Silverside View |



1" of HDPE back-side moderator

2 x 1" of HDPE moderator between chambers

8 channel electronics box

2 x Neutron detection chambers

Position neutron source to this side for optimum performance

Chamber and electronics use MHV connections
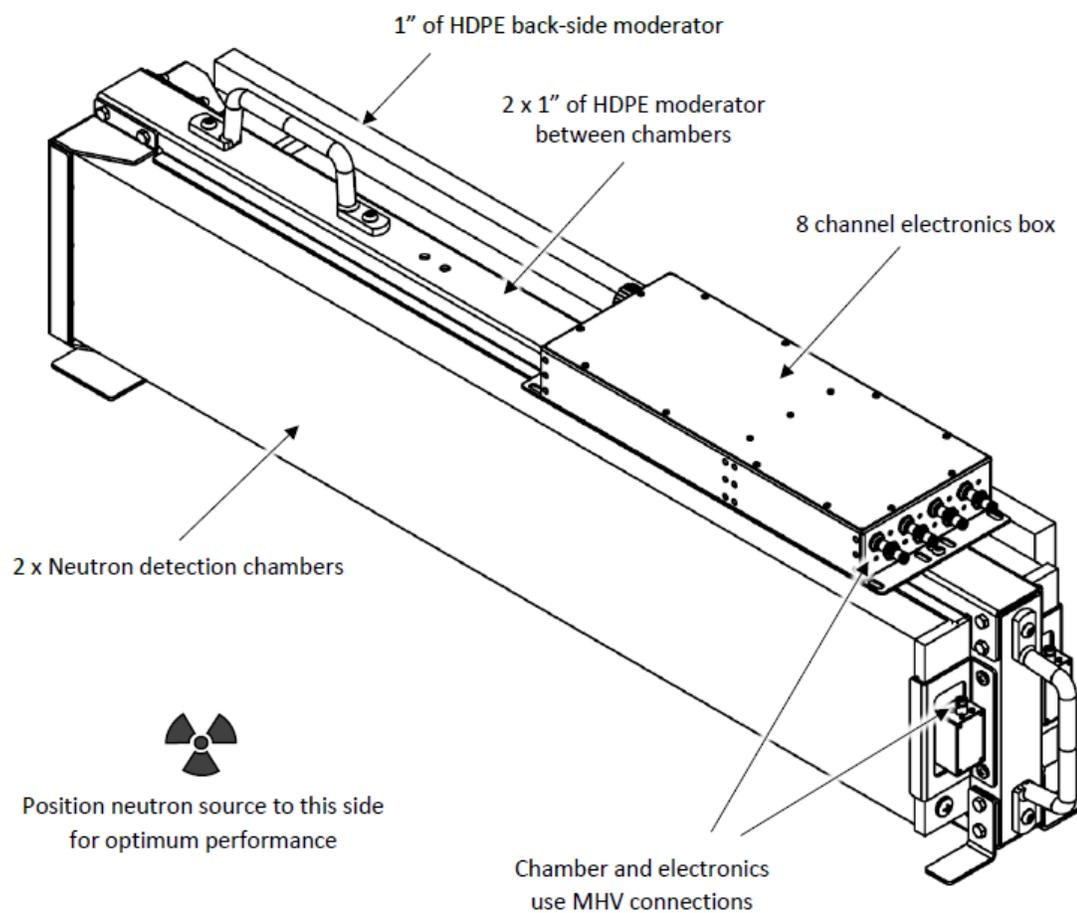
Figure 3.4 Two Base Units Li-6 Detector
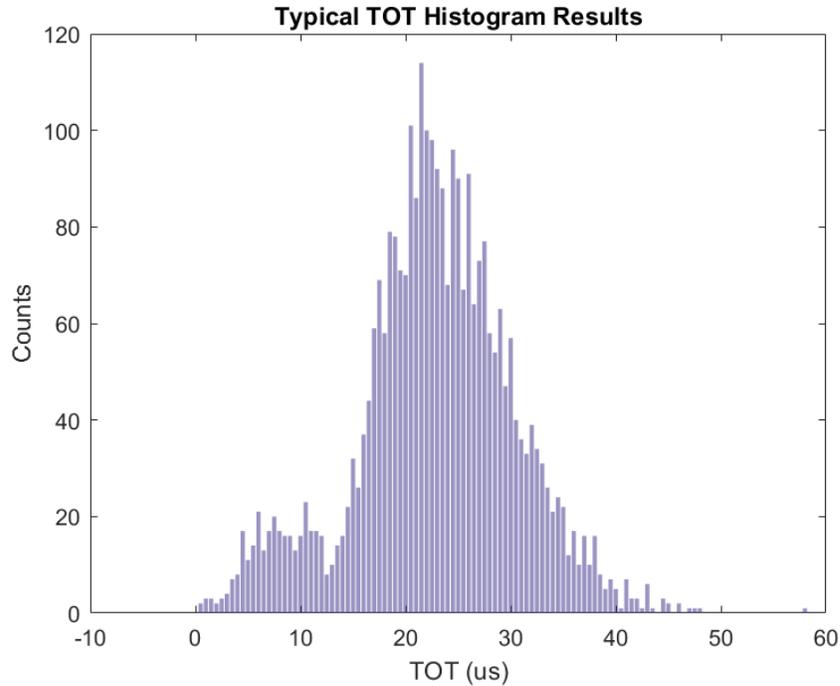
Figure 3.5 Histogram of counts versus TOT in a single chamber detector

## 3.3 DD neutron generator

The UTA-1 can be driven by external neutron sources such as a Cf-252 neutron source, a neutron generator, or a superconducting electron linac coupled to a photoneutron converter. Neutrons are continuously emitted from radioactive sources, thereby emitting radioactivity at all times. However, in neutron generators, like deuterium-deuterium (DD) or linac with photoneutron converter, there is no further emission of radioactivity (neutrons/gammas) when the generator is turned off. Thus, for the preliminary transient analysis of neutrons, DD generator is coupled to the UTA-1 assembly. 2.5 MeV neutrons are obtained from the generator through the DD fusion reaction.

$$^2H + {}^2H = n + {}^3He + 3.266 MeV, \quad E_n = 2.5\ MeV$$
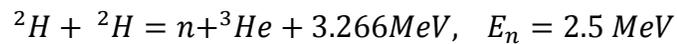
Figure 3.6 Starfire nGen-300 DD neutron generator

A neutron generator produces neutrons through a fusion reaction by accelerating charged particles onto a target. In a DD generator, targets are usually made of metal hydrides, which increases the density of hydrogen in the target. A typical DD neutron generator consists of a source to generate positive ions which are then accelerated, using diode structure, to a hydride target containing either deuterium, tritium or a mixture of the two. The positive ions are generated using a cold cathode, or Penning, ion source. This ion source is a hollow cylindrical anode, with cathode plates at each end of the anode, usually connected to ground. A magnetic field is applied coaxially within the ion source using an external magnet.

On introducing deuterium gas into the anode, ionization of the gas occurs due to the electric field produced between the anode and cathodes. The orientation of electric and magnetic fields creates electron confinement in this plasma. This forces the electrons to oscillate back and forth in helical trajectories. Secondary electrons may be created due to the loss of some low energy electrons which strike the anode. However, most of the electrons remain trapped and ionize more gas molecules to sustain the plasma. The ions are not similarly trapped, and when they strike the cathodes, they also release secondary electrons, which enter the plasma and help sustain it. Ions, however, can escape the chamber into the acceleration section of the tube through a hole at the center of one of the cathodes, called the exit cathode.

In this experiment, a Starfire nGen-300 DD neutron generator is used. The specifications of the DD neutron generator is given in table 3.3.

Table 3.3 Starfire nGen-300 Specifications

| Neutron Output | |
|---|---|
| Time-averaged yield | $10^7$ n/sec |
| Pulsed DD Neutron Energy | 2.5 MeV |
| Ion Source Type | ECR-coupled plasma |
| Pulse Rate | Single shot to 200 kHz |
| Pulse Width | 5-1000 μsec |
| Pulse Rise/Fall time | <5 μsec |
| Nominal Duty Factor | 4-10% |
| Max Neutron Flux | $>2 \times 10^7$ n/cm$^2$*s during pulse |
| **Power and Operations** | |
| Operating voltage | 150 kV |
| Power Requirements | 400 W |
| **System Information** | |
| Neutron Source Dimension | 3" OD x 19.6" L (7.6 cm OD x 46 cm L); without shroud |
| Neutron Source Weight | 11 lbs, 9 oz. |
| Supporting Hardware Dimension | 6.25" W x 10" H x 15.75" L (31 cm W x 31 cm H x 31 cm L) |
| Supporting Hardware Weight | 29 lbs, 6 oz. + 5.5lb battery |
| Integrated cooling w/cowling Dimensions | 3.5" OD x 22" long |
| Battery Operation Time | 45 min (at 4% duty factor); 30 min (at 10% duty factor) |

## 3.4  Experimental setup

Besides UTA-1, the DD neutron generator and the Li-6 detector, other equipment such as an HPGe detector, a NaI scintillation detector and a He-3 rem ball are part of the experimental setup. An HPGe detector and NaI scintillation detector are used for gamma ray spectroscopy while the He-3 rem ball is used for neutron dose measurements. Appropriate electronics such as the pre-amplifiers, amplifiers, oscilloscope, high voltage supplies and multi-channel analyzer (MCA) are used to support the HPGe and NaI detectors. A picture of the experimental setup is shown in figure 3.7.

Figure 3.7 Experimental setup for the transient analysis of neutrons in UTA-1.

Table 3.4 List of equipment's

| Equipment | Make/Model |
|---|---|
| Uranium Target Assembly | Niowave Inc./UTA-1 |
| Li-6 neutron detector | Silverside Detectors Inc. |
| DD neutron generator | Starfire/nGen-300 |
| HPGe gamma-ray detector | Ortec/GEM 10-70 |
| NaI scintillation detector | Amptek Inc./76BR76(3M-HV-E3-X5) |
| He-3 rem ball | Ludlum Inc./2241-4 |
| Oscilloscope | Tektronix/TDS 3014B |
| High voltage supply | Ortec/659 |
| Amplifier | Ortec/572 |
| Multi-channel analyzer (MCA) | Ortec/928 MCB |

# 4.   NEUTRON BEHAVIOR IN THE UTA-1+DD SYSTEM

The transient analysis of neutrons has application in the field of active interrogation (AI) for the detection of SNM and medical radioisotope production. Using a DD neutron source, transient analysis of neutrons is carried out to examine the neutron detector behavior at different time stamps in the UTA-1 assembly. For AI applications, one needs to scan the cargo container in the smallest possible time interval. With the Li-6 neutron detector, the smallest possible time interval can be achieved when the neutron count rate is recorded on microsecond/millisecond timescales. The neutron balance equations, derived from first principles, are used to model the neutron die-away over time. Differential Die-Away Analysis (DDAA) is one of the techniques used for detecting SNM such as U-235 and Pu-239. DDAA models exist in the literature and researchers have studied neutron die-away signals in different scenarios [27]–[30]. The present analysis examines the neutron population at different time stamps and the corresponding Li-6 count rate. Since UTA-1 is a subcritical assembly, we expect the neutron population to die-away over time. Further, we assess the neutron die-away for the non-fueled UTA-1+DD system, which replicates a cargo container with no SNM.

## 4.1   The behavior of the neutron population

To understand the behavior of the neutron population in the UTA-1+DD system, we look closely into the experimental setup (figure 3.7). Source neutrons produced by the DD generator are born in the center of the UTA barrel. These source neutrons cause fission in the fuel rods and produce additional fission neutrons. The DD source, natural uranium, and LEU fuel rods constitute the center region of the entire UTA-1+DD system. This region is surrounded by a moderator, i.e. $H_2O$. The center region and the moderator can be homogenized to obtain region I. Region I is then surrounded by a reflector/absorber, in this case concrete blocks. The concrete blocks constitute the outer region II of the setup. The Li-6 detector is placed in region II. An overview of the simplified two region UTA-1+DD setup is shown in figure 4.1.

Concrete acts as a neutron moderator and reflector. The 2.5 MeV neutrons from the DD generator and the fission neutrons are produced at the center of the UTA barrel. These neutrons quickly slow down to thermal energies due to the presence of the moderator. A fraction of these neutrons leaks out of the assembly. The neutrons that leak out of the assembly travel isotropically in all directions and are subject to various scattering events outside the UTA barrel. These scattering events now occur in a new medium i.e. region II. There is a finite probability for the scattered neutrons to reach the Li-6 detector and be recorded as a count. In other words, the die-away of the neutron population will depend on the region in which the Li-6 detector is placed.

We start with the general balance equation to understand the spatial and time behavior of neutrons in the UTA-1+DD system. The neutrons are assumed to be monoenergetic and the cross-section values are assumed to be constant (i.e. 1-group, homogenized system). In such a system, the neutron population, which is a combined function of space and time, can be separated in its time and space dependence as follows.

$$\phi(r,t) = \varphi(r) * \psi(t) \dots \dots (4.1)$$

where $\phi(r,t)$ = space and time dependent neutron flux,

$\varphi(r)$ = space dependent neutron flux, and

$\psi(t)$ = time dependent neutron flux.
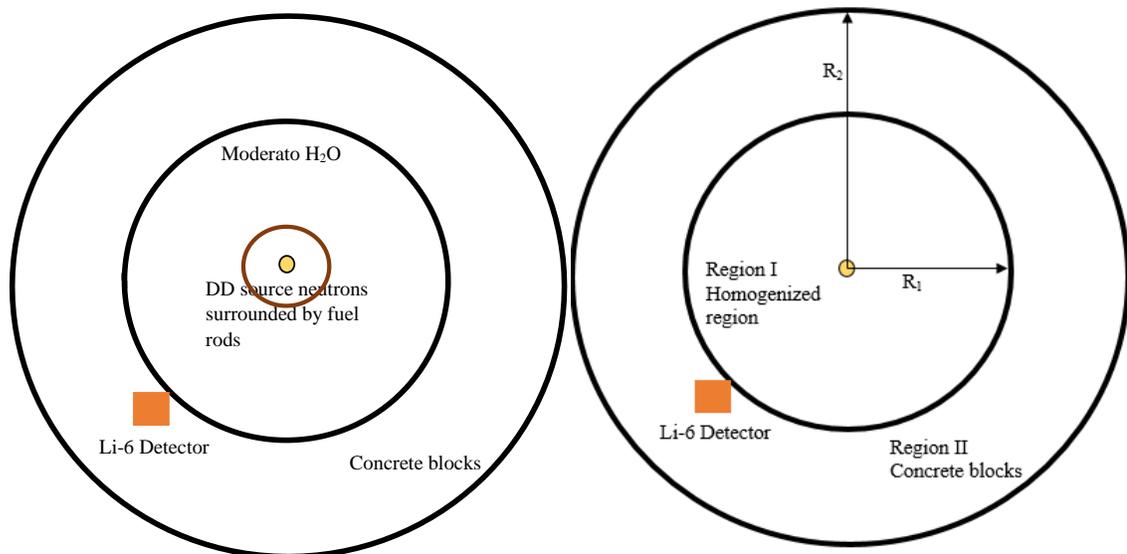


Figure 4.1 Simplified two region UTA-1+DD system.

The general balance equations in region I and region II can be written as follows:

$$[Rate\ of\ change\ in\ \#\ neutrons\ in\ V]$$
$$= [Rate\ of\ production\ of\ neutrons\ in\ V]$$
$$- [Rate\ of\ absorption\ of\ neutrons\ in\ V]$$
$$- [Rate\ of\ leakage\ of\ neutrons\ from\ V]\ \dots\dots (4.2)$$

In region I, we have

$$\frac{1}{\bar{v}}\int_{V_1}\frac{d\phi_1(r,t)}{dt}dV_1$$

$$= \int_{V_1}\nu_p\Sigma_f\phi_1(r,t)dV_1 + \int_{V_1}\sum_k\lambda_k c_k(r,t)dV_1 + \int_{A_2}\overrightarrow{J_2^-}(R_1,t)dA_2$$

$$- \int_{A_1}\overrightarrow{J_1^+}(R_1,t)dA_1 - \int_{V_1}\Sigma_{a1}\phi_1(r,t)dV_1, \qquad 0 \le r \le R_1 \ \dots\dots (4.3a)$$

and in region II, we have

$$\frac{1}{\bar{v}}\int_{V_2}\frac{d\phi_2(r,t)}{dt}dV_2 = \int_{A_1}\overrightarrow{J_1^+}(R_1,t)dA_1 - \int_{A_2}\overrightarrow{J_2^+}(R_2,t)dA_2 - \int_{V_2}\Sigma_{a2}\phi_2(r,t)dV_2,$$

$$R_1 \le r \le R_2 \ \dots\dots (4.3b)$$

where $\phi_i(r,t)$ = neutron flux in region i,

$\quad \overrightarrow{J_i^{\pm}}$ = partial neutron current in region i,

$\quad \Sigma_f$ = thermal fission cross-section,

$\quad \Sigma_{ai}$ = thermal absorption cross-section of region i,

$\quad \nu_p$ = prompt neutron yield,

$\quad \lambda_k$ = decay constant in k[th] delay group,

$\quad c_k$ = k[th] precursor concentration,

$\quad V_i$ = volume of region i,

$\quad A_i$ = area of region i,

$\quad \bar{v}$ = average neutron velocity,

$\quad R_1$ = radius of region I, and

$\quad R_2$ = radius of region II from the center.

The source terms in region I are the neutrons that diffuse partially from region II to region I at the interface, fission prompt neutrons and fission delayed neutrons. The last two terms

on the RHS of eq. (4.3a) represents the losses of neutrons in region I. These losses are due to the partial diffusion of neutrons from region I to region II and the absorption of neutrons in region I. Since there is no external source or fissile material present in region II, the only source of neutrons in region II is the neutrons leaking out of region I. The two loss terms in region II i.e. absorption and leakage are represented in eq. (4.3b).

### 4.1.1 Spatial distribution of neutrons

The spatial and time dependent neutron flux is solved separately. As all of the DD source neutrons are produced at the center of the UTA assembly, we assume a point source of neutrons in region I and no neutron source in region II. The spatial distribution of neutrons can be represented by the diffusion equation in the two regions.

$$\frac{1}{r^2}\frac{d}{dr}\left[r^2\frac{d}{dr}\,\varphi_1(r)\right] - \frac{1}{L_1^2}(1-k)\varphi_1(r) = 0, \qquad 0 < r \le R_1 \ldots\ldots (4.4a)$$

$$\frac{1}{r^2}\frac{d}{dr}\left[r^2\frac{d}{dr}\,\varphi_2(r)\right] - \frac{1}{L_2^2}\,\varphi_2(r) = 0, \qquad R_1 < r \le R_2 \ldots\ldots (4.4b)$$

where $k$ = k-value of UTA-1+DD system,

$L_1^2 = D_1/\Sigma_{a1}$ = diffusion length in region I,

$L_2^2 = D_2/\Sigma_{a2}$ = diffusion length in region II,

$D_i$ = diffusion coefficient in region i,

$\Sigma_{ai}$ = macroscopic absorption cross-section in region I,

$R_1$ = radius of region I, and

$R_2$ = radius of region II from the center.

The solutions to eq. (4.4a) and eq. (4.4b) are exponentials and can be written as follows:

$$\varphi_1(r) = \frac{A_1}{r}\exp\left(\frac{\sqrt{(1-k)}*r}{L_1}\right) + \frac{A_2}{r}\exp\left(-\frac{\sqrt{(1-k)}*r}{L_1}\right), \quad 0 < r$$

$$\le R_1 \ldots\ldots\ldots (4.5a)$$

$$\varphi_2(r) = \frac{A_3}{r}\exp\left(\frac{r}{L_2}\right) + \frac{A_4}{r}\exp\left(-\frac{r}{L_2}\right), \quad R_1 \le r \le R_2 \ldots\ldots\ldots (4.5b)$$

where the constants $A_1$, $A_2$, $A_3$ and $A_4$ are evaluated using the boundary and the interface conditions. Considering the extrapolated distance, these conditions are given as follows:

$$\lim_{r\to 0} 4\pi r^2\left[-D_1\frac{d}{dr}\varphi_1(r)\right] = S \ldots\ldots\ldots (4.6a)$$

$$\varphi_1(r)_{R_1} = \varphi_2(r)_{R_1} \ldots\ldots\ldots (4.6b)$$

$$D_1 \left[ \frac{d}{dr} \varphi_1(r) \right]_{R_1} = D_2 \left[ \frac{d}{dr} \varphi_2(r) \right]_{R_1} \ldots\ldots\ldots (4.6c)$$

$$\varphi_2(R_2 + (0.71 * 3 * D_2)) = 0 \ldots\ldots\ldots (4.6d)$$

where $S$ = DD source neutron intensity.

The four constants were evaluated symbolically using Wolfram Mathematica and the simplified expression for $\varphi_1(r)$ and $\varphi_2(r)$ were obtained (see Appendix A).

### 4.1.2  Time behavior of neutron population

Region I is a multiplying medium with an external source and region II is a non-multiplying medium. The neutron transients in region I and region II will be governed by two separate sets of equations. The point kinetics model is used to study transients in region I. In region II, the neutron population will simply increase/decrease exponentially. The transient equations derived in this section show the behavior of the neutron population when the external source is turned off.

The point kinetic equations predict total neutron flux level at any given instant of time by considering the prompt neutrons and the six delayed neutron groups. When the neutron source is turned off, the point kinetics model shows that there is a sudden decrease in the population of prompt neutrons. This decrease is caused due to absorption, leakage, and a reduction in fission rate. This drop may look instantaneous but in reality the prompt neutrons stay for some period of time (couple hundreds of microseconds to milliseconds) before their population drops to low levels. The decay of prompt neutrons is exponential, and they greatly affect the neutron population at the detector on millisecond timescales.

At the time of shutdown, the delayed neutron population does not decrease as rapidly as the prompt neutron population. This is primarily due to the continuous $\beta^-$ decay of the fission products, which leads to the production of delayed neutrons. The amount of fission products present in the assembly depends on the power at which the assembly was operating. The generation rate of the delayed neutrons changes slowly on the second time scales, but on the microsecond time scales this rate may not change slowly.   Both prompt and delayed neutrons exist at the time of shut down and therefore it is necessary to consider

both prompt and delayed neutrons in predicting neutron count rates on millisecond time scales.

The total neutron current can be expressed as the sum of two partial currents as follows [31]:

$$\vec{J}(r,t) = \vec{J^+}(r,t) - \vec{J^-}(r,t) \dots\dots (4.7a)$$

$$\vec{J^\pm}(r) = \frac{1}{4}\phi(r,t).\hat{u} \pm \frac{1}{2}\vec{J}(r) \dots\dots (4.7b)$$

$$\vec{J}(r,t) = -D\psi(t)\nabla\varphi(r) \dots\dots (4.7c)$$

where $\hat{u}$ is a unit vector. Using eq. (4.7b) and eq. (4.7c), the partial currents in eq. (4.3a) and eq. (4.3b) can be rewritten as follows:

$$\int_{A_1} \vec{J_1^+}(R_1,t)dA_1 = \int_{V_1} \nabla.\vec{J_1^+}(R_1,t)dV_1$$

$$= \int_{V_1} \nabla.\left(\frac{1}{4}\widetilde{\psi_1}(t)\widetilde{\varphi_1}(R_1).\hat{u} - \frac{1}{2}D_1\widetilde{\psi_1}(t)\nabla\widetilde{\varphi_1}(r)|_{R_1}\right)dV_1$$

$$= -\frac{1}{2}\int_{V_1} D_1\widetilde{\psi_1}(t)\nabla^2\widetilde{\varphi_1}(r)|_{R_1}dV_1$$

$$= -\frac{1}{2}\int_{V_2} D_2\widetilde{\psi_2}(t)\nabla^2\widetilde{\varphi_2}(r)|_{R_1}dV_2 \dots\dots (4.8a)$$

Similarly,

$$\int_{A_2} \vec{J_2^-}(R_1,t)dA_2 = \frac{1}{2}\int_{V_2} D_2\widetilde{\psi_2}(t)\nabla^2\widetilde{\varphi_2}(r)|_{R_1}dV_2$$

$$= \frac{1}{2}\int_{V_1} D_1\widetilde{\psi_1}(t)\nabla^2\widetilde{\varphi_1}(r)|_{R_1}dV_1 \dots\dots (4.8b)$$

$$\int_{A_2} \vec{J_2^+}(R_2,t)dA_2 = -\frac{1}{2}\int_{V_2} D_2\widetilde{\psi_2}(t)\nabla^2\widetilde{\varphi_2}(r)|_{R_2}dV_2 \dots\dots (4.8c)$$

where $\widetilde{\varphi_\iota}(r)$ = space dependent neutron flux in region i, and

$\widetilde{\psi_\iota}(t)$ = time dependent neutron flux in region i.

Using eq. (4.8a) and eq. (4.8b), eq. (4.3a) can be rewritten as

$$\frac{1}{\bar{v}} \int\limits_{V_1} \frac{d\phi_1(r,t)}{dt} dV_1$$

$$= \int\limits_{V_1} v_p \Sigma_f \phi_1(r,t) dV_1 + \int\limits_{V_1} \sum_k \lambda_k c_k(r,t) + \frac{1}{2} \int\limits_{V_1} D_1 \widetilde{\psi_1}(t) \nabla^2 \widetilde{\varphi_1}(r)|_{R_1} dV_1$$

$$+ \frac{1}{2} \int\limits_{V_1} D_1 \widetilde{\psi_1}(t) \nabla^2 \widetilde{\varphi_1}(r)|_{R_1} dV_1 - \int\limits_{V_1} \Sigma_{a1} \phi_1(r,t) dV_1 \,\dots\dots(4.9)$$

Since eq. (4.9) is true for any volume, we can write,

$$\frac{\varphi_1(r)}{\bar{v}} \frac{d\psi_1(t)}{dt} = D_1 \psi_1(t) \nabla^2 \varphi_1(r)|_{R_1} + \varphi_1(r)(v_p \Sigma_f - \Sigma_{a1})\psi_1(t)$$

$$+ \sum_k \lambda_k C_k(r,t) \,\dots\dots(4.10a)$$

where

$$\frac{dC_k(r,t)}{dt} = \frac{\beta_k}{\Lambda} \phi_1(r,t) - \lambda_k C_k(r,t) \,\dots\dots(4.10b)$$

where $C_k = k^{th}$ precursor concentration integrated over the volume,

$\varphi(r)$ = volume integrated spatial distribution of neutrons, and

$\psi(t)$ = volume integrated temporal distribution of neutrons.

Similarly, eq. (4.3b) can be written as

$$\frac{\varphi_2(r)}{\bar{v}} \frac{d\psi_2(t)}{dt} = \frac{1}{2} D_2 \psi_2(t) \nabla^2 \varphi_2(r)|_{R_2} - \varphi_2(r)\Sigma_{a2}\psi_2(t)$$

$$- \frac{1}{2} D_2 \psi_2(t) \nabla^2 \varphi_2(r)|_{R_1} \,\dots\dots(4.10c)$$

Since at $r = 0$, the external DD neutron source is placed, the neutron transients in region I at $r = 0$ can be described by point kinetics equations, i.e. eq. (4.10) reduces to the point kinetics equation.

$$\frac{d\psi_1(t)}{dt} = \frac{S(t)}{\Lambda} + \frac{(\rho - \beta)}{\Lambda} \psi_1(t) + \sum_k \lambda_k C_k(t) \,\dots\dots(4.11a)$$

$$\frac{dC_k(t)}{dt} = \frac{\beta_k}{\Lambda} \psi_1(t) - \lambda_k C_k(t) \,\dots\dots(4.11b)$$

where $S$ = external neutron source,

$$\rho = \frac{1}{k} = \frac{\Sigma_{a1} + D_1 B^2}{v\Sigma_f} = \text{reactivity},$$

$\nu$ = total fission neutron yield,

$B^2$ = geometric buckling,

$\beta_i$ = delayed neutron fraction for i$^{th}$ group, and

$\Lambda = \frac{1}{\bar{v}\nu\Sigma_f}$ = neutron generation time

and the neutron transients in region II at any distance r is given as,

$$\frac{\varphi_2(r)}{\bar{v}}\frac{d\psi_2(t)}{dt} = \frac{1}{2}D_2\psi_2(t)\nabla^2\varphi_2(r)|_{R_2} - \varphi_2(r)\Sigma_{a2}\psi_2(t)$$

$$- \frac{1}{2}D_2\psi_2(t)\nabla^2\varphi_2(r)|_{R_1} \dots\dots (4.11c)$$

Eq. (4.11) describes the time behavior of neutrons in region I and region II.

## 4.2 Non-fueled UTA-1+DD system

In the absence of the uranium fuel, region I gets further simplified. Now region I consists of only the moderator and the external neutron source. Because there is no fissionable material present in region I, the need to homogenize region I is eliminated. Therefore, the parameters such as diffusion length and the diffusion coefficient in region I are now that of the moderator. Both region I and region II are non-multiplying mediums. To predict the time behavior of the neutron population, we use the similar approach as before to set up the spatial and time distribution of the neutron population. The spatial distribution of the neutron population, in the case of no uranium, is described by the same set of equations, as in the case of uranium fuel (eq. (4.4)), but with $k = 0$

$$\frac{1}{r^2}\frac{d}{dr}\left[r^2\frac{d}{dr}\varphi_1(r)\right] - \frac{1}{L_1^2}\varphi_1(r) = 0, \qquad 0 < r \le R_1 \dots\dots (4.12a)$$

$$\frac{1}{r^2}\frac{d}{dr}\left[r^2\frac{d}{dr}\varphi_2(r)\right] - \frac{1}{L_2^2}\varphi_2(r) = 0, \qquad R_1 \le r \le R_2 \dots\dots (4.12b)$$

The solution to eq. (4.12) is given as

$$\varphi_1(r) = \frac{a_1}{r}\exp\left(\frac{r}{L_1}\right) + \frac{a_2}{r}\exp\left(-\frac{r}{L_1}\right), \qquad 0 < r \le R_1 \dots\dots (4.13a)$$

$$\varphi_2(r) = \frac{a_3}{r}\exp\left(\frac{r}{L_2}\right) + \frac{a_4}{r}\exp\left(-\frac{r}{L_2}\right), \qquad R_1 \le r \le R_2 \dots\dots (4.13b)$$

where the constants $a_i$ are evaluated using the same boundary conditions described in eq. (4.6).

The zero multiplication of the neutrons in region I and region II will result in the exponential decay of the neutron flux over time, when the external source is turned off. Depending on the detector's location, i.e. region I versus region II, neutron counts will die-away with the corresponding characteristics times. For simplicity we assume that when the external neutron source is turned ON, the neutrons immediately distribute themselves spatially. Therefore, the space dependent neutron flux will provide the initial value at the detector's location for transient analysis. The die-away of the neutrons in region I and region II is given by

$$n_1(t) = n_{01} * \exp\left(-\frac{t}{\tau_1}\right) \dots \dots (4.14a)$$

$$n_2(t) = n_{02} * \exp\left(-\frac{t}{\tau_2}\right) \dots \dots (4.15b)$$

where $n_i(t)$ = neutron population in region i at time $t$,

$n_{0i}$ = initial neutron population in region i, and

$\tau_i$ = die-away time in region i.

The neutron die-away (also called mean lifetime) is defined as the time between the birth of the neutron and its loss due to absorption or leakage. This mean lifetime, $\tau$, is composed of two major components, a mean moderation time $\tau_{mod}$, and a mean diffusion time $\tau_{diff}$. The mean diffusion time is defined as the *"average time that a neutron spends in an infinite system before it is captured"* and the mean moderation time is the *"time required for neutrons to slow down to the cutoff of the moderation region at about 1 eV"*[23].

$$\tau = \tau_{mod} + \tau_{diff}$$

$$= \frac{2}{\xi \Sigma_s v_m} + \frac{1}{\Sigma_a(E_0) v_0} \dots \dots (4.16)$$

where $\xi$ = average change in lethargy per collision,

$v_m$ = neutron velocity corresponding to moderation energy 1 eV,

$v_0$ = neutron velocity corresponding to thermal energy 0.0253 eV,

$\Sigma_s$ = scattering cross-section of the medium, and

$\Sigma_a(E_0)$ = absorption cross-section of the medium at 0.0253 eV.

The neutron die-away time given by eq. (4.16) is for an infinite medium. Thus, for a finite system, the mean lifetime of the neutron is less than $\tau$.

## 5.   SOLUTION TO THE NEUTRON TRANSIENT EQUATIONS

In the previous chapter, the general neutron transient equations, for a simplified two region problem, are obtained using first principles. The space and time dependent neutron population is assumed to be separable to simplify the problem. The balance equations obtained in region I and region II account for the diffusion of neutrons across the two regions, the production of neutrons from fission and the DD generator in region I and the losses due to leakage. Using eq. (4.5), the spatial distribution of the neutron population is obtained. This predicts the initial neutron population at the center of region I and at the detector's location in region II.  Applying this initial condition to eq. (4.11), we study the transient behavior of neutrons in the two regions. The solution to the transient equations are obtained numerically using finite backward Euler differences.

$$\frac{d\Psi_i}{dt} = \frac{\Psi_i - \Psi_{i-1}}{\Delta t} \quad \text{... ...} \ (5.1)$$

where $\Delta t$ = time interval between two time stamps.

The DD generator used to produce source neutrons is pulsed with a frequency of 100 Hz and 2% duty cycle. This yields a characteristic pulse of 10 milliseconds (0.2 milliseconds with neutron source ON and 9.8 milliseconds with neutron source OFF). Therefore, in the transient equations, the external neutron source is turned ON for 0.2 milliseconds and turned OFF for 9.8 milliseconds.

### 5.1   Neutron transient in region I

Since at $r = 0$, all the DD source neutrons are born, we first study the time behavior of neutrons at the center of region I. This behavior is described by the point kinetics equations, i.e. eq. (4.11a) and eq. (4.11b). Rewriting these equations, we have

$$\frac{d\psi_1(t)}{dt} = \frac{S(t)}{\Lambda} + \frac{(\rho - \beta)}{\Lambda}\psi_1(t) + \sum_k \lambda_k C_k \quad \text{... ...} \ (4.11a)$$

$$\frac{dC_k(t)}{dt} = \frac{\beta_k}{\Lambda}\psi_1(t) - \lambda_k C_k(t) \quad \text{... ...} \ (4.11b)$$

Eq. (4.11a) and eq. (4.11b) can be written in a matrix form as follows:

$$\frac{d\Psi}{dt} = A\Psi + S \ldots \ldots (5.2)$$

where $\Psi = \begin{bmatrix} \psi_1(t) \\ C_1(t) \\ C_2(t) \\ C_3(t) \\ C_4(t) \\ C_5(t) \\ C_6(t) \end{bmatrix}$,

$$A = \begin{bmatrix} (\rho - \beta)/\Lambda & \lambda_1 & \lambda_2 & \lambda_3 & \lambda_4 & \lambda_5 & \lambda_6 \\ \beta_1/\Lambda & -\lambda_1 & 0 & 0 & 0 & 0 & 0 \\ \beta_2/\Lambda & 0 & -\lambda_2 & 0 & 0 & 0 & 0 \\ \beta_3/\Lambda & 0 & 0 & -\lambda_3 & 0 & 0 & 0 \\ \beta_4/\Lambda & 0 & 0 & 0 & -\lambda_4 & 0 & 0 \\ \beta_5/\Lambda & 0 & 0 & 0 & 0 & -\lambda_5 & 0 \\ \beta_6/\Lambda & 0 & 0 & 0 & 0 & 0 & -\lambda_6 \end{bmatrix} \text{ and}$$

$$S = \begin{bmatrix} S/\Lambda \\ 0 \\ 0 \\ 0 \\ 0 \\ 0 \\ 0 \end{bmatrix}$$

In general, using eq. (5.1) and eq. (5.2), the neutron population at any given time stamp can be written as

$$\frac{d\Psi_n}{dt} = \frac{\Psi_n - \Psi_{n-1}}{\Delta t} = A\Psi_n + S$$

$$\therefore \Psi_n - \Psi_{n-1} = \Delta t * A * \Psi_n + \Delta t * S$$

$$\therefore \Psi_{n-1} + (\Delta t * A - I)\Psi_n = -\Delta t * S \ldots \ldots (5.3)$$

where $I$ is a (7 x 7) unit matrix. We assume that the fuel inside the UTA-1 assembly is fresh fuel, i.e. there are zero fission neutrons present in the fuel. Neglecting the spontaneous fission of U-235 and U-238 in the fresh fuel, the initial conditions required to solve eq. (5.2) are as follows:

$$\Psi_0 = \begin{bmatrix} \psi(t=0) \\ C_1(t=0) \\ C_2(t=0) \\ C_3(t=0) \\ C_4(t=0) \\ C_5(t=0) \\ C_6(t=0) \end{bmatrix} = \begin{bmatrix} 0 \\ 0 \\ 0 \\ 0 \\ 0 \\ 0 \\ 0 \end{bmatrix} \quad \dots\dots (5.4)$$

The solution to eq. (5.2), using Euler backward difference is

$$\begin{bmatrix} 1 & 0 & 0 & 0 & 0 & 0 & 0 \\ 1 & p & 0 & 0 & 0 & 0 & 0 \\ 0 & 1 & p & 0 & 0 & 0 & 0 \\ \vdots & \vdots & \ddots & \ddots & 0 & 0 & 0 \\ \vdots & \vdots & \vdots & \ddots & \ddots & 0 & 0 \\ \vdots & \vdots & \vdots & \vdots & \ddots & \ddots & 0 \\ 0 & 0 & 0 & 0 & 0 & 1 & p \end{bmatrix} * \begin{bmatrix} \Psi_{10} \\ \Psi_{11} \\ \Psi_{12} \\ \vdots \\ \vdots \\ \vdots \\ \Psi_{1n} \end{bmatrix} = \begin{bmatrix} 0 \\ S*(-\Delta t) \\ S*(-\Delta t) \\ \vdots \\ \vdots \\ \vdots \\ S*(-\Delta t) \end{bmatrix} \quad \dots\dots (5.5)$$

where $p = (\Delta t * A - I)$. Eq. (5.5) is of the form $P * \Psi = S_{ext}$. Each $\Psi_{1n}$ in the matrix $\Psi$ is a (7 x 1) column matrix. This makes the size of the matrix $\Psi$ (7n x 1). The size of the matrix $A$ is (7 x 7). Thus, each element in matrix $P$ is a (7 x 7) matrix, resulting in a (7n x 7n) matrix $P$. Similarly, the size of the matrix $S_{ext}$ is (7n x 1), since $S$ is a (7x1) column matrix. Eq. (5.6) can then be used to obtain the neutron population at different time stamps, in region I.

$$\Psi = Inverse(P) * S_{ext} \dots\dots\dots (5.6)$$

Table 5.1 Weighted delayed neutron fractions

| Delayed neutron Group | Delayed neutron fractions | | Weighted Fractions |
|---|---|---|---|
| | U-235 | U-238 | |
| 1 | 0.00021 | 0.0002 | 0.0002093 |
| 2 | 0.00141 | 0.0022 | 0.0014653 |
| 3 | 0.00127 | 0.0025 | 0.0013561 |
| 4 | 0.00255 | 0.0061 | 0.0027985 |
| 5 | 0.00074 | 0.0035 | 0.0009332 |
| 6 | 0.00027 | 0.0012 | 0.0003351 |

Table 5.2 Design parameters of UTA-1+DD system

| | |
|---|---|
| DD source neutron intensity | $2.50 \times 10^7$ n/sec |
| $k_{eff}$ of UTA-1+DD system (determined using MCNP) | 0.412 |
| Multiplication factor, M [$1/(1-k_{eff})$] | 1.70 |
| Neutron emission rate from the system [(Source intensity) – (Source intensity * M)] | $1.75 \times 10^7$ n/sec |
| Spontaneous fission (SF) of U-238 | 230.4 n/sec |
| Total neutron yield for U-235 | 2.44 n/fission |
| Total neutron yield for U-238 | 2.82 n/fission |
| Total Fission Rate | $7.11 \times 10^6$ fission/sec |
| U-235 fission rate | $6.62 \times 10^6$ fission/sec |
| U-238 fission rate | $4.98 \times 10^5$ fission/sec |
| U-238 total fission rate (including SF of U-238) | $4.98 \times 10^5$ fission/sec |
| Neutron generation lifetime ($\Lambda$) | $2.01 \times 10^{-4}$ sec |

Since the fuel in the UTA-1 assembly is a combination of U-235 and U-238, the delayed neutron fraction $\beta_i$ is weighted to obtain a single value for each delayed neutron group. The weighting is done using eq. (5.7). Calculations using MCNP have determined that in UTA-1, 93% of the fissions take place in U-235 and 7% of the fissions take place in U-238. Table 5.1 provides the weighted delayed neutron fraction for each group of delayed neutrons and table 5.2 summarizes the important design parameters of the UTA-1+DD system.

$$\beta_i = \sum_j P_j * \beta_{ij} \dots \dots \dots (5.7)$$

where $P_j$ = fraction of power generated by $j^{th}$ isotope, and

$\beta_{ij}$ = Delayed neutron fraction of $i^{th}$ delayed group for $j^{th}$ isotope.

To obtain the precursor decay constants, we average the U-235 and U-238 precursor decay constants in the six delayed groups. This can be done because the isotope dependence of the decay constant is not very pronounced. Most of them differ only within their

statistical errors (see table 5.3). It can be clearly seen that the decay constants of U-238, Pu-239 and Pu-240 are comparable with those of U-235.

Table 5.3 Precursor decay constants in six delayed groups for various isotopes [32]

| Delay Group | Pu-239 | Pu-240 | |
|---|---|---|---|
| 1 | 0.0129±0.0002 | 0.0129±0.0004 | |
| 2 | 0.0311±0.0005 | 0.0313±0.0005 | |
| 3 | 0.134±0.003 | 0.135±0.011 | |
| 4 | 0.331±0.012 | 0.333±0.031 | |
| 5 | 1.26±0.12 | 1.36±0.21 | |
| 6 | 3.21±0.26 | 4.04±0.78 | |
| | U-238 | U-235 | Averaged U-235 & U-238 |
| 1 | 0.0132±0.0003 | 0.0127±0.0002 | 0.01295 |
| 2 | 0.0321±0.0006 | 0.0317±0.0008 | 0.0319 |
| 3 | 0.139±0.005 | 0.115±0.003 | 0.127 |
| 4 | 0.358±0.014 | 0.311±0.008 | 0.3345 |
| 5 | 1.41±0.07 | 1.40±0.081 | 1.405 |
| 6 | 4.02±0.21 | 3.87±0.37 | 3.945 |

MATLAB is used to solve the point kinetics equations represented in eq. (5.5). The neutron and precursors populations are assumed to be zero at time $t = 0$. The build up of the neutron and precursors population over time are considered in determining the total neutron population at different time stamps.
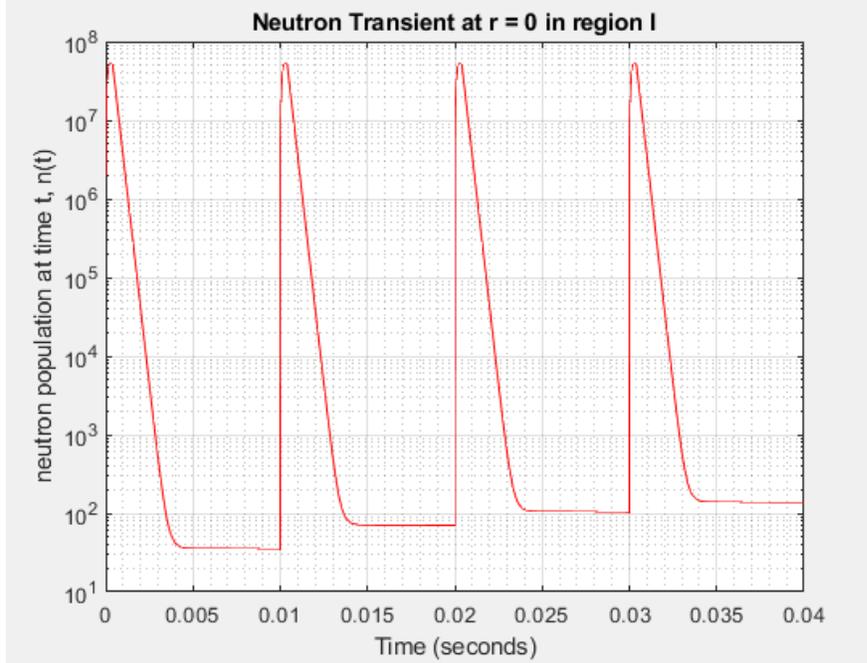
Figure 5.1 Neutron transient at $r = 0$ in region I, using point kinetics.

## 5.2 Neutron transients in Region II

Before we use eq. (4.11c) to evaluate the neutron population at different time stamps in region II, we obtain the initial neutron population at the detector's location in region II. The spatial distribution of neutrons described by eq. (4.4) predicts this initial condition.

### 5.2.1 Solution to the space dependent neutron flux

Before using eq. (4.5) to obtain the spatial distribution of the neutron population, the diffusion parameters in region I and region II are calculated. In the simplified two region problem, region I is a homogenized region of fuel and moderator. Thus, the cross-section values and the diffusion length in region I are homogenized. The homogenized macroscopic cross-sections can be obtained as

$$\Sigma_{Homogenized} = \frac{\Sigma^F + \Sigma^M \left(\frac{V_M}{V_F}\right) \zeta}{1 + \left(\frac{V_M}{V_F}\right) \zeta} \; \ldots \ldots (5.8)$$

$$\zeta = \frac{\phi_M}{\phi_F} \; \ldots \ldots (5.9)$$

where $\Sigma^F$ = macroscopic cross-section of fuel,

$\Sigma^M$ = macroscopic cross-section of moderator,

$V_M$ = volume of the moderator, and

$V_F$ = volume of the fuel.

The factor, $\zeta$, is the thermal disadvantage factor and it is defined as the ratio of the average flux in the moderator to that in the fuel. For a very small assembly, like UTA-1, this thermal disadvantage factor is close to unity and hence it can be neglected. In a homogeneous mixture of fuel and moderator, the homogenized diffusion coefficient, $D_{Homogenized}$, is essentially the diffusion coefficient for the moderator. This is because the concentration of the fuel in the moderator is small. Therefore, the homogenized diffusion length in region I is obtained as

$$L^2_{Homogenized} = \frac{D_{Homogenized}}{\Sigma_{aHomogenized}} = \frac{D_{moderator}}{\Sigma_{aHomogenized}} \dots\dots (5.10)$$

where $\Sigma_{aHomogenized}$ is the homogenized macroscopic absorption cross-section. To obtain the cross-sections and diffusion parameters in region II, ordinary 2.300 g/cm³ concrete (NIST) is used. The composition of concrete, ordinary (NIST), is specified in a report from the Pacific Northwest National Laboratory, Richland (see table 5.4). Table 5.5 summarizes all the diffusion parameters required to obtain the spatial distribution of neutrons. A plot of the spatial distribution of neutrons in region I and region II is shown in figure 5.2.

Table 5.4 Composition of ordinary concrete (NIST) [33]

| Elements | Weight Fraction | Atomic mass, A (amu) |
|---|---|---|
| H | 0.0221 | 1.00797 |
| C | 0.002484 | 12.011 |
| O | 0.57493 | 15.9994 |
| Mg | 0.001266 | 24.305 |
| Al | 0.019953 | 26.98154 |
| Si | 0.304627 | 28.0855 |
| Na | 0.015208 | 39.0983 |
| K | 0.010045 | 39.0983 |
| Ca | 0.042951 | 40.08 |
| Fe | 0.006435 | 55.847 |
| | | |
| Concrete | | 21.4435818 |

Table 5.5 Calculated diffusion parameters in region I and region II

| Homogenized fuel and moderator region, region I | |
|---|---|
| Radius $(R_1)$ | 28 cm |
| Diffusion coefficient $(D_1)$ | 0.142 cm |
| Absorption cross-section | 0.068795 cm$^{-1}$ |
| Diffusion length $(L_1^2)$ | 2.0641 cm$^2$ |
| **2.300 g/cm$^3$ concrete, region II** | |
| Radius $(R_2)$ | 38 cm |
| Atomic mass $(A_{concrete})$ | 21.444 amu |
| Scattering cross-section $\Sigma_{s(concrete)}$ | 0.33596 cm$^{-1}$ |
| $\mu = \dfrac{2}{3 * A_{concrete}}$ | 0.0311 |
| Diffusion coefficient $\left(D_2 = \dfrac{1}{3\Sigma_{s(concrete)}(1-\mu)}\right)$ | 1.024 cm |
| Absorption cross-section | 0.00693 cm$^{-1}$ |
| Diffusion length $(L_2^2)$ | 147.794 cm$^2$ |
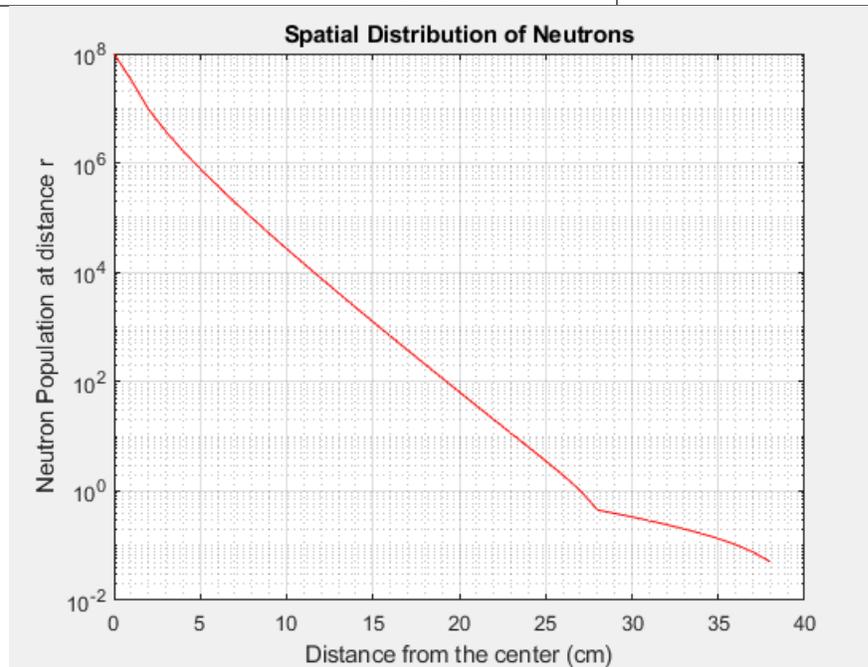


Figure 5.2 Spatial distribution of neutrons in region I and region II

## 5.2.2 Solution to the transient equation in region II

Once the initial condition is set, we can obtain the solution to eq. (4.11c). This equation is also solved numerically. Because it is assumed that the neutrons immediately distribute themselves spatially when the DD generator is turned ON, the neutron population at any distance $r$ in region II remains constant for the entire ON period. When the external source is turned OFF, the die-away of the neutron population over time is governed by eq. (4.11c). Using Euler's backward difference, we can rewrite eq. (4.11c) in matrix form as follows:

$$
\begin{bmatrix}
1 & 0 & 0 & 0 & \cdots & \cdots & 0 \\
1 & q & 0 & 0 & \cdots & \cdots & 0 \\
0 & 1 & q & 0 & \cdots & \cdots & 0 \\
\vdots & \vdots & \ddots & \ddots & \cdots & \cdots & 0 \\
\vdots & \vdots & \vdots & \ddots & \ddots & \cdots & 0 \\
\vdots & \vdots & \vdots & \vdots & \ddots & \ddots & 0 \\
0 & 0 & 0 & 0 & 0 & 1 & q
\end{bmatrix}
*
\begin{bmatrix}
\Psi_{20} \\
\Psi_{21} \\
\Psi_{22} \\
\vdots \\
\vdots \\
\vdots \\
\Psi_{2n}
\end{bmatrix}
=
\begin{bmatrix}
Int \\
0 \\
0 \\
\vdots \\
\vdots \\
\vdots \\
0
\end{bmatrix}
\quad \cdots \cdots (5.11)
$$

where $Int$ = initial neutron population at any distance $r$ in region II, and

$$
q = \Delta t * \bar{v} * \left( \frac{1}{2\varphi(r)} D_2 \nabla^2 \varphi_2(r)|_{R_2} - \frac{1}{2\varphi(r)} D_2 \nabla^2 \varphi_2(r)|_{R_1} - \Sigma_{a2} \right) - 1.
$$

Using MATLAB, eq. (5.11) is solved for a fixed $r$. Figure 5.3 shows the transient behavior of neutrons in region II.
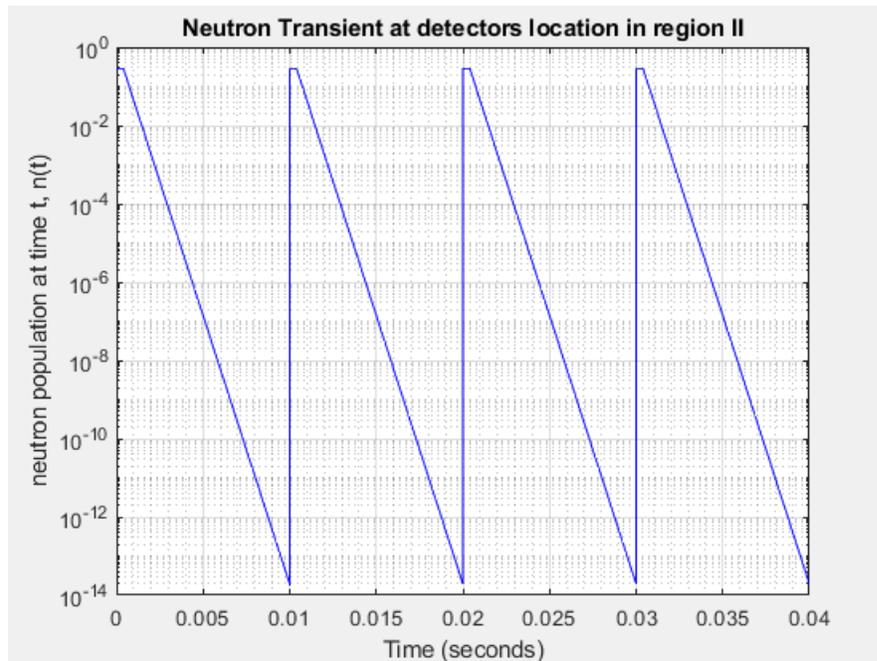


Figure 5.3 Neutron transient in region II

The solution to the transient equations in region I and region II provides a better understanding of the behavior of neutron population over time. Since the detector is placed far away from the center of the UTA-1 barrel, not many neutron events will be recorded per DD generator pulse. If the generator is operated for a sufficiently long period of time, an averaged transient behavior can be measured. This averaged transient behavior can be compared with the predicted model. One can be more precise in the predicted model by averaging out the predicted transient behavior. A detailed explanation on the averaging of the neutron transient behavior is given section 6.1.

# 6. MEASURED TRANSIENT BEHAVIOR OF NEUTRONS

The predicted transient behavior of neutrons is verified experimentally. The experimental data provides an understanding as to how far the predicted model is from the reality. The experiment is performed at Niowave Inc. facility in Lansing, Michigan. Various measurements are taken to study the temporal behavior of neutrons inside the UTA-1+DD system. All these measurements are made using the Silverside Li-6 neutron detector. The entire experiment is comprised of three parts. The first part includes background measurements. The second part of the experiment consists of UTA-1+DD system with a k-value of 0.412 and the third part consists of UTA-1+DD system without the uranium fuel. The raw data obtained from the Li-6 detector is then analyzed using a post processing utility code.

## 6.1 UTA-1+DD system with $k = 0.412$

An R&D pulsed DD generator, nGen 300, from Starfire Industries is used to perform transient measurements in the UTA-1+DD system. The UTA barrel is filled with the uranium fuel and light water and the entire UTA-1+DD system has a k-value of 0.412. The external neutron source is operating at 100.003655 Hz frequency with an accelerating voltage of 80 kV for one run and 120 kV for another. Transient measurements for each accelerating voltages are performed. The generator yields a characteristics pulse with 9.9 milliseconds period (0.2 milliseconds ON and 9.7 milliseconds OFF). At 80 kV, the DD generator produces $6.8 * 10^5$ neutrons/second and at 120 kV $2.0 * 10^6$ neutrons/second. Robert Stubbers from Starfire industries pointed out that this R&D device operates at reduced intensity than that specified in table 3.3.

The Li-6 detector provides output in list mode. Every event recorded by the detector has the electronic module ID, time (in microseconds and seconds), and the pulse height channel number. Silverside recommends to set the lower level discriminator (LLD) to channel 230, to eliminate the gamma events. Therefore, in the raw data, events with pulse height less than 230 are ignored. The raw data in the Li-6 detector is recorded using a Quaesta NPM3100E neuchrometer module.

| ◢ | A | B | C | D | E |
|---|---|---|---|---|---|
| 1 | Pulse # | NPM Id | PulseHt | Time(sec) | Time(microsec) |
| 2 | 0 | 21 | 502 | 0 | 0 |
| 3 | 1 | 21 | 421 | 6.38E-05 | 63.75 |
| 4 | 2 | 21 | 421 | 9.38E-05 | 93.75 |
| 5 | 3 | 21 | 421 | 0.000101 | 100.875 |
| 6 | 4 | 21 | 245 | 0.000232 | 231.875 |
| 7 | 5 | 21 | 354 | 0.000327 | 326.875 |
| 8 | 6 | 21 | 373 | 0.001262 | 1261.875 |

Figure 6.1 Screenshot of the Li-6 panel raw data .csv file using Quaesta NPM3100E
neuchrometer.

A binning algorithm is developed to analyze the raw data. Initially the bin width is set to 1 second and a plot of counts per bin versus time is generated, figure 6.2. This plot clearly shows that the count rate, when the DD source is operating at 120 kV, is higher than the count rate of 80 kV DD accelerating voltage. Both 120 kV and 80 kV have counts much higher than the background counts, demonstrating the multiplication of neutrons in the system. However figure 6.2 does not provide any information about the individual pulses and the general transient behavior of neutrons in the UTA-1+DD system. Therefore, the bin size is reduced to 10 microseconds and an average measured pulse is plotted. Since the neutron pulsing from the DD generator is periodic, we decide to mathematically average the counts and obtain an average measured pulse. Every transient pulse is not identical. This is because of the buildup of the delayed neutron precursors. The initial pulses, starting from a fresh fuel loading, do not see the effect of delayed neutron precursors. Over time, the precursors concentration builds up resulting in higher count rate. Therefore, this mathematical averaging results in an asymptote region which is higher than the original background. The asymptote region is clearly seen in figure 6.3. The average pulse provides useful information about the rate at which neutrons decay in the UTA-1+DD system when the DD generator is turned off.
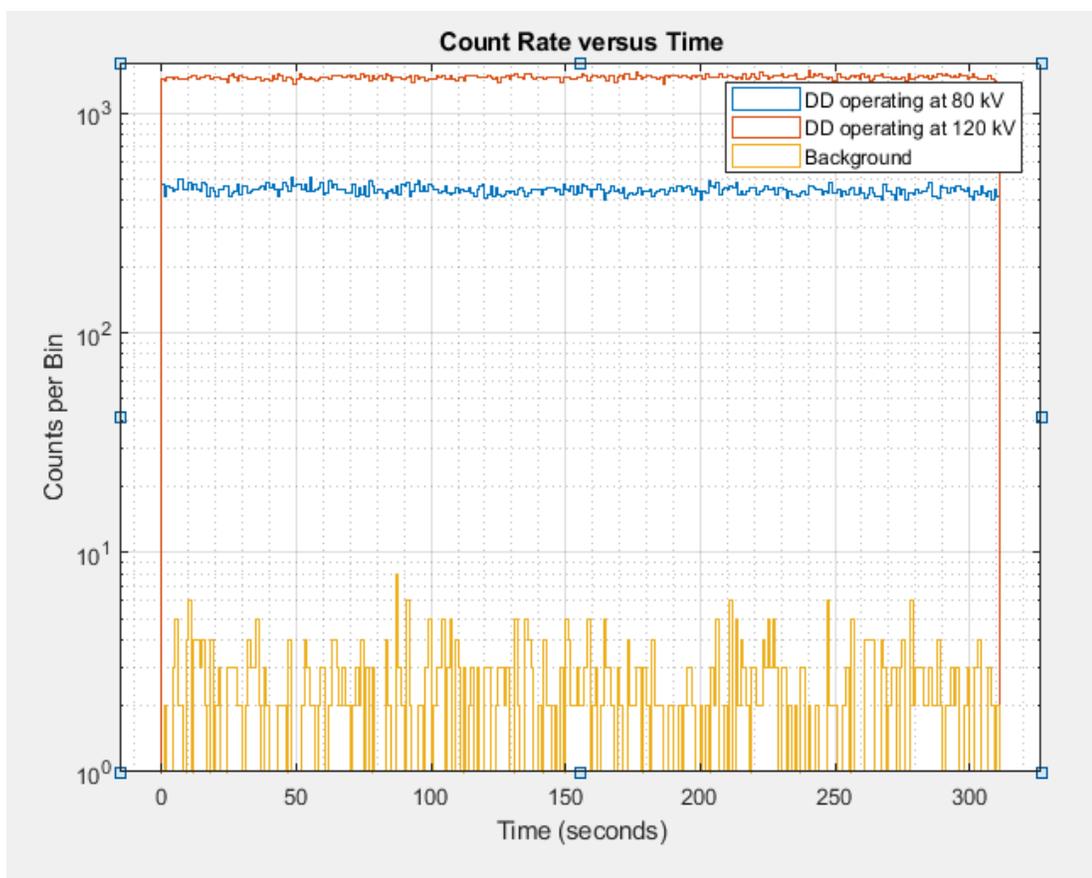
Figure 6.2 Plot of count rate versus time with bin width set to 1 second.

With bin width set to 10 microseconds, a 9.99 milliseconds pulse will occupy 999 bins. This implies that the first pulse will occupy bins from 1 to 999, the second pulse will occupy bins from 1000 to 1998 and so on. The counts in the bins 1, 1000, 1999, 2998 ….. are averaged to obtain the counts in the first bin of the averaged pulse. Similarly, the counts in the bins 2, 1001, 2000, 2999 …. are averaged to obtain the counts in the second bin of the averaged pulse. This averaging method is repeated to obtain counts in each bin of the averaged pulse. Figure 6.3 shows an average measured pulse for 80 kV and 120 kV accelerating voltage.
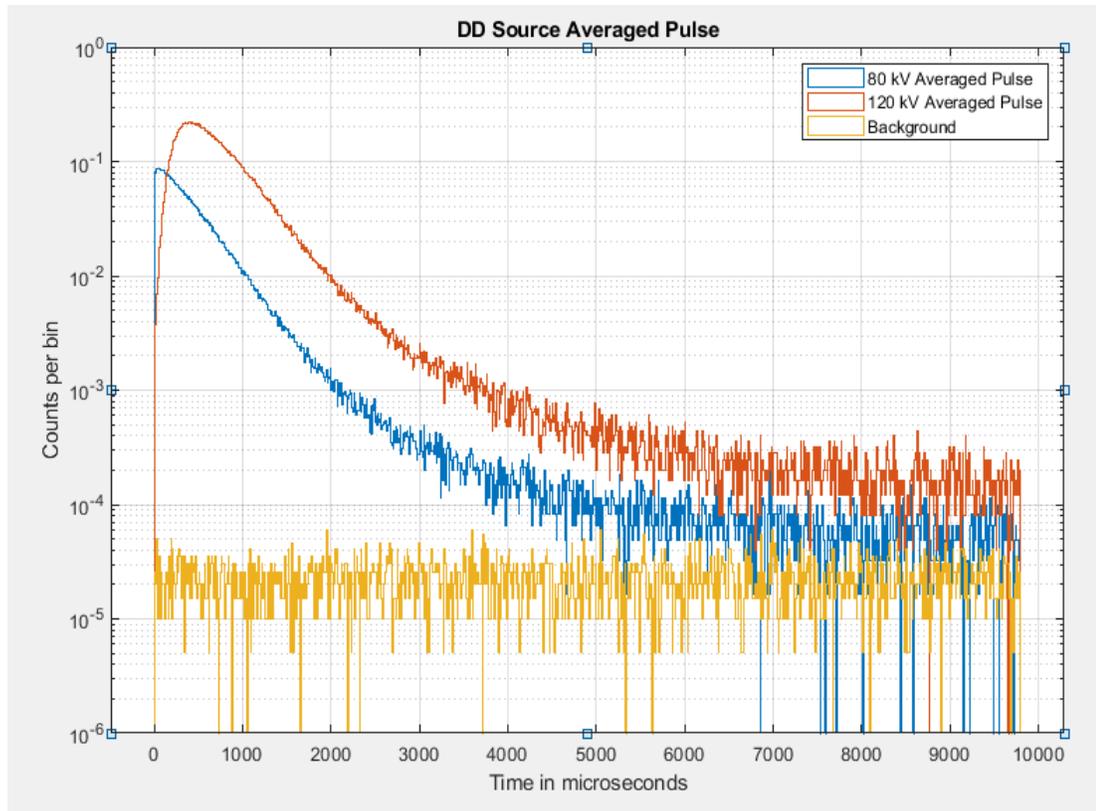
Figure 6.3 Average measured pulse from the DD generator.

### 6.1.1 Comparison with the predicted model

The neutron transient shown in figure 5.3 cannot be directly compared with the experimental data. Since figure 6.3 is an averaged pulse, the predicted pulse must also be averaged. The neutron population is calculated from time $t = 0$ to time $t = 1800\ seconds$. With 100 Hz frequency, 180,000 pulses will be produced in 1800 seconds. At the completion of the pulse, the delayed neutron precursors produce additional fission neutrons. Before the start of the next pulse, there are already some neutrons (coming from the delayed precursors) present in the system. Therefore, when the next pulse arrives, there is a new elevated external source term, which is DD source neutrons plus the neutrons produced by the delayed neutron precursor concentration from the preceding pulse. In the predicted behavior, the number of neutrons produced by the delayed precursors are obtained by multiplying the delayed precursor concentration, at the end of each pulse, with their corresponding decay constant (eq. (6.1)).

$$S_{delayed} = \sum_{i=1}^{6} C_i\lambda_i \ldots \ldots (6.1)$$

where $S_{delayed}$ = number of neutrons produced by delayed precursors,

$C_i$ = i[th] group precursor concentration at the end of the pulse, and

$\lambda_i$ = decay constant in i[th] delay group.

Since the detector is placed in region II, the measured average pulse is compared with the predicted average pulse in region II. Figure 6.4 shows a normalized plot to compare the average predicted pulse with the average measured pulse. To account for the measured background in figure 6.4 a ratio of average background counts to the peak counts (120 kV) is computed. This factor is then multiplied with the normalized background.
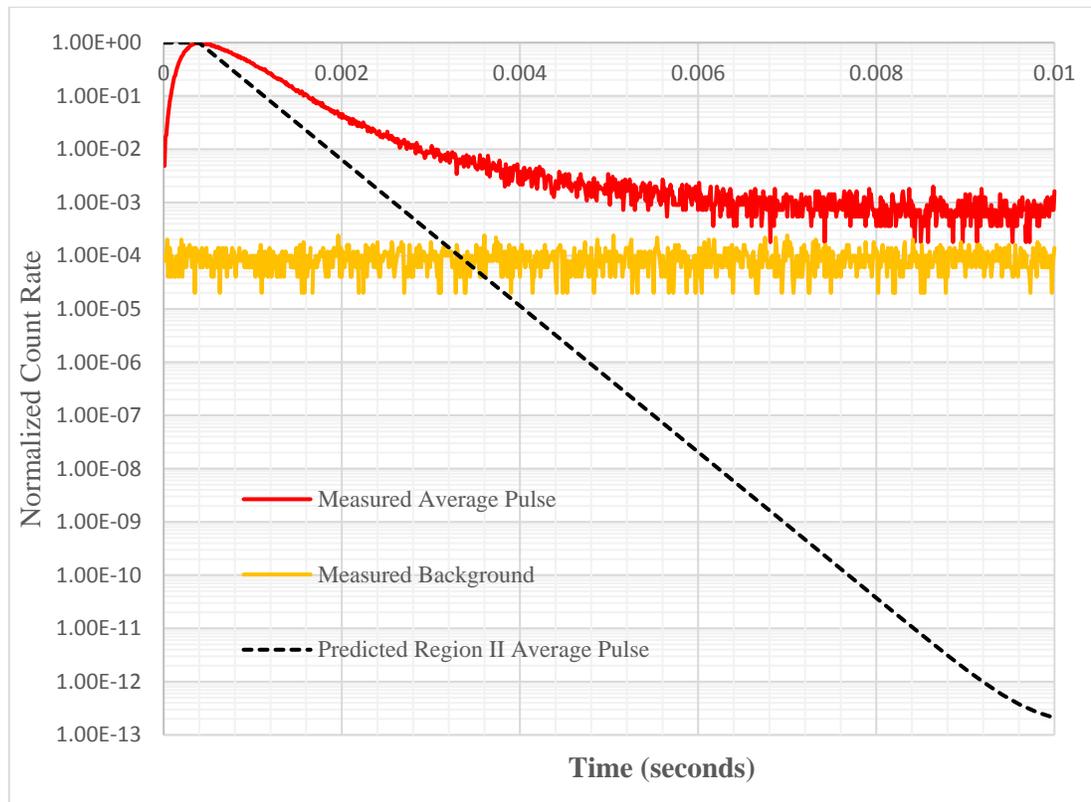


Figure 6.4 Comparison of average measured 120 kV pulse with the region II average predicted pulse (background is not accounted for in this average predicted pulse).

From figure 6.4 the predicted neutron population decays much faster than the measured neutron population. This is because of the simplifications and the assumptions made while solving the transient equations. The transient equations were solved with the homogenization of the fuel and the moderator. However, in reality, the mixture of the fuel

and moderator is not 100% homogeneous. Further the predicted model assumed ordinary 2.300 g/cm$^3$ (NIST) concrete in region II. The blocks used in the experimental setup are cinder blocks. Having known the exact composition of the blocks used in the experimental setup, the predictions could be closer to the reality. Also, the predicted model uses thermal cross-section values in the transient equations. This affects the calculated decay of the neutron population as a thermal neutron is more likely to be absorbed than a fast neutron.

The real system is far more complex than the simplified two region problem shown in figure 4.1. When calculating the neutron population at different time stamps, it is assumed that the new neutron source, coming from the delayed neutron precursors, at the start of each pulse is a point source. This assumption is not necessarily quite true because neutrons from the delayed precursors may not be born at the center of the region I. These neutrons can be released from their precursors anywhere in region I making the delayed source a distributed neutron source. Therefore, at the beginning of each pulse there is an external point neutron source and a distributed source. Analytically solving a two region problem with a point source and a distributed source is very complex.
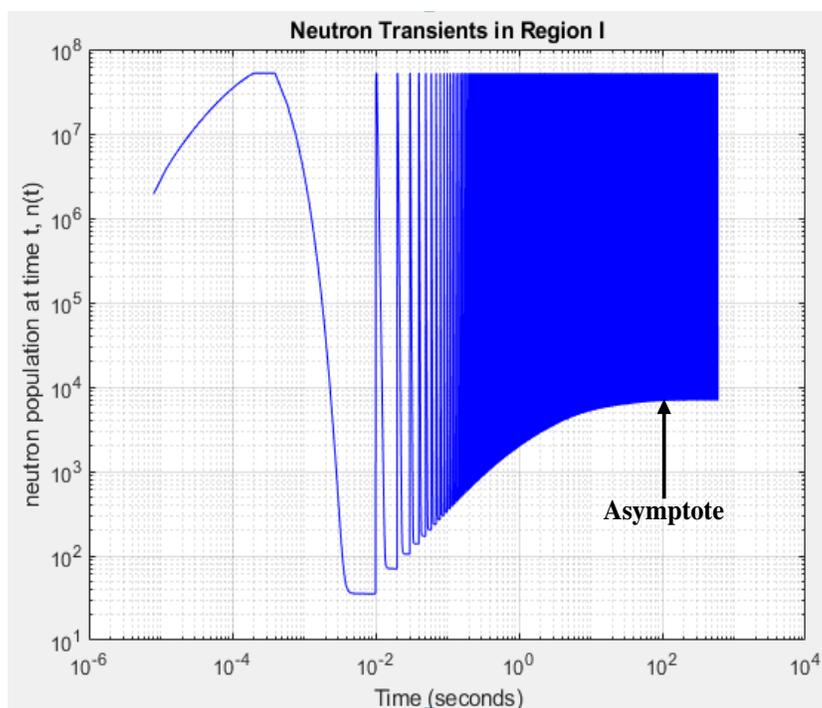


Figure 6.5 The 10 minutes warm-up of the DD generator saturates the delayed neutron precursors in region I, resulting in an asymptote.

The 10 milliseconds period of the DD generator pulse is faster than the half-life of the shortest-lived delayed precursor (~0.2 seconds). However, when pulsed at this fast rate for a sufficiently long period of time, all the delayed precursors will attain saturation in region I. This saturation of the delayed neutron precursors will be like a steady-state behavior of a typical power reactor. A power reactor operates at steady-state until shut down. At the time of shutdown, there is a prompt drop in the neutron flux, which occurs almost instantly (on second time scales) of the reactivity change, followed by the decay of delayed precursors. Similarly, on saturating the delayed precursors before the transient measurement, an asymptote would be established in region I (refer figure 6.5). This asymptote imitates steady-state behavior and is expected to be significantly higher than the measured background.

The neutrons produced by the saturated delayed precursors in region I will continuously diffuse into region II and result in an asymptote in region II (due to the saturation in region I). Therefore, when the DD generator is turned OFF, the count rate on the Li-6 detector is expected to drop until it reaches the asymptote. The asymptote is seen in the average measured pulse. However, the predicted region II pulse shown in figure 6.4 does not reflect this asymptote. The predicted neutron population is continuously dropping even when the delayed precursors in region I have saturated. This is due to the decoupling of the region I and region II neutron fluxes in the transient equations (eq. 4.11). The decoupling does not correctly account for the diffusion of neutrons from the delayed precursors across the two regions, resulting in the continuous drop of calculated neutron population in region II. The assumptions and the boundary/interface conditions used to solve the space and time dependent neutron balance equations resulted in this decoupling.

An average predicted pulse is obtained, in the same way as region II, for the neutron population in region I. This predicted average pulse in region I is compared with the measured average pulse (figure 6.6). The asymptote due to the saturation of the delayed precursors is clearly seen in the region I predicted average pulse. This gives confidence that the transient equations developed for region I are correctly accounting for the neutrons from the delayed precursors.

Once the delayed precursors have saturated in region I, the neutron population in region II will simply follow the neutron population in region I. It is also seen from figure

6.4 and figure 6.6 that when the DD generator is turned off, the decay rate in region I is faster than the decay rate in region II. When the neutron population in region I decays much faster than the neutron population in region II, the die-away of the neutron population will be dominated by the slower decay rate of region II. Therefore, the Li-6 detector's response will follow region II until the saturation of the delayed precursors in region I and then follow region I (figure 6.7).
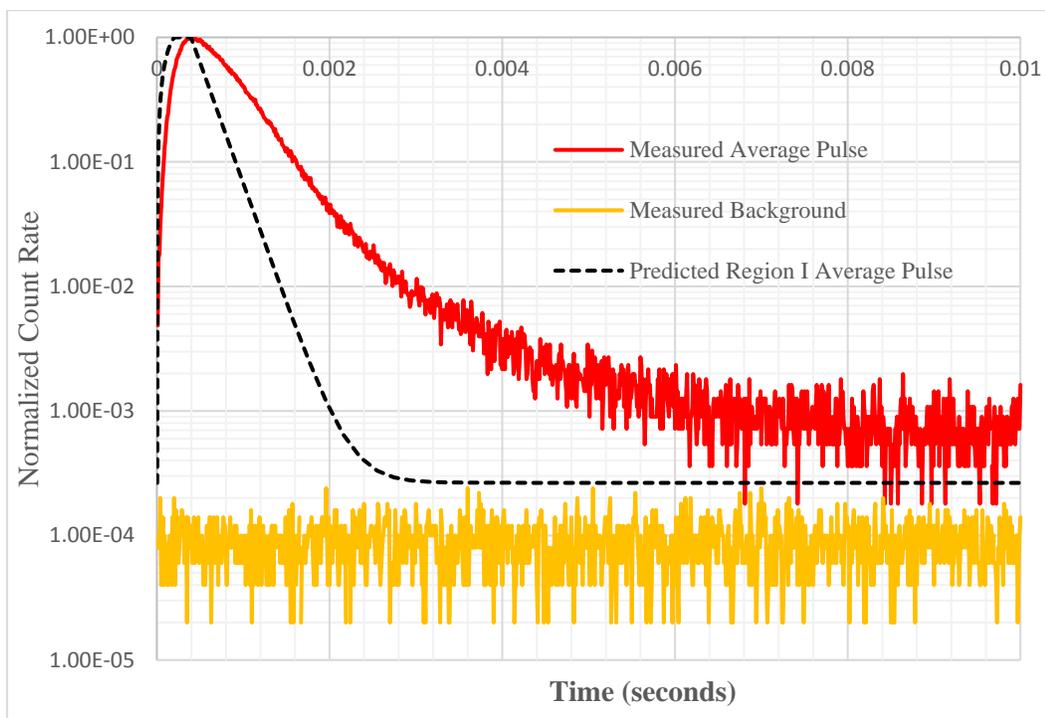


Figure 6.6 Comparison of average measured 120 kV pulse with the region I average predicted pulse (background is not accounted for in this average predicted pulse).

A more detailed explanation for the exact time window in which the detector's response will follow region II is given in chapter 7.

Also, before the Li-6 detector was turned on to record the counts, the DD neutron generator was warmed up for a long period of time. This was done intentionally to produce a significant concentration of delayed precursors. Partially, it was also done to obtain maximum source neutrons from the DD generator. The warming up of the DD generator caused initial fissions in the uranium fuel which resulted in the production of the fission neutrons and the delayed neutron precursors. This constituted a new baseline, much above the measured background, before the detector was turned on for transient measurements. The new baseline is the consequence of the fission neutrons and the decay of delayed

precursors. The predicted detector's response shown in figure 6.7 accounts for this warming up of the DD generator.
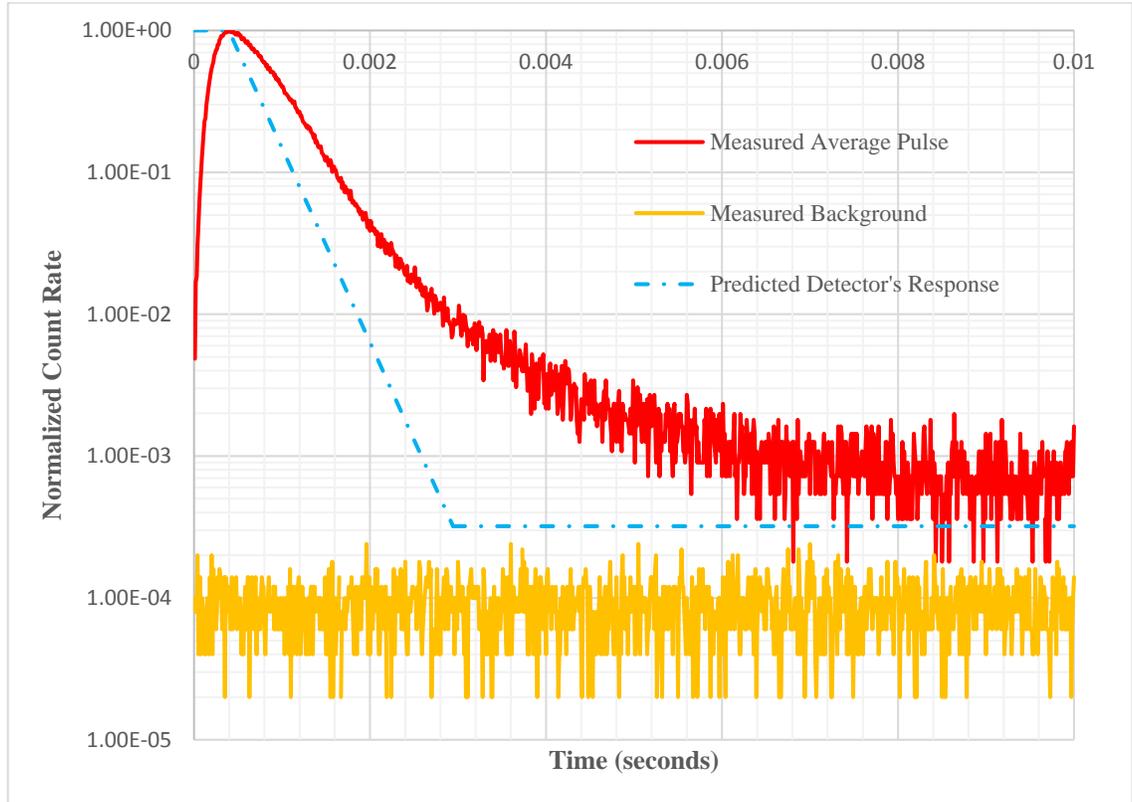


Figure 6.7 Comparison of average measured 120 kV pulse with the expected predicted behavior.

## 6.1.2    Error calculations

The measured raw data is subject to error analysis to find the uncertainty in the average measured pulse. Since neutron measurements are random events, Poisson statistics is applied to find the uncertainty in each bin. The method of weighted least squares [34] is used, as the uncertainty in each bin is different. We assume that there is negligible uncertainty in the time measurements i.e. error in time $t_i$ is negligible. Figure 6.8 is the measured average pulse with error bars. The error bars extend one standard deviation on each side of the measured count rate, and the line is the least-squares best fit. The best fit line is given by the following equation:

$$y = P + Qt \ldots \ldots (6.2)$$

where $y_i$ = natural log of counts in each bin of the average measured pulse,

$t_i$ = time stamp,

$$P = \frac{\sum w_i t_i^2 \sum w_i y_i - \sum w_i t_i \sum w_i t_i y_i}{\sum w_i \sum w_i t_i^2 - (\sum w_i t_i)^2},$$

$$Q = \frac{\sum w_i \sum w_i t_i y_i - \sum w_i t_i \sum w_i y_i}{\sum w_i \sum w_i t_i^2 - (\sum w_i t_i)^2},$$

$$w_i = \frac{1}{\sigma_i^2}, \text{ and}$$

$$\sigma_i = \text{error in } y_i.$$

The best fit line provides information about the rate at which the neutrons are dying away in the UTA-1+DD system. Table 6.1 lists the die-away times for the case of 80 kV accelerating voltage and 120 kV accelerating voltage.

Table 6.1 Measured neutron die-away times

|  | DD generator operation | Measured |
|---|---|---|
| **UTA-1+DD system with uranium fuel** | 120 kV operating voltage with 2% duty cycle (2.0E+06 n/sec peak intensity) | 520.461±0.346 microseconds |
|  | 80 kV operating voltage with 2% duty cycle (6.5E+04 n/sec peak intensity) | 452.294±1.235 microseconds |
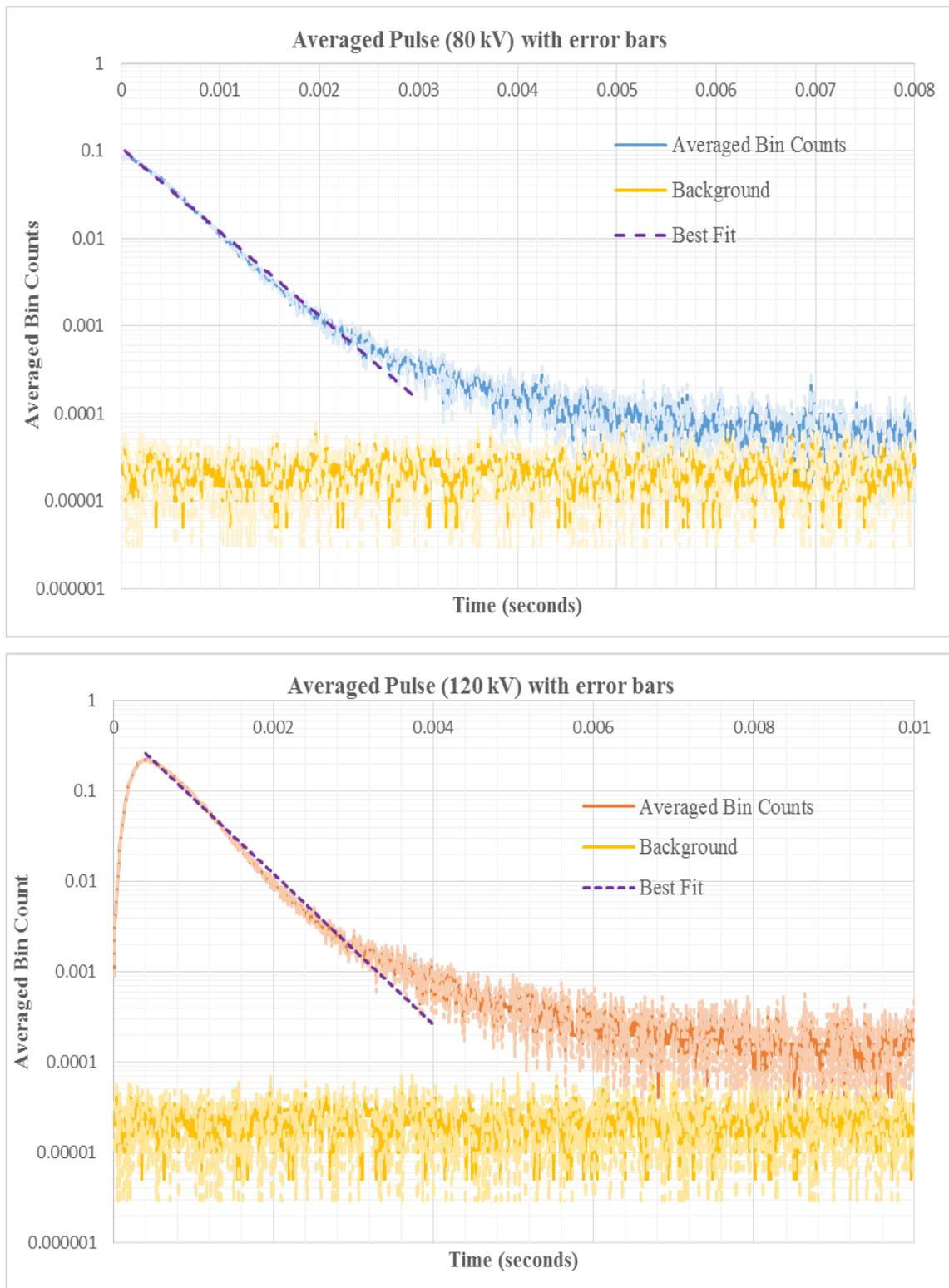
Figure 6.8 Average measured pulse with error bars

## 6.2    UTA-1+DD system without uranium fuel

The transient measurement is repeated with no uranium fuel loaded into the UTA barrel. The experimental setup is the same as in the case of uranium fuel. In this set of measurements, the DD generator is operating at 120 kV accelerating voltage, 100 Hz frequency and 6% duty cycle. This yielded a characteristic pulse with a 10 millisecond period (0.6 milliseconds with source ON and 9.4 milliseconds with source OFF). A measured average pulse is plotted in a similar fashion as described in section 6.1. The uncertainties in the experimental data is determined and a best fit line is plotted. The inverse of the slope of this best fit line specifies the neutron die-away time in the case of no uranium fuel. Figure 6.9 shows the average measured pulse for the case of no uranium fuel in the UTA-1+DD system.
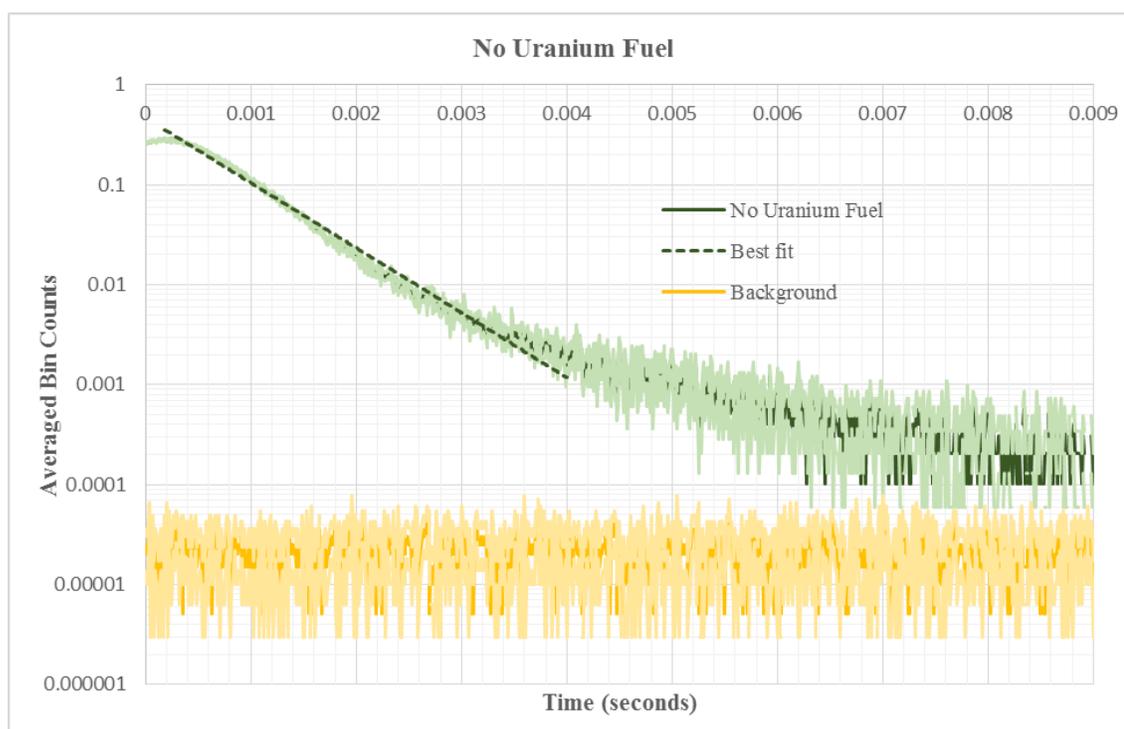


Figure 6.9 Average measured pulse for no uranium fuel case with error bars

The Li-6 detector is placed in region II. Therefore, the die-away of the neutron population will be determined by the diffusion parameters in region II. For 2.300 g/cm$^3$ (NIST) concrete, the mean lifetime of the neutron in an infinite medium, according to eq. (4.16), is calculated as 661 microseconds (table 6.3). Since concrete is a mixture of elements, the average lethargy change is given by eq. (6.3).

$$\bar{\xi} = \frac{1}{\Sigma_s} \sum_i \xi_i \Sigma_s^{(i)} \ldots \ldots (6.3)$$

where $\bar{\xi}$ = average lethargy change in a mixture of elements,

$\Sigma_s$ = total macroscopic scattering cross-section,

$\xi_i$ = average lethargy change in i[th] element of the mixture, and

$\Sigma_s$ = macroscopic scattering cross-section in i[th] element of the mixture.

The measured neutron die-away time is 668 microseconds. Since the predicted die-away is for an infinite medium, the measured die-away time should be less than the predicted value. However, the measured time is slightly greater than the predicted value. This is due to the fact that the concrete blocks used in the experimental setup are not NIST concrete.

Table 6.2 list the predicted and the measured neutron die-away times for the case of no uranium fuel loaded into the UTA-1+DD system.

Table 6.2 Predicted and measured die-away time for the case of no uranium fuel.

| | DD generator operation | Predicted | Measured |
|---|---|---|---|
| **UTA-1+DD system with no uranium fuel** | With 6% duty cycle (2.50E+07 n/sec peak intensity) | 661 microseconds (infinite medium) | 668.605±0.772 microseconds |

Table 6.3 Neutron die-away time in 2.300 g/cm$^3$ (NIST) concrete

| Elements | Weight Fraction | Absorption cross-section (barns) | Scattering cross-section (barns) | Atomic mass A (amu) | No of atoms $N_i$ in concrete | Macroscopic Absorption cross-section (cm$^{-1}$) | Macroscopic Scattering cross-section (cm$^{-1}$) | $\alpha$ $(A-1)^2/(A+1)^2$ | Average lethargy change |
|---|---|---|---|---|---|---|---|---|---|
| H | 0.0221 | 0.3326 | 82.02 | 1.00797 | 1.43E+21 | 4.75E-04 | 1.17E-01 | 1.58E-05 | 1.00E+00 |
| C | 0.002484 | 0.0035 | 5.551 | 12.011 | 1.60E+20 | 5.62E-07 | 8.91E-04 | 7.16E-01 | 1.58E-01 |
| O | 0.57493 | 0.00019 | 4.232 | 15.9994 | 3.71E+22 | 7.06E-06 | 1.57E-01 | 7.79E-01 | 1.20E-01 |
| Mg | 0.001266 | 0.063 | 3.71 | 24.305 | 8.18E+19 | 5.15E-06 | 3.03E-04 | 8.48E-01 | 8.01E-02 |
| Al | 0.019953 | 0.231 | 1.503 | 26.98154 | 1.29E+21 | 2.98E-04 | 1.94E-03 | 8.62E-01 | 7.23E-02 |
| Si | 0.304627 | 0.171 | 2.167 | 28.0855 | 1.97E+22 | 3.37E-03 | 4.26E-02 | 8.67E-01 | 6.96E-02 |
| Na | 0.015208 | 0.53 | 3.28 | 39.0983 | 9.82E+20 | 5.21E-04 | 3.22E-03 | 9.03E-01 | 5.03E-02 |
| K | 0.010045 | 2.1 | 1.96 | 39.0983 | 6.49E+20 | 1.36E-03 | 1.27E-03 | 9.03E-01 | 5.03E-02 |
| Ca | 0.042951 | 0.43 | 2.83 | 40.08 | 2.77E+21 | 1.19E-03 | 7.85E-03 | 9.05E-01 | 4.91E-02 |
| Fe | 0.006435 | 2.56 | 11.62 | 55.847 | 4.16E+20 | 1.06E-03 | 4.83E-03 | 9.31E-01 | 3.54E-02 |
| | | | | | | | | | |
| Total | 9.90E-01 | | | 2.14E+01 | | 6.93E-03 | 3.36E-01 | | 4.15E-01 |
| | | | | | | | | | |
| | | | | | | | | | |
| | | | | | Diffusion Time (sec) | 6.56E-04 | | | |
| | | | | | Moderation Time (sec) | 5.18432E-06 | | | |
| | | | | | Die-away Time (microsec) | 6.61E+02 | | | |

The model developed to predict the transient behavior of neutrons in the UTA-1+DD system agrees to quite an extent with the observed transient behavior. In the case of fuel loaded UTA-1+DD system, the model predicts that the neutron population will rise and then drop to an asymptote region. The predicted rate at which the neutron population is decaying is much faster than the measured rate. This difference is partially to do with the choice of material in region II of the simplified two region problem (figure 4.1). The model also suggests that the neutron population will reach an asymptote. The asymptote region acts as a "background" for the predicted count rate. The warming up of the DD generator for a long period of time, prior to transient measurement, determines this asymptote. If there is fissionable material present in the system, then the warming up of the generator will result in an asymptote much higher than the measured background and this effect is seen in the experimental measurements. However, in the case of no uranium fuel, the model predicts that the neutron population will die-away with a characteristic die-away time. The neutron population will continue to drop until it reaches the measured background levels. The dying away of the neutrons over time is determined by the absorption and scattering cross-sections of the region in which the detector is placed. This predicted behavior of neutrons in absence of uranium fuel is well reflected in the experimental data. The developed model is not aiming to provide the exact count rate that the detector will record during transient measurements. It is aiming to understand the trends and the behavior of neutrons in a system which is subject to transient measurements in the presence and absence of fissionable material.

## 7. EXTENSION OF THE MODEL TO DIFFERENT K-VALUES

The transient model developed for a simplified two region problem provides a general understanding on the behavior of neutrons. It is learnt that the developed model has limitations because of the nature by which the transient equations are solved. These limitations are mainly because of the assumptions made to simplify the transient equations. The model works very well in predicting the neutron population, for varying k-values, on microseconds/milliseconds time stamps in region I. However, the model tends to become less accurate in region II with increasing k-values. It is realized that the developed model provides useful information about the neutron transients in region II, only when the neutron population in region I decays much faster than the neutron population in region II.
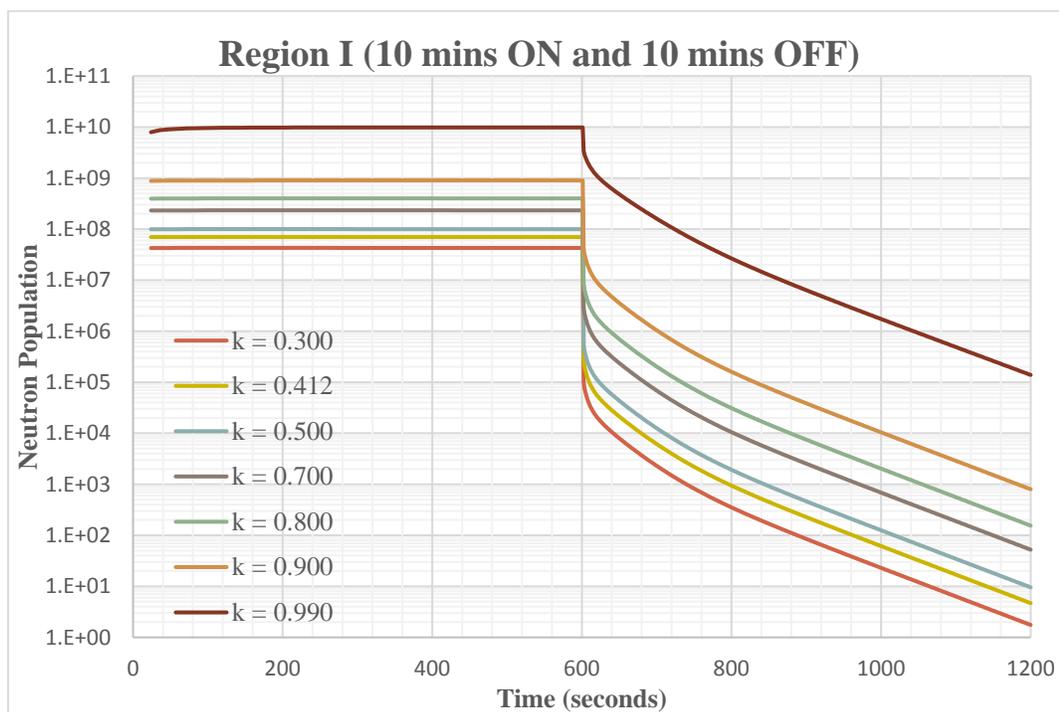


Figure 7.1 Neutron transients for different k-values in region I with external source ON for 10 mins and OFF for 10 mins.

Further investigations are made to find the exact window in which the assumptions of the developed model retain their validity in region I and region II. To find this exact window, a simple case is considered in which the external neutron source, i.e. DD generator, is continuously ON for 10 minutes and then turned OFF to study the die-away of the

neutron population. In 10 minutes ON, the neutron population in region I will attain steady-state. Also, the delayed neutron precursors, produced as a result of the fission reaction, will saturate in this ON period. The figure 7.1 and 7.2 represent the neutron behavior in region I and region II with external source ON for 10 minutes and OFF for 10 minutes.
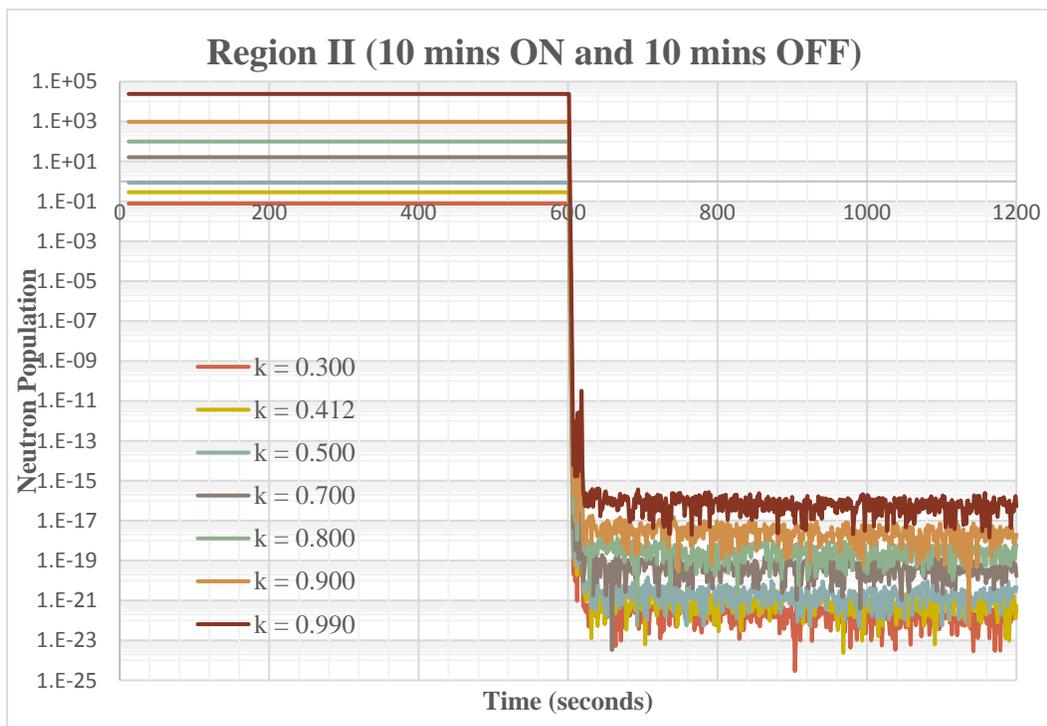


Figure 7.2 Neutron transients for different k-values in region II with external source ON for 10 mins and OFF for 10 mins.

From figure 7.2, no matter what the k-value of the system is, the calculated neutron population in region II drops by the same order of magnitude. Intuitively, we know that this is not true because the neutrons that leak from region I act as a source to region II. This leakage of neutrons from region I increases with increasing k-value of the system, thereby resulting in an increased source term in region II. Currently, the developed model assumes that during the ON period of the pulsed DD generator, the neutron population attains steady-state and immediately distributes itself throughout region I and region II. The spatial distribution of the neutrons in the simplified two region problem provides the initial value, at the detector's location in region II, to the transient equation, eq. (4.11c). On obtaining this initial value, the neutron behavior in region II is described by the eq. (4.11c). This particular transient equation in region II is not accounting for the continuous diffusion of additional fission neutrons, produced by the delayed precursors, from region I into region

II, completely decoupling region II neutron flux from the region I neutron flux. This decoupling is the consequence of the use of boundary/interface conditions to simplify the solution to the transient equations. Therefore, with increasing k-value, only the initial condition is changing in region II and the transient behavior remains unchanged. Note that in figure 7.2, when the neutron population drops below $10^{-13}$ magnitude, the numerical solution falls apart. Anything below this threshold magnitude is simply numerical error and no useful information about the neutron flux is obtained.

To determine the exact window in which the decay rate in region I is much faster than the decay rate in region II, the die-away of the neutron population within 4 milliseconds of external source cutoff is observed. Figures 7.3 and 7.4 show the decay of the calculated neutron population in region I and II, up to 4 milliseconds after the external source is turned OFF.
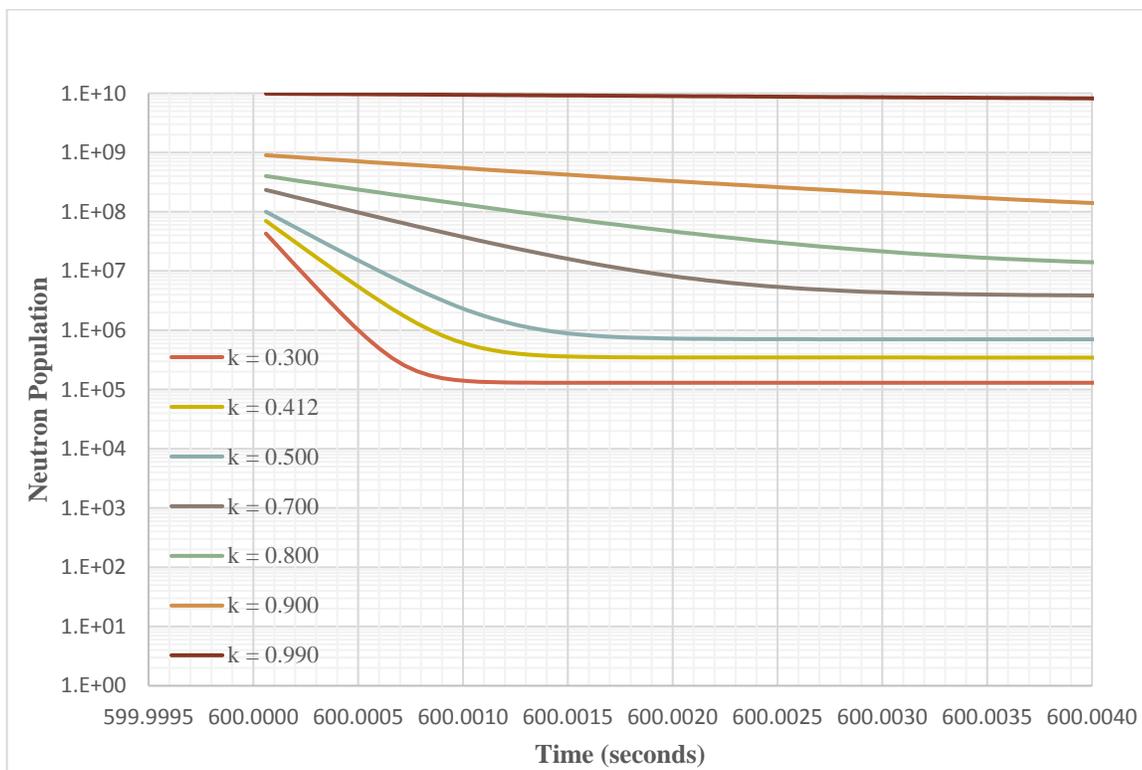


Figure 7.3 Die-away of the neutron population in region I, 4 milliseconds after cutoff (10 mins ON)
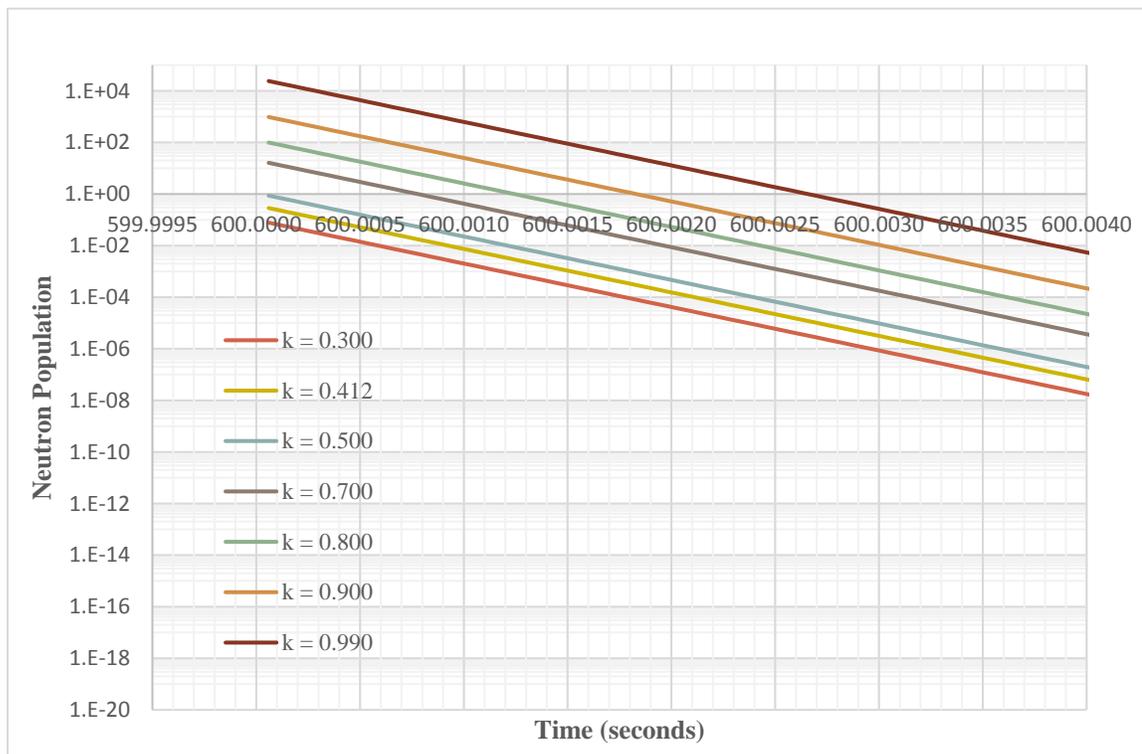
Figure 7.4 Die-away of the neutron population in region II, 4 milliseconds after cutoff (10 mins ON)

In region I, when the external neutron source is turned OFF, there is a prompt drop followed by the slow decay of the delayed neutron precursors, figure 7.3. It is seen that the decay rate in region I is significantly decreasing with increasing k-value. At low k-values, i.e. up to $k \sim 0.5$, the prompt drop of the neutron population is very fast followed by an asymptote region. This asymptote region is because of the neutrons produced by the delayed neutron precursors. With increasing k-value, this asymptote region elevates indicating the lift of the delayed precursor concentration. Also, the leveling of the neutron population to the asymptote region shifts to the right of the graph (figure 7.3) with increasing k-value. This right shift is indicating whether the transient behavior is being dominated by the prompt neutron drop or by the long-term transients due to the delayed precursors. When the subcritical multiplication is approaching criticality, the rate at which neutron population decays in region I is significantly slower. This is to be expected since at higher k-values, the neutrons will multiply rapidly due to increased fission rate. Increased fission rate will result in increased delayed precursor concentration, producing

additional fission neutrons. Therefore, when $k = 0.990$, it is seen from figure 7.3 that the neutron population hardly undergoes any transients and levels off very quickly on a milliseconds timescale when the external neutron source is turned OFF. If the longest-lived precursor concentration is saturated in region I, for low k-values, the prompt neutron drop occurs in less than 2 milliseconds after cutoff followed by a very slow decay of the neutron population from the delayed precursors. For high k-values, the effect of the delayed precursors is not seen within 4 milliseconds of cutoff because of the slow prompt neutron drop. Thus, it can be inferred from figure 7.3 that in the case of low k-values of the system, the decay of the neutron population is very slow after the prompt drop. However, in the case of high k-values, the prompt drop takes longer on the millisecond time steps.

In the cases when the decay rate in region I is higher (or the same) than the decay rate in region II, the transient behavior in region II will follow region I. Therefore, in general, the Li-6 detector's response will heavily depend on the decay rates in region I and region II. The detector will follow region II when region I decays much faster than region II and follow region I otherwise. The slope of the curves in figure 7.3 and 7.4 determines the decay rate in region I and II respectively. To determine the time at which the Li-6 detector's response will follow region II, the slope of the curve, in figure 7.3, at every $i^{th}$ time step is computed with respect to $(i-1)^{th}$ time step (eq. (7.1)).

$$(Slope)_i = \frac{N_i - N_{i-1}}{t_i - t_{i-1}} \quad \ldots \ldots (7.1)$$

where $N_i$ = Neutron population at $i^{th}$ time step, and

$\quad N_{i-1}$ = Neutron population at $(i-1)^{th}$ time step.

This slope changes significantly at every time step during the prompt neutron drop. When the decay of the neutron population is dominated by the decay of delayed neutron precursors, the slope changes by small amounts at every time step. The switching from significant slope change to small slope change in region I determines the time step at which the Li-6 detector's response will stop following region II. With increase in the k-value of the system, the switching of the detector's response will happen early on milliseconds time scales. For high subcritical multiplications of the system, the detector will always follow the decay rate of region I as region I is decaying much slower than region II. The expected detector's response for low and high k-value is shown in figure 7.5.
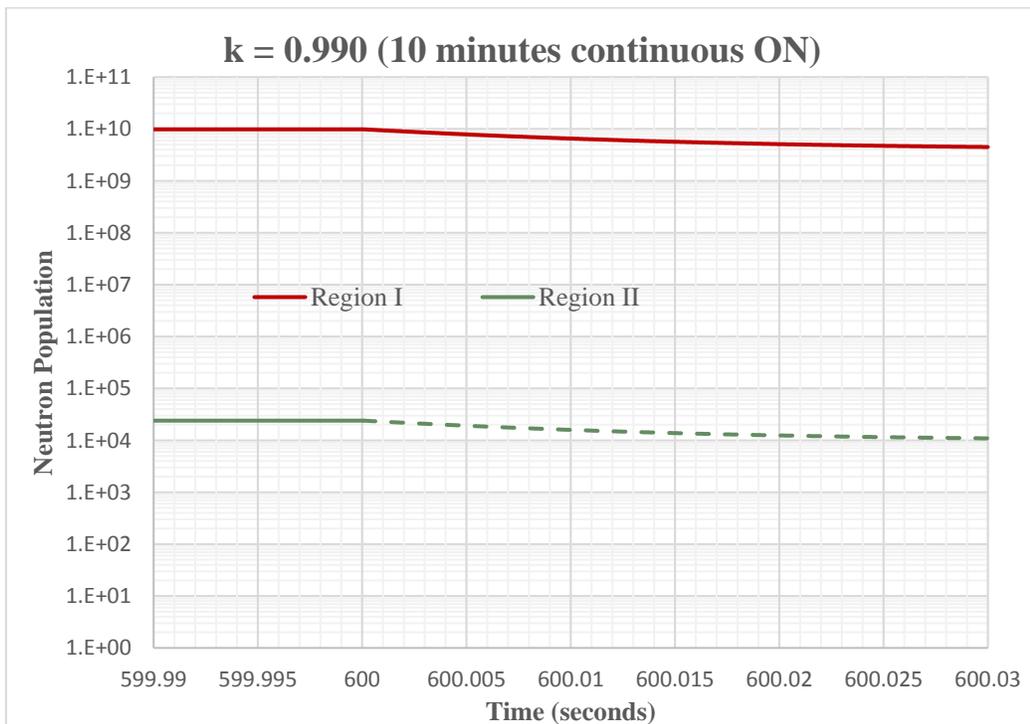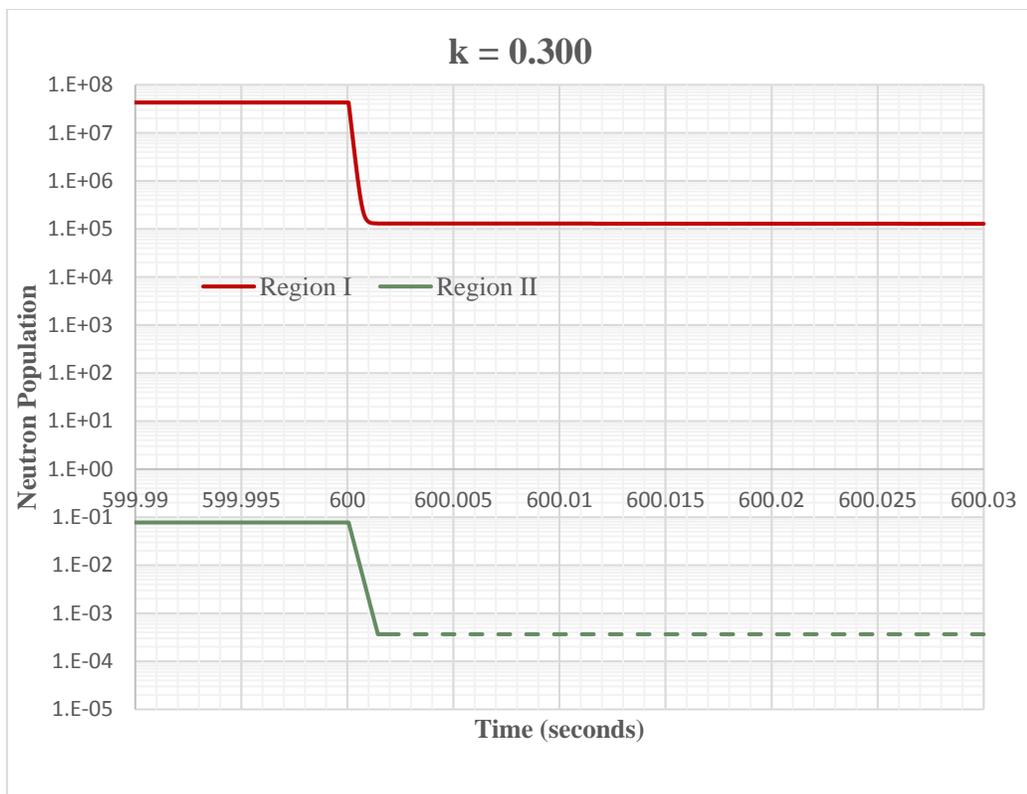
Figure 7.5 Expected correct behavior of neutrons in region II for k = 0.300 and k = 0.990 (Dotted line indicates that neutron behavior in region II will follow neutron behavior in region I at that time step (currently the model does not take that into account))

# 8. CONCLUSIONS AND INFERENCES

The transient analysis of neutrons performed using UTA-1 and a pulsed DD neutron generator is a preliminary test done to understand the neutron behavior in the subcritical uranium assembly. On comparing uranium and no uranium measurements, we can conclude that on turning ON the DD source beam, the following effects are seen:

1) In the first five milliseconds, the neutron population rises and then decays. In this time, the decay is mainly dominated by the diffusion parameters in region II i.e. the region in which the detector is placed.

2) After 5 milliseconds, if no uranium fuel is present, the neutron population will continue to decay exponentially until the count rate drops to background level.

3) However, in the presence of the fuel, the additional fission neutrons from the delayed neutron precursors will result in a new baseline. This baseline will continue to produce counts on the detector and establish an asymptote region.

The developed model is capable of understanding the neutron behavior on microsecond time stamps in the UTA-1+DD system. For low k-values, the model can predict the Li-6 detector's response in this time stamps. At high subcritical multiplication, the predictions are not very accurate. Knowing the exact composition of the material in region II, the model can determine the rate at which neutron count rate will drop to asymptote/background levels. If the detector is placed in region I, than the model can also provide information about the k-value of the system. The measured transient behavior shows that for $k = 0.412$, not many neutrons are produced from the delayed precursors (figure 6.5), which is to be expected with low subcritical multiplication and low external neutron source.

For active interrogation applications, this understanding of the simplified two region system provides useful information about the operating parameters of the accelerator based SNM detection techniques. The UTA-1+DD system is just a preliminary study to understand the behavior of fission and source neutrons after cutoff. This preliminary study provides a basis to distinguish the presence and absence of SNM in real life cargo scanning. Let's consider the case in which the cargo container under inspection contains SNM. In

this case, when the external neutron source, prior to transient analysis, is pulsed for a sufficiently long period of time, the delayed precursors will buildup and attain saturation. This saturation will slow down the decay rate of the neutron population inside the cargo container. Now the detector, which is placed outside the cargo container (i.e. region II), will follow the transient behavior in region I (region I is the cargo container). When subject to transient analysis after cutoff, the neutron population will decay and level off at the asymptote, which is the consequence of the delayed precursors producing additional fission neutrons. In the case of no SNM inside the container, the initial pulsing of the external accelerator will not establish any asymptote level. In this case, the neutron population inside the cargo container will decay at a faster rate (region I decays faster than region II). Therefore, the neutron population at the detector's location will continue to fall to background levels at a rate determined by region II.

The amount of SNM present is proportional to the subcritical multiplication. Since the die-away of the neutron population is observed on microsecond/millisecond time stamps, information on the prompt neutron drop is present in the collected data. From the point kinetics model, eq. (4.11a) and eq. (4.11b), the prompt neutron drop is determined by three parameters, i.e. reactivity $\rho$, total delayed neutron fraction $\beta$ and neutron generation time $\Lambda$.

$$prompt\ neutron\ jump = \frac{\rho - \beta}{\Lambda}$$

The reactivity $\rho$ is directly linked to the subcritical multiplication. The leveling of the neutron population to the asymptote region is related to the buildup of the delayed precursor concentration. This built up of the precursor concentration depends on the delayed neutron fraction, $\beta$. For different SNM, $\beta$ is different. If additional information about the type of isotope present in the cargo container could be obtained, one can determine the delayed neutron fraction and thereby calculate the k-value.

The UTA-1 can further be used to produce medical radioisotopes such as Tc-99m by producing Mo-99. The k-value of the assembly can be raised to 0.99 to obtain full-fledged production of Mo-99 and other important isotopes. A photoneutron converter, such as lead-bismuth eutectic (LBE), connected to the electron linac can be used to obtain source neutrons to drive the assembly for isotope production applications. For radioisotope

applications, ensuring subcriticality of the target assembly is very important for safe operations of the system. Knowing the exact k-value of the system is always beneficial. Using the die-away of the neutron population after cutoff, the k-value at which the system is operating can be determined from the prompt neutron drop. This could help in deciding the operating conditions of the accelerator driven target assembly. From figure 7.3, clearly for low k-values of the target assembly, the prompt drop occurs in the first 5 milliseconds after cutoff. This implies that the exact k-value could be determined within 5 to 10 milliseconds of cutoff. For high k-values, the long term transient, figure 7.1, will provide information on the subcritical multiplication.

The entire setup, i.e. superconducting electron linac and photoneutron converter is capable of producing high intensity source neutrons (of the order of $10^{15}$ n/sec). This can provide a testbed for material irradiation studies. The UTA-1 being a subcritical uranium assembly and not being a commercial power reactor, its cost of building and operations is reduced. Further the use of LEU and not HEU reduces the regulatory burden and the non-proliferation issues.

# 9. PROPOSED FUTURE WORK

Starting from the first principles, transient equations are developed in a simplified two region problem. Certain assumptions and simplifications are made to obtain solutions to these equations. These simplifications impose limitations on the developed model. The limitations can be minimized by developing a three region (or multi region) system instead of two region. In a three-region system, region I could be comprised of the fuel and external neutron source, region II could be comprised of the moderator and region III could be the reflector/absorber. This eliminates the need to homogenize the fuel and all of the moderator, more closely representing the real system. The homogenization of the fuel and moderator drastically affects the diffusion parameters and cross-section values, thereby affecting the modeled transient behavior.

In region II, it is assumed that when the pulsed DD generator is turned ON, the neutrons appear instantaneously at the detector's location. This assumption is not quite true because of the neutron flight time. A neutron will take a finite amount of time to travel from the point where it is born to the detector's location in region II. When operating in microseconds/milliseconds time stamps, it is worthwhile to study the effect of neutron flight time on the transient behavior. The current model assumes constant neutron flux at the detector's location during the pulse ON period. Since the rise of the neutron flux is exponential in region I, according to the point kinetics model, the neutron flux in region II will also rise exponentially. The neutron time of flight should be able to account for this exponential increase at the detector's location. Considering the neutron flight time in the predicted model, one could closely couple the fluctuations in the neutron populations in region I with region II (fluctuations are due to subcritical multiplication and fission reactions).

Further investigation is required to study the effect of pulsing the external neutron source at different frequencies and duty cycles. The model does good job in predicting the transient behavior of neutrons in region I. Pulsing the external neutron source at different frequencies and duty cycles will help in understanding the time required to saturate the precursor concentration in region I. With this information one can decide on how long the external source will have to be pulsed so that the decay rate is region I becomes slower
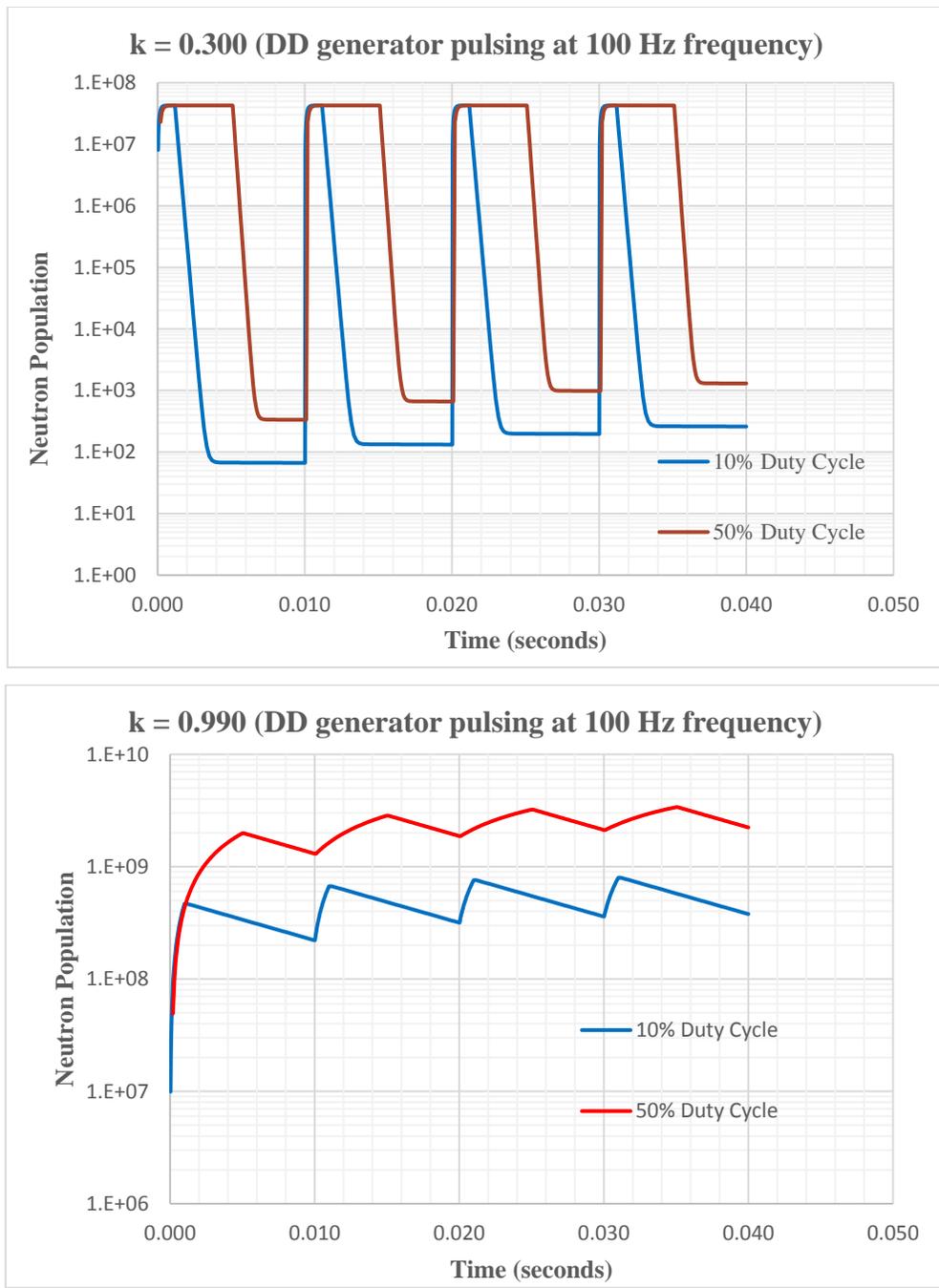
Figure 9.1 Effect of running the DD generator at different duty cycles on the neutron transient behavior in region I (for k = 0.300 and k = 0.990)

than the decay rate in region II. Under such circumstances, the two region model reduces to a single region model, as the neutron population in region II at different time stamps will be some constant times the neutron population in region I at that time stamp. This constant can be determined using the spatial distribution of the neutron population.

For high and low subcritical multiplication of the system, the effect of 10% and 50% duty cycle on the neutron transients in shown in figure 9.1. Clearly the built up of the delayed neutron precursors is significantly affected by the duty cycle of the DD generator. In the case of high k-value, the prompt drop takes longer on millisecond time scales. Therefore, during the pulse OFF time, the decay of the neutron population is mainly dominated by the prompt neutrons.

Additional analysis is needed to couple the neutron flux in region I and region II. This coupling of the flux into the transient equations will accurately account for the built up of the delayed precursors concentration in region II. Currently the solution to the transient equations are obtained assuming separability of variables. Solving the equations without separating the variables could result in better predictions.

It will be valuable in using the known composition of the reflector/moderator in the experimental setup. This will result in the exact diffusion values in the developed model. Finally, additional measurements with varying k-values will provide benchmarking data and a better understanding of the neutron transient behavior.

# APPENDIX A. WOLFRAM MATHEMATICA SYNTAX TO EVALUATE THE SPATIAL DISTRIBUTION OF NEUTRONS

A Wolfram Mathematica code is developed to solve the spatial distribution of neutrons in the simplified two region problem. The syntax requires homogenized diffusion coefficient of neutrons in region I $D_1$, homogenized macroscopic absorption cross-section of neutrons in region I $\Sigma_{a1}$, macroscopic scattering cross-section in region II $\Sigma_{s2}$, macroscopic absorption cross-section in region II $\Sigma_{a2}$, region II mass in amu $A$ and the k-value of the UTA-1+DD system as inputs. The output of the code is the simplified expression for the neutron flux in region I and region II in terms of the external neutron source strength.

```
In[1]:= Clear[Phi1, Phi2, C1, C2, C3, C4, r, L1, L2, f1, f2, f3, f4,
        ff, X, D1, D2, S, D1, D2, sigmaA1, sigmaA2, R1, R2, kinf, k, Bsqu]
```

```
In[2]:= Phi1[r_] = C1 * E^ (Sqrt[1 - k] * r / L1) / r + C2 * E^ (-Sqrt[1 - k] * r / L1) / r
```

$$\text{Out[2]= } \frac{C2\, e^{-\frac{\sqrt{1-k}\, r}{L1}}}{r} + \frac{C1\, e^{\frac{\sqrt{1-k}\, r}{L1}}}{r}$$

```
In[3]:= Phi2[r_] = C3 * E^ (r / L2) / r + C4 * E^ (-r / L2) / r
```

$$\text{Out[3]= } \frac{C4\, e^{-\frac{r}{L2}}}{r} + \frac{C3\, e^{\frac{r}{L2}}}{r}$$

```
In[4]:= X = 4 * Pi * r^2 * (-D1) * Phi1'[r] - S
```

$$\text{Out[4]= } -4\, D1\, \pi \left( -\frac{C2\, e^{-\frac{\sqrt{1-k}\, r}{L1}}}{r^2} - \frac{C1\, e^{\frac{\sqrt{1-k}\, r}{L1}}}{r^2} - \frac{C2\, e^{-\frac{\sqrt{1-k}\, r}{L1}}\sqrt{1-k}}{L1\, r} + \frac{C1\, e^{\frac{\sqrt{1-k}\, r}{L1}}\sqrt{1-k}}{L1\, r} \right) r^2 - S$$

```
In[5]:= ff[r_] = Simplify[X]
```

$$\text{Out[5]= } \frac{1}{L1} \left( 4\, C1\, D1\, e^{\frac{\sqrt{1-k}\, r}{L1}}\, \pi \left( L1 - \sqrt{1-k}\, r \right) + 4\, C2\, D1\, e^{-\frac{\sqrt{1-k}\, r}{L1}}\, \pi \left( L1 + \sqrt{1-k}\, r \right) - L1\, S \right)$$

```
In[6]:= f1 = Simplify[ff[0]]
```

$$\text{Out[6]= } 4\, C1\, D1\, \pi + 4\, C2\, D1\, \pi - S$$

```
In[7]:= f2 = Phi1[R1] - Phi2[R1]
```

$$\text{Out[7]= } \frac{C2\, e^{-\frac{\sqrt{1-k}\, R1}{L1}}}{R1} + \frac{C1\, e^{\frac{\sqrt{1-k}\, R1}{L1}}}{R1} - \frac{C4\, e^{-\frac{R1}{L2}}}{R1} - \frac{C3\, e^{\frac{R1}{L2}}}{R1}$$

```
In[8]:= f3 = D1 * Phi1'[R1] - D2 * Phi2'[R1]
```

$$\text{Out[8]= } D1 \left( -\frac{C2\, e^{-\frac{\sqrt{1-k}\, R1}{L1}}}{R1^2} - \frac{C1\, e^{\frac{\sqrt{1-k}\, R1}{L1}}}{R1^2} - \frac{C2\, e^{-\frac{\sqrt{1-k}\, R1}{L1}}\sqrt{1-k}}{L1\, R1} + \frac{C1\, e^{\frac{\sqrt{1-k}\, R1}{L1}}\sqrt{1-k}}{L1\, R1} \right) - $$

$$D2 \left( -\frac{C4\, e^{-\frac{R1}{L2}}}{R1^2} - \frac{C3\, e^{\frac{R1}{L2}}}{R1^2} - \frac{C4\, e^{-\frac{R1}{L2}}}{L2\, R1} + \frac{C3\, e^{\frac{R1}{L2}}}{L2\, R1} \right)$$

In[9]:= `f4 = Phi2[(R2 + (0.71 * 3 * D2))]`

Out[9]= $\dfrac{C4\, e^{-\frac{2.13\, D2 + R2}{L2}}}{2.13\, D2 + R2} + \dfrac{C3\, e^{\frac{2.13\, D2 + R2}{L2}}}{2.13\, D2 + R2}$

In[10]:= `sol = Solve[f1 == 0 && f2 == 0 && f3 == 0 && f4 == 0, {C1, C2, C3, C4}]`

Out[10]= $\{\{$C1 $\rightarrow$

$-\left(\left(\left(1.\left(0.+1.\left(-1.\left(\frac{1}{R1}1.\,e^{\frac{R1}{L2}}\left(\frac{D2\,e^{-\frac{1.\,R1}{L2}}}{R1^2}+\frac{D2\,e^{-\frac{1.\,R1}{L2}}}{L2\,R1}\right)-\frac{1}{R1}1.\,e^{-\frac{1.\,R1}{L2}}\left(\frac{D2\,e^{\frac{R1}{L2}}}{R1^2}-\frac{1.\,D2\,e^{\frac{R1}{L2}}}{L2\,R1}\right)\right)\left(0.-\left(1.\right.\right.\right.\right.\right.\right.$

$e^{-\frac{1.\,\sqrt{1.-1.\,k}\,R1}{L1}-\frac{1.\,(2.13\,D2+R2)}{L2}}\Big)\Big/\left(R1\,(2.13\,D2+R2)\right)\Big)+$

$\left(-\frac{1}{R1}1.\,e^{-\frac{1.\,R1}{L2}}\left(-\frac{1}{R1^2}1.\,D1\,e^{-\frac{1.\,\sqrt{1.-1.\,k}\,R1}{L1}}-\left(1.\,D1\,e^{-\frac{1.\,\sqrt{1.-1.\,k}\,R1}{L1}}\sqrt{1.-1.\,k}\right)\Big/(L1\,R1)\right)-\right.$

$\frac{1}{R1}1.\,e^{-\frac{1.\,\sqrt{1.-1.\,k}\,R1}{L1}}\left(\frac{D2\,e^{-\frac{1.\,R1}{L2}}}{R1^2}+\frac{D2\,e^{-\frac{1.\,R1}{L2}}}{L2\,R1}\right)\right)$

$\left(\left(1.\,e^{\frac{R1}{L2}-\frac{1.\,(2.13\,D2+R2)}{L2}}\right)\Big/\left(R1\,(2.13\,D2+R2)\right)-\frac{1.\,e^{-\frac{1.\,R1}{L2}+\frac{2.13\,D2+R2}{L2}}}{R1\,(2.13\,D2+R2)}\right)\right)S\right)\Big/$

$\left(-12.5664\,D1\left(-1.\left(\frac{1}{R1}1.\,e^{\frac{R1}{L2}}\left(\frac{D2\,e^{-\frac{1.\,R1}{L2}}}{R1^2}+\frac{D2\,e^{-\frac{1.\,R1}{L2}}}{L2\,R1}\right)-\frac{1}{R1}1.\,e^{-\frac{1.\,R1}{L2}}\left(\frac{D2\,e^{\frac{R1}{L2}}}{R1^2}-\frac{1.\,D2\,e^{\frac{R1}{L2}}}{L2\,R1}\right)\right)\right.$

$\left(0.-\left(1.\,e^{-\frac{1.\,\sqrt{1.-1.\,k}\,R1}{L1}-\frac{1.\,(2.13\,D2+R2)}{L2}}\right)\Big/\left(R1\,(2.13\,D2+R2)\right)\right)+$

$\left(-\frac{1}{R1}1.\,e^{-\frac{1.\,R1}{L2}}\left(-\frac{1}{R1^2}1.\,D1\,e^{-\frac{1.\,\sqrt{1.-1.\,k}\,R1}{L1}}-\left(1.\,D1\,e^{-\frac{1.\,\sqrt{1.-1.\,k}\,R1}{L1}}\sqrt{1.-1.\,k}\right)\Big/(L1\,R1)\right)-\right.$

$\frac{1}{R1}1.\,e^{-\frac{1.\,\sqrt{1.-1.\,k}\,R1}{L1}}\left(\frac{D2\,e^{-\frac{1.\,R1}{L2}}}{R1^2}+\frac{D2\,e^{-\frac{1.\,R1}{L2}}}{L2\,R1}\right)\right)\left(\frac{1.\,e^{\frac{R1}{L2}-\frac{1.\,(2.13\,D2+R2)}{L2}}}{R1\,(2.13\,D2+R2)}-\frac{1.\,e^{-\frac{1.\,R1}{L2}+\frac{2.13\,D2+R2}{L2}}}{R1\,(2.13\,D2+R2)}\right)+$

$12.5664\,D1\left(-1.\left(\frac{1}{R1}1.\,e^{\frac{R1}{L2}}\left(\frac{D2\,e^{-\frac{1.\,R1}{L2}}}{R1^2}+\frac{D2\,e^{-\frac{1.\,R1}{L2}}}{L2\,R1}\right)-\frac{1}{R1}1.\,e^{-\frac{1.\,R1}{L2}}\left(\frac{D2\,e^{\frac{R1}{L2}}}{R1^2}-\frac{1.\,D2\,e^{\frac{R1}{L2}}}{L2\,R1}\right)\right)\right.$

$\left(0.-\left(1.\,e^{\frac{\sqrt{1.-1.\,k}\,R1}{L1}-\frac{1.\,(2.13\,D2+R2)}{L2}}\right)\Big/\left(R1\,(2.13\,D2+R2)\right)\right)+$

$\left(-\frac{1}{R1}1.\,e^{-\frac{1.\,R1}{L2}}\left(-\frac{1.\,D1\,e^{\frac{\sqrt{1.-1.\,k}\,R1}{L1}}}{R1^2}+\left(D1\,e^{\frac{\sqrt{1.-1.\,k}\,R1}{L1}}\sqrt{1.-1.\,k}\right)\Big/(L1\,R1)\right)-\frac{1}{R1}\right.$

$1.\,e^{\frac{\sqrt{1.-1.\,k}\,R1}{L1}}\left(\frac{D2\,e^{-\frac{1.\,R1}{L2}}}{R1^2}+\frac{D2\,e^{-\frac{1.\,R1}{L2}}}{L2\,R1}\right)\right)\left(\frac{1.\,e^{\frac{R1}{L2}-\frac{1.\,(2.13\,D2+R2)}{L2}}}{R1\,(2.13\,D2+R2)}-\frac{1.\,e^{-\frac{1.\,R1}{L2}+\frac{2.13\,D2+R2}{L2}}}{R1\,(2.13\,D2+R2)}\right)\right)\right)\right),$

$$C2 \rightarrow \Bigg( 0.0795775 \Bigg( -1.74393 \times 10^{-16} \, D1 \, e^{\frac{2.\,R1}{L2}} \, L1 \, L2 \, S + 1.74393 \times 10^{-16} \, D2 \, e^{\frac{2.\,R1}{L2}} \, L1 \, L2 \, S +$$

$$1.\, D1 \, e^{\frac{2.\,\sqrt{1.-1.\,k}\,\,R1}{L1}+\frac{2.\,R1}{L2}} \, L1 \, L2 \, S - 1.\, D2 \, e^{\frac{2.\,\sqrt{1.-1.\,k}\,\,R1}{L1}+\frac{2.\,R1}{L2}} \, L1 \, L2 \, S +$$

$$1.74393 \times 10^{-16} \, D1 \, e^{\frac{4.26\,D2}{L2}+\frac{2.\,R2}{L2}} \, L1 \, L2 \, S - 1.74393 \times 10^{-16} \, D2 \, e^{\frac{4.26\,D2}{L2}+\frac{2.\,R2}{L2}} \, L1 \, L2 \, S -$$

$$1.\, D1 \, e^{\frac{4.26\,D2}{L2}+\frac{2.\,\sqrt{1.-1.\,k}\,\,R1}{L1}+\frac{2.\,R2}{L2}} \, L1 \, L2 \, S + 1.\, D2 \, e^{\frac{4.26\,D2}{L2}+\frac{2.\,\sqrt{1.-1.\,k}\,\,R1}{L1}+\frac{2.\,R2}{L2}} \, L1 \, L2 \, S -$$

$$1.74393 \times 10^{-16} \, D2 \, e^{\frac{2.\,R1}{L2}} \, L1 \, R1 \, S + 1.\, D2 \, e^{\frac{2.\,\sqrt{1.-1.\,k}\,\,R1}{L1}+\frac{2.\,R1}{L2}} \, L1 \, R1 \, S -$$

$$1.74393 \times 10^{-16} \, D2 \, e^{\frac{4.26\,D2}{L2}+\frac{2.\,R2}{L2}} \, L1 \, R1 \, S + 1.\, D2 \, e^{\frac{4.26\,D2}{L2}+\frac{2.\,\sqrt{1.-1.\,k}\,\,R1}{L1}+\frac{2.\,R2}{L2}} \, L1 \, R1 \, S -$$

$$1.74393 \times 10^{-16} \, D1 \, e^{\frac{2.\,R1}{L2}} \, \sqrt{1.-1.\,k} \, L2 \, R1 \, S - 1.\, D1 \, e^{\frac{2.\,\sqrt{1.-1.\,k}\,\,R1}{L1}+\frac{2.\,R1}{L2}} \, \sqrt{1.-1.\,k} \, L2 \, R1 \, S +$$

$$1.74393 \times 10^{-16} \, D1 \, e^{\frac{4.26\,D2}{L2}+\frac{2.\,R2}{L2}} \, \sqrt{1.-1.\,k} \, L2 \, R1 \, S +$$

$$1.\, D1 \, e^{\frac{4.26\,D2}{L2}+\frac{2.\,\sqrt{1.-1.\,k}\,\,R1}{L1}+\frac{2.\,R2}{L2}} \, \sqrt{1.-1.\,k} \, L2 \, R1 \, S \Bigg) \Bigg) \Bigg/$$

$$\Bigg( D1 \Bigg( -1.\, D1 \, e^{\frac{2.\,R1}{L2}} \, L1 \, L2 + 1.\, D2 \, e^{\frac{2.\,R1}{L2}} \, L1 \, L2 + 1.\, D1 \, e^{\frac{2.\,\sqrt{1.-1.\,k}\,\,R1}{L1}+\frac{2.\,R1}{L2}} \, L1 \, L2 -$$

$$1.\, D2 \, e^{\frac{2.\,\sqrt{1.-1.\,k}\,\,R1}{L1}+\frac{2.\,R1}{L2}} \, L1 \, L2 + 1.\, D1 \, e^{\frac{4.26\,D2}{L2}+\frac{2.\,R2}{L2}} \, L1 \, L2 - 1.\, D2 \, e^{\frac{4.26\,D2}{L2}+\frac{2.\,R2}{L2}} \, L1 \, L2 -$$

$$1.\, D1 \, e^{\frac{4.26\,D2}{L2}+\frac{2.\,\sqrt{1.-1.\,k}\,\,R1}{L1}+\frac{2.\,R2}{L2}} \, L1 \, L2 + 1.\, D2 \, e^{\frac{4.26\,D2}{L2}+\frac{2.\,\sqrt{1.-1.\,k}\,\,R1}{L1}+\frac{2.\,R2}{L2}} \, L1 \, L2 - 1.\, D2 \, e^{\frac{2.\,R1}{L2}} \, L1 \, R1 +$$

$$1.\, D2 \, e^{\frac{2.\,\sqrt{1.-1.\,k}\,\,R1}{L1}+\frac{2.\,R1}{L2}} \, L1 \, R1 - 1.\, D2 \, e^{\frac{4.26\,D2}{L2}+\frac{2.\,R2}{L2}} \, L1 \, R1 + 1.\, D2 \, e^{\frac{4.26\,D2}{L2}+\frac{2.\,\sqrt{1.-1.\,k}\,\,R1}{L1}+\frac{2.\,R2}{L2}} \, L1 \, R1 -$$

$$1.\, D1 \, e^{\frac{2.\,R1}{L2}} \, \sqrt{1.-1.\,k} \, L2 \, R1 - 1.\, D1 \, e^{\frac{2.\,\sqrt{1.-1.\,k}\,\,R1}{L1}+\frac{2.\,R1}{L2}} \, \sqrt{1.-1.\,k} \, L2 \, R1 +$$

$$1.\, D1 \, e^{\frac{4.26\,D2}{L2}+\frac{2.\,R2}{L2}} \, \sqrt{1.-1.\,k} \, L2 \, R1 + 1.\, D1 \, e^{\frac{4.26\,D2}{L2}+\frac{2.\,\sqrt{1.-1.\,k}\,\,R1}{L1}+\frac{2.\,R2}{L2}} \, \sqrt{1.-1.\,k} \, L2 \, R1 \Bigg) \Bigg),$$

$$C3 \rightarrow \Bigg( 0.0795775 \, e^{-\frac{1.\,\sqrt{1.-1.\,k}\,\,R1}{L1}} \Bigg( 1.74393 \times 10^{-16} \, D1 \, e^{\frac{3.\,R1}{L2}} \, L1 \, L2 \, S - 1.74393 \times 10^{-16} \, D2 \, e^{\frac{3.\,R1}{L2}} \, L1 \, L2 \, S -$$

$$2.22045 \times 10^{-16} \, D1 \, e^{\frac{2.\,\sqrt{1.-1.\,k}\,\,R1}{L1}+\frac{3.\,R1}{L2}} \, L1 \, L2 \, S + 2.22045 \times 10^{-16} \, D2 \, e^{\frac{2.\,\sqrt{1.-1.\,k}\,\,R1}{L1}+\frac{3.\,R1}{L2}} \, L1 \, L2 \, S -$$

$$1.74393 \times 10^{-16} \, D1 \, e^{\frac{4.26\,D2}{L2}+\frac{1.\,R1}{L2}+\frac{2.\,R2}{L2}} \, L1 \, L2 \, S + 1.74393 \times 10^{-16} \, D2 \, e^{\frac{4.26\,D2}{L2}+\frac{1.\,R1}{L2}+\frac{2.\,R2}{L2}} \, L1 \, L2 \, S +$$

$$2.22045 \times 10^{-16} \, D1 \, e^{\frac{4.26\,D2}{L2}+\frac{2.\,\sqrt{1.-1.\,k}\,\,R1}{L1}+\frac{1.\,R1}{L2}+\frac{2.\,R2}{L2}} \, L1 \, L2 \, S -$$

$$2.22045 \times 10^{-16} \, D2 \, e^{\frac{4.26\,D2}{L2}+\frac{2.\,\sqrt{1.-1.\,k}\,\,R1}{L1}+\frac{1.\,R1}{L2}+\frac{2.\,R2}{L2}} \, L1 \, L2 \, S + 1.74393 \times 10^{-16} \, D2 \, e^{\frac{3.\,R1}{L2}} \, L1 \, R1 \, S -$$

$$2.22045 \times 10^{-16} \, D2 \, e^{\frac{2.\,\sqrt{1.-1.\,k}\,\,R1}{L1}+\frac{3.\,R1}{L2}} \, L1 \, R1 \, S + 1.74393 \times 10^{-16} \, D2 \, e^{\frac{4.26\,D2}{L2}+\frac{1.\,R1}{L2}+\frac{2.\,R2}{L2}} \, L1 \, R1 \, S -$$

$$2.22045 \times 10^{-16} \, D2 \, e^{\frac{4.26\,D2}{L2}+\frac{2.\,\sqrt{1.-1.\,k}\,\,R1}{L1}+\frac{1.\,R1}{L2}+\frac{2.\,R2}{L2}} \, L1 \, R1 \, S +$$

$$1.74393 \times 10^{-16} \, D1 \, e^{\frac{3.\,R1}{L2}} \, \sqrt{1.-1.\,k} \, L2 \, R1 \, S + 2.\, D1 \, e^{\frac{2.\,\sqrt{1.-1.\,k}\,\,R1}{L1}+\frac{3.\,R1}{L2}} \, \sqrt{1.-1.\,k} \, L2 \, R1 \, S -$$

$$1.74393 \times 10^{-16} \, D1 \, e^{\frac{4.26\,D2}{L2}+\frac{1.\,R1}{L2}+\frac{2.\,R2}{L2}} \, \sqrt{1.-1.\,k} \, L2 \, R1 \, S -$$

$$2.\, D1 \, e^{\frac{4.26\,D2}{L2}+\frac{2.\,\sqrt{1.-1.\,k}\,\,R1}{L1}+\frac{1.\,R1}{L2}+\frac{2.\,R2}{L2}} \, \sqrt{1.-1.\,k} \, L2 \, R1 \, S \Bigg) \Bigg) \Bigg/$$

$$\left( D1 \left( 1.\, e^{\frac{2.\,R1}{L2}} - 1.\, e^{\frac{4.26\,D2}{L2}+\frac{2.\,R2}{L2}} \right) \left( 1.\,D1\, e^{\frac{2.\,R1}{L2}} L1\,L2 - 1.\,D2\, e^{\frac{2.\,R1}{L2}} L1\,L2 - 1.\,D1\, e^{\frac{2.\,\sqrt{1.-1.\,k}\,R1}{L1}+\frac{2.\,R1}{L2}} L1\,L2 + \right. \right.$$

$$1.\,D2\, e^{\frac{2.\,\sqrt{1.-1.\,k}\,R1}{L1}+\frac{2.\,R1}{L2}} L1\,L2 - 1.\,D1\, e^{\frac{4.26\,D2}{L2}+\frac{2.\,R2}{L2}} L1\,L2 + 1.\,D2\, e^{\frac{4.26\,D2}{L2}+\frac{2.\,R2}{L2}} L1\,L2 +$$

$$1.\,D1\, e^{\frac{4.26\,D2}{L2}+\frac{2.\,\sqrt{1.-1.\,k}\,R1}{L1}+\frac{2.\,R2}{L2}} L1\,L2 - 1.\,D2\, e^{\frac{4.26\,D2}{L2}+\frac{2.\,\sqrt{1.-1.\,k}\,R1}{L1}+\frac{2.\,R2}{L2}} L1\,L2 + 1.\,D2\, e^{\frac{2.\,R1}{L2}} L1\,R1 -$$

$$1.\,D2\, e^{\frac{2.\,\sqrt{1.-1.\,k}\,R1}{L1}+\frac{2.\,R1}{L2}} L1\,R1 + 1.\,D2\, e^{\frac{4.26\,D2}{L2}+\frac{2.\,R2}{L2}} L1\,R1 - 1.\,D2\, e^{\frac{4.26\,D2}{L2}+\frac{2.\,\sqrt{1.-1.\,k}\,R1}{L1}+\frac{2.\,R2}{L2}} L1\,R1 +$$

$$1.\,D1\, e^{\frac{2.\,R1}{L2}} \sqrt{1.-1.\,k}\, L2\,R1 + 1.\,D1\, e^{\frac{2.\,\sqrt{1.-1.\,k}\,R1}{L1}+\frac{2.\,R1}{L2}} \sqrt{1.-1.\,k}\, L2\,R1 -$$

$$\left. \left. 1.\,D1\, e^{\frac{4.26\,D2}{L2}+\frac{2.\,R2}{L2}} \sqrt{1.-1.\,k}\, L2\,R1 - 1.\,D1\, e^{\frac{4.26\,D2}{L2}+\frac{2.\,\sqrt{1.-1.\,k}\,R1}{L1}+\frac{2.\,R2}{L2}} \sqrt{1.-1.\,k}\, L2\,R1 \right) \right),$$

$$C4 \to \left( 0.0795775\, e^{-\frac{1.\,\sqrt{1.-1.\,k}\,R1}{L1}} \left( 1.74393\times10^{-16}\,D1\, e^{\frac{4.26\,D2}{L2}+\frac{3.\,R1}{L2}+\frac{2.\,R2}{L2}} L1\,L2\,S - \right. \right.$$

$$1.74393\times10^{-16}\,D2\, e^{\frac{4.26\,D2}{L2}+\frac{3.\,R1}{L2}+\frac{2.\,R2}{L2}} L1\,L2\,S - 2.22045\times10^{-16}\,D1\, e^{\frac{4.26\,D2}{L2}+\frac{2.\,\sqrt{1.-1.\,k}\,R1}{L1}+\frac{3.\,R1}{L2}+\frac{2.\,R2}{L2}} L1\,L2\,S +$$

$$2.22045\times10^{-16}\,D2\, e^{\frac{4.26\,D2}{L2}+\frac{2.\,\sqrt{1.-1.\,k}\,R1}{L1}+\frac{3.\,R1}{L2}+\frac{2.\,R2}{L2}} L1\,L2\,S - 1.74393\times10^{-16}\,D1\, e^{\frac{8.52\,D2}{L2}+\frac{1.\,R1}{L2}+\frac{4.\,R2}{L2}} L1\,L2\,S +$$

$$1.74393\times10^{-16}\,D2\, e^{\frac{8.52\,D2}{L2}+\frac{1.\,R1}{L2}+\frac{4.\,R2}{L2}} L1\,L2\,S + 2.22045\times10^{-16}\,D1\, e^{\frac{8.52\,D2}{L2}+\frac{2.\,\sqrt{1.-1.\,k}\,R1}{L1}+\frac{1.\,R1}{L2}+\frac{4.\,R2}{L2}} L1\,L2\,S -$$

$$2.22045\times10^{-16}\,D2\, e^{\frac{8.52\,D2}{L2}+\frac{2.\,\sqrt{1.-1.\,k}\,R1}{L1}+\frac{1.\,R1}{L2}+\frac{4.\,R2}{L2}} L1\,L2\,S +$$

$$1.74393\times10^{-16}\,D2\, e^{\frac{4.26\,D2}{L2}+\frac{3.\,R1}{L2}+\frac{2.\,R2}{L2}} L1\,R1\,S - 2.22045\times10^{-16}\,D2\, e^{\frac{4.26\,D2}{L2}+\frac{2.\,\sqrt{1.-1.\,k}\,R1}{L1}+\frac{3.\,R1}{L2}+\frac{2.\,R2}{L2}} L1\,R1\,S +$$

$$1.74393\times10^{-16}\,D2\, e^{\frac{8.52\,D2}{L2}+\frac{1.\,R1}{L2}+\frac{4.\,R2}{L2}} L1\,R1\,S - 2.22045\times10^{-16}\,D2\, e^{\frac{8.52\,D2}{L2}+\frac{2.\,\sqrt{1.-1.\,k}\,R1}{L1}+\frac{1.\,R1}{L2}+\frac{4.\,R2}{L2}} L1\,R1\,S +$$

$$1.74393\times10^{-16}\,D1\, e^{\frac{4.26\,D2}{L2}+\frac{3.\,R1}{L2}+\frac{2.\,R2}{L2}} \sqrt{1.-1.\,k}\, L2\,R1\,S +$$

$$2.\,D1\, e^{\frac{4.26\,D2}{L2}+\frac{2.\,\sqrt{1.-1.\,k}\,R1}{L1}+\frac{3.\,R1}{L2}+\frac{2.\,R2}{L2}} \sqrt{1.-1.\,k}\, L2\,R1\,S - 1.74393\times10^{-16}\,D1\, e^{\frac{8.52\,D2}{L2}+\frac{1.\,R1}{L2}+\frac{4.\,R2}{L2}}$$

$$\left. \left. \sqrt{1.-1.\,k}\, L2\,R1\,S - 2.\,D1\, e^{\frac{8.52\,D2}{L2}+\frac{2.\,\sqrt{1.-1.\,k}\,R1}{L1}+\frac{1.\,R1}{L2}+\frac{4.\,R2}{L2}} \sqrt{1.-1.\,k}\, L2\,R1\,S \right) \right) \Big/$$

$$\left( D1 \left( -1.\, e^{\frac{2.\,R1}{L2}} + 1.\, e^{\frac{4.26\,D2}{L2}+\frac{2.\,R2}{L2}} \right) \left( 1.\,D1\, e^{\frac{2.\,R1}{L2}} L1\,L2 - 1.\,D2\, e^{\frac{2.\,R1}{L2}} L1\,L2 - 1.\,D1\, e^{\frac{2.\,\sqrt{1.-1.\,k}\,R1}{L1}+\frac{2.\,R1}{L2}} L1\,L2 + \right. \right.$$

$$1.\,D2\, e^{\frac{2.\,\sqrt{1.-1.\,k}\,R1}{L1}+\frac{2.\,R1}{L2}} L1\,L2 - 1.\,D1\, e^{\frac{4.26\,D2}{L2}+\frac{2.\,R2}{L2}} L1\,L2 + 1.\,D2\, e^{\frac{4.26\,D2}{L2}+\frac{2.\,R2}{L2}} L1\,L2 +$$

$$1.\,D1\, e^{\frac{4.26\,D2}{L2}+\frac{2.\,\sqrt{1.-1.\,k}\,R1}{L1}+\frac{2.\,R2}{L2}} L1\,L2 - 1.\,D2\, e^{\frac{4.26\,D2}{L2}+\frac{2.\,\sqrt{1.-1.\,k}\,R1}{L1}+\frac{2.\,R2}{L2}} L1\,L2 + 1.\,D2\, e^{\frac{2.\,R1}{L2}} L1\,R1 -$$

$$1.\,D2\, e^{\frac{2.\,\sqrt{1.-1.\,k}\,R1}{L1}+\frac{2.\,R1}{L2}} L1\,R1 + 1.\,D2\, e^{\frac{4.26\,D2}{L2}+\frac{2.\,R2}{L2}} L1\,R1 - 1.\,D2\, e^{\frac{4.26\,D2}{L2}+\frac{2.\,\sqrt{1.-1.\,k}\,R1}{L1}+\frac{2.\,R2}{L2}} L1\,R1 +$$

$$1.\,D1\, e^{\frac{2.\,R1}{L2}} \sqrt{1.-1.\,k}\, L2\,R1 + 1.\,D1\, e^{\frac{2.\,\sqrt{1.-1.\,k}\,R1}{L1}+\frac{2.\,R1}{L2}} \sqrt{1.-1.\,k}\, L2\,R1 -$$

$$\left. \left. \left. 1.\,D1\, e^{\frac{4.26\,D2}{L2}+\frac{2.\,R2}{L2}} \sqrt{1.-1.\,k}\, L2\,R1 - 1.\,D1\, e^{\frac{4.26\,D2}{L2}+\frac{2.\,\sqrt{1.-1.\,k}\,R1}{L1}+\frac{2.\,R2}{L2}} \sqrt{1.-1.\,k}\, L2\,R1 \right) \right) \right\} \right\}$$

In[11]:= **C1 = C1 /. sol[[1]]**

Out[11]= $-\left( \left( 1. \left( 0. + 1. \left( -1. \left( \frac{1}{R1} 1.\, e^{\frac{R1}{L2}} \left( \frac{D2\, e^{-\frac{1.\,R1}{L2}}}{R1^2} + \frac{D2\, e^{-\frac{1.\,R1}{L2}}}{L2\,R1} \right) - \frac{1}{R1} 1.\, e^{-\frac{1.\,R1}{L2}} \left( \frac{D2\, e^{\frac{R1}{L2}}}{R1^2} - \frac{1.\,D2\, e^{\frac{R1}{L2}}}{L2\,R1} \right) \right) \right. \right. \right. \right.$

$\left. \left. \left. \left( 0. - \left( 1.\, e^{-\frac{1.\,\sqrt{1.-1.\,k}\,R1}{L1}-\frac{1.\,(2.13\,D2+R2)}{L2}} \right) \Big/ \left( R1\,(2.13\,D2+R2) \right) \right) \right) + \right.$

$$\left(-\frac{1}{R1}1.\,e^{-\frac{1.\,R1}{L2}}\left(-\frac{1}{R1^2}1.\,D1\,e^{-\frac{1.\,\sqrt{1.-1.\,k}\,R1}{L1}}-\left(1.\,D1\,e^{-\frac{1.\,\sqrt{1.-1.\,k}\,R1}{L1}}\sqrt{1.-1.\,k}\right)\right)\Big/(L1\,R1)\right)-\frac{1}{R1}$$

$$1.\,e^{-\frac{1.\,\sqrt{1.-1.\,k}\,R1}{L1}}\left(\frac{D2\,e^{-\frac{1.\,R1}{L2}}}{R1^2}+\frac{D2\,e^{-\frac{1.\,R1}{L2}}}{L2\,R1}\right)\right)\left(\frac{1.\,e^{\frac{R1}{L2}-\frac{1.\,(2.13\,D2+R2)}{L2}}}{R1\,(2.13\,D2+R2)}-\frac{1.\,e^{-\frac{1.\,R1}{L2}+\frac{2.13\,D2+R2}{L2}}}{R1\,(2.13\,D2+R2)}\right)\right)S\Bigg)\Bigg/$$

$$\Bigg(-12.5664\,D1\left(-1.\left(\frac{1}{R1}1.\,e^{\frac{R1}{L2}}\left(\frac{D2\,e^{-\frac{1.\,R1}{L2}}}{R1^2}+\frac{D2\,e^{-\frac{1.\,R1}{L2}}}{L2\,R1}\right)-\frac{1}{R1}1.\,e^{-\frac{1.\,R1}{L2}}\left(\frac{D2\,e^{\frac{R1}{L2}}}{R1^2}-\frac{1.\,D2\,e^{\frac{R1}{L2}}}{L2\,R1}\right)\right)\right.$$

$$\left(0.-\left(1.\,e^{-\frac{1.\,\sqrt{1.-1.\,k}\,R1}{L1}-\frac{1.\,(2.13\,D2+R2)}{L2}}\right)\right)\Big/(R1\,(2.13\,D2+R2))\Bigg)+$$

$$\left(-\frac{1}{R1}1.\,e^{-\frac{1.\,R1}{L2}}\left(-\frac{1}{R1^2}1.\,D1\,e^{-\frac{1.\,\sqrt{1.-1.\,k}\,R1}{L1}}-\left(1.\,D1\,e^{-\frac{1.\,\sqrt{1.-1.\,k}\,R1}{L1}}\sqrt{1.-1.\,k}\right)\right)\Big/(L1\,R1)\right)-$$

$$\frac{1}{R1}1.\,e^{-\frac{1.\,\sqrt{1.-1.\,k}\,R1}{L1}}\left(\frac{D2\,e^{-\frac{1.\,R1}{L2}}}{R1^2}+\frac{D2\,e^{-\frac{1.\,R1}{L2}}}{L2\,R1}\right)\right)\left(\frac{1.\,e^{\frac{R1}{L2}-\frac{1.\,(2.13\,D2+R2)}{L2}}}{R1\,(2.13\,D2+R2)}-\frac{1.\,e^{-\frac{1.\,R1}{L2}+\frac{2.13\,D2+R2}{L2}}}{R1\,(2.13\,D2+R2)}\right)\Bigg)+$$

$$12.5664\,D1\left(-1.\left(\frac{1}{R1}1.\,e^{\frac{R1}{L2}}\left(\frac{D2\,e^{-\frac{1.\,R1}{L2}}}{R1^2}+\frac{D2\,e^{-\frac{1.\,R1}{L2}}}{L2\,R1}\right)-\frac{1}{R1}1.\,e^{-\frac{1.\,R1}{L2}}\left(\frac{D2\,e^{\frac{R1}{L2}}}{R1^2}-\frac{1.\,D2\,e^{\frac{R1}{L2}}}{L2\,R1}\right)\right)\right.$$

$$\left(0.-\left(1.\,e^{\frac{\sqrt{1.-1.\,k}\,R1}{L1}-\frac{1.\,(2.13\,D2+R2)}{L2}}\right)\right)\Big/(R1\,(2.13\,D2+R2))\Bigg)+$$

$$\left(-\frac{1}{R1}1.\,e^{-\frac{1.\,R1}{L2}}\left(-\frac{1.\,D1\,e^{\frac{\sqrt{1.-1.\,k}\,R1}{L1}}}{R1^2}+\left(D1\,e^{\frac{\sqrt{1.-1.\,k}\,R1}{L1}}\sqrt{1.-1.\,k}\right)\right)\Big/(L1\,R1)\right)-\frac{1}{R1}$$

$$1.\,e^{\frac{\sqrt{1.-1.\,k}\,R1}{L1}}\left(\frac{D2\,e^{-\frac{1.\,R1}{L2}}}{R1^2}+\frac{D2\,e^{-\frac{1.\,R1}{L2}}}{L2\,R1}\right)\right)\left(\frac{1.\,e^{\frac{R1}{L2}-\frac{1.\,(2.13\,D2+R2)}{L2}}}{R1\,(2.13\,D2+R2)}-\frac{1.\,e^{-\frac{1.\,R1}{L2}+\frac{2.13\,D2+R2}{L2}}}{R1\,(2.13\,D2+R2)}\right)\Bigg)\Bigg)$$

In[12]:= **C2 = C2 /. sol[[1]]**

Out[12]= $\Bigg(0.0795775\left(-1.74393\times10^{-16}\,D1\,e^{\frac{2.\,R1}{L2}}L1\,L2\,S+1.74393\times10^{-16}\,D2\,e^{\frac{2.\,R1}{L2}}L1\,L2\,S+\right.$

$1.\,D1\,e^{\frac{2.\,\sqrt{1.-1.\,k}\,R1}{L1}+\frac{2.\,R1}{L2}}L1\,L2\,S-1.\,D2\,e^{\frac{2.\,\sqrt{1.-1.\,k}\,R1}{L1}+\frac{2.\,R1}{L2}}L1\,L2\,S+1.74393\times10^{-16}\,D1\,e^{\frac{4.26\,D2}{L2}+\frac{2.\,R2}{L2}}L1\,L2\,S-$

$1.74393\times10^{-16}\,D2\,e^{\frac{4.26\,D2}{L2}+\frac{2.\,R2}{L2}}L1\,L2\,S-1.\,D1\,e^{\frac{4.26\,D2}{L2}+\frac{2.\,\sqrt{1.-1.\,k}\,R1}{L1}+\frac{2.\,R2}{L2}}L1\,L2\,S+$

$1.\,D2\,e^{\frac{4.26\,D2}{L2}+\frac{2.\,\sqrt{1.-1.\,k}\,R1}{L1}+\frac{2.\,R2}{L2}}L1\,L2\,S-1.74393\times10^{-16}\,D2\,e^{\frac{2.\,R1}{L2}}L1\,R1\,S+$

$1.\,D2\,e^{\frac{2.\,\sqrt{1.-1.\,k}\,R1}{L1}+\frac{2.\,R1}{L2}}L1\,R1\,S-1.74393\times10^{-16}\,D2\,e^{\frac{4.26\,D2}{L2}+\frac{2.\,R2}{L2}}L1\,R1\,S+$

$1.\,D2\,e^{\frac{4.26\,D2}{L2}+\frac{2.\,\sqrt{1.-1.\,k}\,R1}{L1}+\frac{2.\,R2}{L2}}L1\,R1\,S-1.74393\times10^{-16}\,D1\,e^{\frac{2.\,R1}{L2}}\sqrt{1.-1.\,k}\,L2\,R1\,S-$

$1.\,D1\,e^{\frac{2.\,\sqrt{1.-1.\,k}\,R1}{L1}+\frac{2.\,R1}{L2}}\sqrt{1.-1.\,k}\,L2\,R1\,S+1.74393\times10^{-16}\,D1\,e^{\frac{4.26\,D2}{L2}+\frac{2.\,R2}{L2}}\sqrt{1.-1.\,k}\,L2\,R1\,S+$

$1.\,D1\,e^{\frac{4.26\,D2}{L2}+\frac{2.\,\sqrt{1.-1.\,k}\,R1}{L1}+\frac{2.\,R2}{L2}}\sqrt{1.-1.\,k}\,L2\,R1\,S\Bigg)\Bigg)\Bigg/$

$$\left( D1 \left( -1.\, D1\, e^{\frac{2.\,R1}{L2}} L1\, L2 + 1.\, D2\, e^{\frac{2.\,R1}{L2}} L1\, L2 + 1.\, D1\, e^{\frac{2.\,\sqrt{1.-1.\,k}\,R1}{L1}+\frac{2.\,R1}{L2}} L1\, L2 - \right. \right.$$

$$1.\, D2\, e^{\frac{2.\,\sqrt{1.-1.\,k}\,R1}{L1}+\frac{2.\,R1}{L2}} L1\, L2 + 1.\, D1\, e^{\frac{4.26\,D2}{L2}+\frac{2.\,R2}{L2}} L1\, L2 - 1.\, D2\, e^{\frac{4.26\,D2}{L2}+\frac{2.\,R2}{L2}} L1\, L2 -$$

$$1.\, D1\, e^{\frac{4.26\,D2}{L2}+\frac{2.\,\sqrt{1.-1.\,k}\,R1}{L1}+\frac{2.\,R2}{L2}} L1\, L2 + 1.\, D2\, e^{\frac{4.26\,D2}{L2}+\frac{2.\,\sqrt{1.-1.\,k}\,R1}{L1}+\frac{2.\,R2}{L2}} L1\, L2 - 1.\, D2\, e^{\frac{2.\,R1}{L2}} L1\, R1 +$$

$$1.\, D2\, e^{\frac{2.\,\sqrt{1.-1.\,k}\,R1}{L1}+\frac{2.\,R1}{L2}} L1\, R1 - 1.\, D2\, e^{\frac{4.26\,D2}{L2}+\frac{2.\,R2}{L2}} L1\, R1 + 1.\, D2\, e^{\frac{4.26\,D2}{L2}+\frac{2.\,\sqrt{1.-1.\,k}\,R1}{L1}+\frac{2.\,R2}{L2}} L1\, R1 -$$

$$1.\, D1\, e^{\frac{2.\,R1}{L2}} \sqrt{1.-1.\,k}\, L2\, R1 - 1.\, D1\, e^{\frac{2.\,\sqrt{1.-1.\,k}\,R1}{L1}+\frac{2.\,R1}{L2}} \sqrt{1.-1.\,k}\, L2\, R1 +$$

$$\left. \left. 1.\, D1\, e^{\frac{4.26\,D2}{L2}+\frac{2.\,R2}{L2}} \sqrt{1.-1.\,k}\, L2\, R1 + 1.\, D1\, e^{\frac{4.26\,D2}{L2}+\frac{2.\,\sqrt{1.-1.\,k}\,R1}{L1}+\frac{2.\,R2}{L2}} \sqrt{1.-1.\,k}\, L2\, R1 \right) \right)$$

In[13]:= **C3 = C3 /. sol[[1]]**

Out[13]= $\left( 0.0795775\, e^{-\frac{1.\,\sqrt{1.-1.\,k}\,R1}{L1}} \right.$

$$\left( 1.74393 \times 10^{-16}\, D1\, e^{\frac{3.\,R1}{L2}} L1\, L2\, S - 1.74393 \times 10^{-16}\, D2\, e^{\frac{3.\,R1}{L2}} L1\, L2\, S - 2.22045 \times 10^{-16}\, D1\, e^{\frac{2.\,\sqrt{1.-1.\,k}\,R1}{L1}+\frac{3.\,R1}{L2}} \right.$$

$$L1\, L2\, S + 2.22045 \times 10^{-16}\, D2\, e^{\frac{2.\,\sqrt{1.-1.\,k}\,R1}{L1}+\frac{3.\,R1}{L2}} L1\, L2\, S - 1.74393 \times 10^{-16}\, D1\, e^{\frac{4.26\,D2}{L2}+\frac{1.\,R1}{L2}+\frac{2.\,R2}{L2}} L1\, L2\, S +$$

$$1.74393 \times 10^{-16}\, D2\, e^{\frac{4.26\,D2}{L2}+\frac{1.\,R1}{L2}+\frac{2.\,R2}{L2}} L1\, L2\, S + 2.22045 \times 10^{-16}\, D1\, e^{\frac{4.26\,D2}{L2}+\frac{2.\,\sqrt{1.-1.\,k}\,R1}{L1}+\frac{1.\,R1}{L2}+\frac{2.\,R2}{L2}} L1\, L2\, S -$$

$$2.22045 \times 10^{-16}\, D2\, e^{\frac{4.26\,D2}{L2}+\frac{2.\,\sqrt{1.-1.\,k}\,R1}{L1}+\frac{1.\,R1}{L2}+\frac{2.\,R2}{L2}} L1\, L2\, S + 1.74393 \times 10^{-16}\, D2\, e^{\frac{3.\,R1}{L2}} L1\, R1\, S -$$

$$2.22045 \times 10^{-16}\, D2\, e^{\frac{2.\,\sqrt{1.-1.\,k}\,R1}{L1}+\frac{3.\,R1}{L2}} L1\, R1\, S + 1.74393 \times 10^{-16}\, D2\, e^{\frac{4.26\,D2}{L2}+\frac{1.\,R1}{L2}+\frac{2.\,R2}{L2}} L1\, R1\, S -$$

$$2.22045 \times 10^{-16}\, D2\, e^{\frac{4.26\,D2}{L2}+\frac{2.\,\sqrt{1.-1.\,k}\,R1}{L1}+\frac{1.\,R1}{L2}+\frac{2.\,R2}{L2}} L1\, R1\, S + 1.74393 \times 10^{-16}\, D1\, e^{\frac{3.\,R1}{L2}} \sqrt{1.-1.\,k}\, L2\, R1\, S +$$

$$2.\, D1\, e^{\frac{2.\,\sqrt{1.-1.\,k}\,R1}{L1}+\frac{3.\,R1}{L2}} \sqrt{1.-1.\,k}\, L2\, R1\, S - 1.74393 \times 10^{-16}\, D1\, e^{\frac{4.26\,D2}{L2}+\frac{1.\,R1}{L2}+\frac{2.\,R2}{L2}} \sqrt{1.-1.\,k}\, L2\, R1\, S -$$

$$\left. 2.\, D1\, e^{\frac{4.26\,D2}{L2}+\frac{2.\,\sqrt{1.-1.\,k}\,R1}{L1}+\frac{1.\,R1}{L2}+\frac{2.\,R2}{L2}} \sqrt{1.-1.\,k}\, L2\, R1\, S \right) \right) \Big/$$

$$\left( D1 \left( 1.\, e^{\frac{2.\,R1}{L2}} - 1.\, e^{\frac{4.26\,D2}{L2}+\frac{2.\,R2}{L2}} \right) \left( 1.\, D1\, e^{\frac{2.\,R1}{L2}} L1\, L2 - 1.\, D2\, e^{\frac{2.\,R1}{L2}} L1\, L2 - 1.\, D1\, e^{\frac{2.\,\sqrt{1.-1.\,k}\,R1}{L1}+\frac{2.\,R1}{L2}} L1\, L2 + \right. \right.$$

$$1.\, D2\, e^{\frac{2.\,\sqrt{1.-1.\,k}\,R1}{L1}+\frac{2.\,R1}{L2}} L1\, L2 - 1.\, D1\, e^{\frac{4.26\,D2}{L2}+\frac{2.\,R2}{L2}} L1\, L2 + 1.\, D2\, e^{\frac{4.26\,D2}{L2}+\frac{2.\,R2}{L2}} L1\, L2 +$$

$$1.\, D1\, e^{\frac{4.26\,D2}{L2}+\frac{2.\,\sqrt{1.-1.\,k}\,R1}{L1}+\frac{2.\,R2}{L2}} L1\, L2 - 1.\, D2\, e^{\frac{4.26\,D2}{L2}+\frac{2.\,\sqrt{1.-1.\,k}\,R1}{L1}+\frac{2.\,R2}{L2}} L1\, L2 + 1.\, D2\, e^{\frac{2.\,R1}{L2}} L1\, R1 -$$

$$1.\, D2\, e^{\frac{2.\,\sqrt{1.-1.\,k}\,R1}{L1}+\frac{2.\,R1}{L2}} L1\, R1 + 1.\, D2\, e^{\frac{4.26\,D2}{L2}+\frac{2.\,R2}{L2}} L1\, R1 - 1.\, D2\, e^{\frac{4.26\,D2}{L2}+\frac{2.\,\sqrt{1.-1.\,k}\,R1}{L1}+\frac{2.\,R2}{L2}} L1\, R1 +$$

$$1.\, D1\, e^{\frac{2.\,R1}{L2}} \sqrt{1.-1.\,k}\, L2\, R1 + 1.\, D1\, e^{\frac{2.\,\sqrt{1.-1.\,k}\,R1}{L1}+\frac{2.\,R1}{L2}} \sqrt{1.-1.\,k}\, L2\, R1 -$$

$$\left. \left. 1.\, D1\, e^{\frac{4.26\,D2}{L2}+\frac{2.\,R2}{L2}} \sqrt{1.-1.\,k}\, L2\, R1 - 1.\, D1\, e^{\frac{4.26\,D2}{L2}+\frac{2.\,\sqrt{1.-1.\,k}\,R1}{L1}+\frac{2.\,R2}{L2}} \sqrt{1.-1.\,k}\, L2\, R1 \right) \right)$$

In[14]:= **C4 = C4 /. sol[[1]]**

Out[14]= $\left( 0.0795775\, e^{-\frac{1.\,\sqrt{1.-1.\,k}\,R1}{L1}} \left( 1.74393 \times 10^{-16}\, D1\, e^{\frac{4.26\,D2}{L2}+\frac{3.\,R1}{L2}+\frac{2.\,R2}{L2}} L1\, L2\, S - \right. \right.$

$1.74393 \times 10^{-16}\, D2\, e^{\frac{4.26\, D2}{L2} + \frac{3.\, R1}{L2} + \frac{2.\, R2}{L2}}\, L1\, L2\, S - 2.22045 \times 10^{-16}\, D1\, e^{\frac{4.26\, D2}{L2} + \frac{2.\, \sqrt{1. - 1.\, k}\, R1}{L1} + \frac{3.\, R1}{L2} + \frac{2.\, R2}{L2}}\, L1\, L2\, S +$

$2.22045 \times 10^{-16}\, D2\, e^{\frac{4.26\, D2}{L2} + \frac{2.\, \sqrt{1. - 1.\, k}\, R1}{L1} + \frac{3.\, R1}{L2} + \frac{2.\, R2}{L2}}\, L1\, L2\, S - 1.74393 \times 10^{-16}\, D1\, e^{\frac{8.52\, D2}{L2} + \frac{1.\, R1}{L2} + \frac{4.\, R2}{L2}}\, L1\, L2\, S +$

$1.74393 \times 10^{-16}\, D2\, e^{\frac{8.52\, D2}{L2} + \frac{1.\, R1}{L2} + \frac{4.\, R2}{L2}}\, L1\, L2\, S + 2.22045 \times 10^{-16}\, D1\, e^{\frac{8.52\, D2}{L2} + \frac{2.\, \sqrt{1. - 1.\, k}\, R1}{L1} + \frac{1.\, R1}{L2} + \frac{4.\, R2}{L2}}\, L1\, L2\, S -$

$2.22045 \times 10^{-16}\, D2\, e^{\frac{8.52\, D2}{L2} + \frac{2.\, \sqrt{1. - 1.\, k}\, R1}{L1} + \frac{1.\, R1}{L2} + \frac{4.\, R2}{L2}}\, L1\, L2\, S +$

$1.74393 \times 10^{-16}\, D2\, e^{\frac{4.26\, D2}{L2} + \frac{3.\, R1}{L2} + \frac{2.\, R2}{L2}}\, L1\, R1\, S - 2.22045 \times 10^{-16}\, D2\, e^{\frac{4.26\, D2}{L2} + \frac{2.\, \sqrt{1. - 1.\, k}\, R1}{L1} + \frac{3.\, R1}{L2} + \frac{2.\, R2}{L2}}\, L1\, R1\, S +$

$1.74393 \times 10^{-16}\, D2\, e^{\frac{8.52\, D2}{L2} + \frac{1.\, R1}{L2} + \frac{4.\, R2}{L2}}\, L1\, R1\, S - 2.22045 \times 10^{-16}\, D2\, e^{\frac{8.52\, D2}{L2} + \frac{2.\, \sqrt{1. - 1.\, k}\, R1}{L1} + \frac{1.\, R1}{L2} + \frac{4.\, R2}{L2}}\, L1\, R1\, S +$

$1.74393 \times 10^{-16}\, D1\, e^{\frac{4.26\, D2}{L2} + \frac{3.\, R1}{L2} + \frac{2.\, R2}{L2}}\, \sqrt{1. - 1.\, k}\, L2\, R1\, S +$

$2.\, D1\, e^{\frac{4.26\, D2}{L2} + \frac{2.\, \sqrt{1. - 1.\, k}\, R1}{L1} + \frac{3.\, R1}{L2} + \frac{2.\, R2}{L2}}\, \sqrt{1. - 1.\, k}\, L2\, R1\, S - 1.74393 \times 10^{-16}\, D1\, e^{\frac{8.52\, D2}{L2} + \frac{1.\, R1}{L2} + \frac{4.\, R2}{L2}}$

$\sqrt{1. - 1.\, k}\, L2\, R1\, S - 2.\, D1\, e^{\frac{8.52\, D2}{L2} + \frac{2.\, \sqrt{1. - 1.\, k}\, R1}{L1} + \frac{1.\, R1}{L2} + \frac{4.\, R2}{L2}}\, \sqrt{1. - 1.\, k}\, L2\, R1\, S \Big)\Big) \Big/$

$\Bigg( D1 \left( -1.\, e^{\frac{2.\, R1}{L2}} + 1.\, e^{\frac{4.26\, D2}{L2} + \frac{2.\, R2}{L2}} \right) \Bigg( 1.\, D1\, e^{\frac{2.\, R1}{L2}}\, L1\, L2 - 1.\, D2\, e^{\frac{2.\, R1}{L2}}\, L1\, L2 - 1.\, D1\, e^{\frac{2.\, \sqrt{1. - 1.\, k}\, R1}{L1} + \frac{2.\, R1}{L2}}\, L1\, L2 +$

$1.\, D2\, e^{\frac{2.\, \sqrt{1. - 1.\, k}\, R1}{L1} + \frac{2.\, R1}{L2}}\, L1\, L2 - 1.\, D1\, e^{\frac{4.26\, D2}{L2} + \frac{2.\, R2}{L2}}\, L1\, L2 + 1.\, D2\, e^{\frac{4.26\, D2}{L2} + \frac{2.\, R2}{L2}}\, L1\, L2 +$

$1.\, D1\, e^{\frac{4.26\, D2}{L2} + \frac{2.\, \sqrt{1. - 1.\, k}\, R1}{L1} + \frac{2.\, R2}{L2}}\, L1\, L2 - 1.\, D2\, e^{\frac{4.26\, D2}{L2} + \frac{2.\, \sqrt{1. - 1.\, k}\, R1}{L1} + \frac{2.\, R2}{L2}}\, L1\, L2 + 1.\, D2\, e^{\frac{2.\, R1}{L2}}\, L1\, R1 -$

$1.\, D2\, e^{\frac{2.\, \sqrt{1. - 1.\, k}\, R1}{L1} + \frac{2.\, R1}{L2}}\, L1\, R1 + 1.\, D2\, e^{\frac{4.26\, D2}{L2} + \frac{2.\, R2}{L2}}\, L1\, R1 - 1.\, D2\, e^{\frac{4.26\, D2}{L2} + \frac{2.\, \sqrt{1. - 1.\, k}\, R1}{L1} + \frac{2.\, R2}{L2}}\, L1\, R1 +$

$1.\, D1\, e^{\frac{2.\, R1}{L2}}\, \sqrt{1. - 1.\, k}\, L2\, R1 + 1.\, D1\, e^{\frac{2.\, \sqrt{1. - 1.\, k}\, R1}{L1} + \frac{2.\, R1}{L2}}\, \sqrt{1. - 1.\, k}\, L2\, R1 -$

$1.\, D1\, e^{\frac{4.26\, D2}{L2} + \frac{2.\, R2}{L2}}\, \sqrt{1. - 1.\, k}\, L2\, R1 - 1.\, D1\, e^{\frac{4.26\, D2}{L2} + \frac{2.\, \sqrt{1. - 1.\, k}\, R1}{L1} + \frac{2.\, R2}{L2}}\, \sqrt{1. - 1.\, k}\, L2\, R1 \Bigg)\Bigg)$

In[15]:= **Simplify[Phi1[r]]**

Out[15]= $\Bigg( e^{-\frac{\sqrt{1 - k}\, r}{L1}} \Bigg( D2\, L1 \Bigg( e^{\frac{4.26\, D2}{L2} + \frac{2.\, \sqrt{1 - k}\, r}{L1} + \frac{2.\, R2}{L2}} \left( -0.0795775\, L2 - 0.0795775\, R1 \right) + e^{\frac{2.\, \sqrt{1 - k}\, r}{L1} + \frac{2.\, R1}{L2}}$

$\left( 0.0795775\, L2 - 0.0795775\, R1 \right) + e^{\frac{4.26\, D2 + 2.\, R2}{L2}} \left( -1.38778 \times 10^{-17}\, L2 - 1.38778 \times 10^{-17}\, R1 \right) +$

$e^{\frac{2.\, R1}{L2}} \left( 1.38778 \times 10^{-17}\, L2 - 1.38778 \times 10^{-17}\, R1 \right) + e^{\frac{2.\, \sqrt{1. - 1.\, k}\, R1}{L1} + \frac{2.\, R1}{L2}}$

$\left( -0.0795775\, L2 + 0.0795775\, R1 \right) + e^{\frac{4.26\, D2}{L2} + \frac{2.\, \sqrt{1. - 1.\, k}\, R1}{L1} + \frac{2.\, R2}{L2}} \left( 0.0795775\, L2 + 0.0795775\, R1 \right) \Bigg) +$

$D1\, L2 \Bigg( e^{\frac{2.\, \sqrt{1. - 1.\, k}\, R1}{L1} + \frac{2.\, R1}{L2}} \left( 0.0795775\, L1 - 0.0795775\, \sqrt{1. - 1.\, k}\, R1 \right) +$

$e^{\frac{2.\, \sqrt{1 - k}\, r}{L1} + \frac{2.\, R1}{L2}} \left( -0.0795775\, L1 - 0.0795775\, \sqrt{1. - 1.\, k}\, R1 \right) +$

$e^{\frac{2.\, R1}{L2}} \left( -1.38778 \times 10^{-17}\, L1 - 1.38778 \times 10^{-17}\, \sqrt{1. - 1.\, k}\, R1 \right) +$

$e^{\frac{4.26\, D2 + 2.\, R2}{L2}} \left( 1.38778 \times 10^{-17}\, L1 + 1.38778 \times 10^{-17}\, \sqrt{1. - 1.\, k}\, R1 \right) +$

$e^{\frac{4.26\, D2}{L2} + \frac{2.\, \sqrt{1 - k}\, r}{L1} + \frac{2.\, R2}{L2}} \left( 0.0795775\, L1 + 0.0795775\, \sqrt{1. - 1.\, k}\, R1 \right) +$

$e^{\frac{4.26\, D2}{L2} + \frac{2.\, \sqrt{1. - 1.\, k}\, R1}{L1} + \frac{2.\, R2}{L2}} \left( -0.0795775\, L1 + 0.0795775\, \sqrt{1. - 1.\, k}\, R1 \right) \Bigg)\Bigg)\, S \Bigg) \Big/$

$$\left( D1\ r \left( D2\ L1 \left( e^{\frac{4.26\,D2+2.\,R2}{L2}} \left( -1.\ L2 - 1.\ R1 \right) + e^{\frac{2.\,R1}{L2}} \left( 1.\ L2 - 1.\ R1 \right) + \right.\right.\right.$$

$$e^{\frac{2.\,\sqrt{1.-1.\,k}\ R1}{L1} + \frac{2.\,R1}{L2}} \left( -1.\ L2 + 1.\ R1 \right) + e^{\frac{4.26\,D2}{L2} + \frac{2.\,\sqrt{1.-1.\,k}\ R1}{L1} + \frac{2.\,R2}{L2}} \left( 1.\ L2 + 1.\ R1 \right) \right) +$$

$$D1\ L2 \left( e^{\frac{2.\,R1}{L2}} \left( -1.\ L1 - 1.\ \sqrt{1.-1.\,k}\ R1 \right) + e^{\frac{2.\,\sqrt{1.-1.\,k}\ R1}{L1} + \frac{2.\,R1}{L2}} \left( 1.\ L1 - 1.\ \sqrt{1.-1.\,k}\ R1 \right) + \right.$$

$$\left.\left.\left. e^{\frac{4.26\,D2}{L2} + \frac{2.\,\sqrt{1.-1.\,k}\ R1}{L1} + \frac{2.\,R2}{L2}} \left( -1.\ L1 + 1.\ \sqrt{1.-1.\,k}\ R1 \right) + e^{\frac{4.26\,D2+2.\,R2}{L2}} \left( 1.\ L1 + 1.\ \sqrt{1.-1.\,k}\ R1 \right) \right)\right)\right)$$

In[16]:= **Simplify[Phi2[r]]**

Out[16]= $\left( e^{-\frac{r}{L2} - \frac{1.\,\sqrt{1.-1.\,k}\ R1}{L1}} \left( D2\ L1 \left( e^{\frac{8.52\,D2\,L1+1.\,L1\,R1+2.\,\sqrt{1.-1.\,k}\ L2\,R1+4.\,L1\,R2}{L1\,L2}} \left( -1.76697 \times 10^{-17}\ L2 - 1.76697 \times 10^{-17}\ R1 \right) + \right.\right.\right.$

$e^{\frac{4.26\,D2\,L1+3.\,L1\,R1+2.\,\sqrt{1.-1.\,k}\ L2\,R1+2.\,L1\,R2}{L1\,L2}} \left( 1.76697 \times 10^{-17}\ L2 - 1.76697 \times 10^{-17}\ R1 \right) +$

$e^{\frac{4.26\,D2+2.\,r+1.\,R1+2.\,R2}{L2}} \left( -1.38778 \times 10^{-17}\ L2 - 1.38778 \times 10^{-17}\ R1 \right) +$

$e^{\frac{2.\,r+3.\,R1}{L2}} \left( 1.38778 \times 10^{-17}\ L2 - 1.38778 \times 10^{-17}\ R1 \right) +$

$e^{\frac{4.26\,D2+3.\,R1+2.\,R2}{L2}} \left( -1.38778 \times 10^{-17}\ L2 + 1.38778 \times 10^{-17}\ R1 \right) +$

$e^{\frac{8.52\,D2+1.\,R1+4.\,R2}{L2}} \left( 1.38778 \times 10^{-17}\ L2 + 1.38778 \times 10^{-17}\ R1 \right) +$

$e^{\frac{2.\,\sqrt{1.-1.\,k}\ R1}{L1} + \frac{2.\,r+3.\,R1}{L2}} \left( -1.76697 \times 10^{-17}\ L2 + 1.76697 \times 10^{-17}\ R1 \right) +$

$\left. e^{\frac{4.26\,D2\,L1+2.\,L1\,r+1.\,L1\,R1+2.\,\sqrt{1.-1.\,k}\ L2\,R1+2.\,L1\,R2}{L1\,L2}} \left( 1.76697 \times 10^{-17}\ L2 + 1.76697 \times 10^{-17}\ R1 \right) \right) +$

$D1\ L2 \left( e^{\frac{2.\,\sqrt{1.-1.\,k}\ R1}{L1} + \frac{2.\,r+3.\,R1}{L2}} \left( 1.76697 \times 10^{-17}\ L1 - 0.159155\ \sqrt{1.-1.\,k}\ R1 \right) + \right.$

$e^{\frac{8.52\,D2\,L1+1.\,L1\,R1+2.\,\sqrt{1.-1.\,k}\ L2\,R1+4.\,L1\,R2}{L1\,L2}} \left( 1.76697 \times 10^{-17}\ L1 - 0.159155\ \sqrt{1.-1.\,k}\ R1 \right) +$

$e^{\frac{2.\,r+3.\,R1}{L2}} \left( -1.38778 \times 10^{-17}\ L1 - 1.38778 \times 10^{-17}\ \sqrt{1.-1.\,k}\ R1 \right) +$

$e^{\frac{8.52\,D2+1.\,R1+4.\,R2}{L2}} \left( -1.38778 \times 10^{-17}\ L1 - 1.38778 \times 10^{-17}\ \sqrt{1.-1.\,k}\ R1 \right) +$

$e^{\frac{4.26\,D2+2.\,r+1.\,R1+2.\,R2}{L2}} \left( 1.38778 \times 10^{-17}\ L1 + 1.38778 \times 10^{-17}\ \sqrt{1.-1.\,k}\ R1 \right) +$

$e^{\frac{4.26\,D2+3.\,R1+2.\,R2}{L2}} \left( 1.38778 \times 10^{-17}\ L1 + 1.38778 \times 10^{-17}\ \sqrt{1.-1.\,k}\ R1 \right) +$

$e^{\frac{4.26\,D2\,L1+2.\,L1\,r+1.\,L1\,R1+2.\,\sqrt{1.-1.\,k}\ L2\,R1+2.\,L1\,R2}{L1\,L2}} \left( -1.76697 \times 10^{-17}\ L1 + 0.159155\ \sqrt{1.-1.\,k}\ R1 \right) +$

$\left.\left.\left. e^{\frac{4.26\,D2\,L1+3.\,L1\,R1+2.\,\sqrt{1.-1.\,k}\ L2\,R1+2.\,L1\,R2}{L1\,L2}} \left( -1.76697 \times 10^{-17}\ L1 + 0.159155\ \sqrt{1.-1.\,k}\ R1 \right) \right)\right)\ S\right) \Bigg/$

$\left( D1 \left( 1.\ e^{\frac{2.\,R1}{L2}} - 1.\ e^{\frac{4.26\,D2+2.\,R2}{L2}} \right) r \left( D2\ L1 \left( e^{\frac{4.26\,D2+2.\,R2}{L2}} \left( -1.\ L2 - 1.\ R1 \right) + e^{\frac{2.\,R1}{L2}} \left( 1.\ L2 - 1.\ R1 \right) + \right.\right.\right.$

$e^{\frac{2.\,\sqrt{1.-1.\,k}\ R1}{L1} + \frac{2.\,R1}{L2}} \left( -1.\ L2 + 1.\ R1 \right) + e^{\frac{4.26\,D2}{L2} + \frac{2.\,\sqrt{1.-1.\,k}\ R1}{L1} + \frac{2.\,R2}{L2}} \left( 1.\ L2 + 1.\ R1 \right) \right) +$

$D1\ L2 \left( e^{\frac{2.\,R1}{L2}} \left( -1.\ L1 - 1.\ \sqrt{1.-1.\,k}\ R1 \right) + e^{\frac{2.\,\sqrt{1.-1.\,k}\ R1}{L1} + \frac{2.\,R1}{L2}} \left( 1.\ L1 - 1.\ \sqrt{1.-1.\,k}\ R1 \right) + \right.$

$\left.\left.\left. e^{\frac{4.26\,D2}{L2} + \frac{2.\,\sqrt{1.-1.\,k}\ R1}{L1} + \frac{2.\,R2}{L2}} \left( -1.\ L1 + 1.\ \sqrt{1.-1.\,k}\ R1 \right) + e^{\frac{4.26\,D2+2.\,R2}{L2}} \left( 1.\ L1 + 1.\ \sqrt{1.-1.\,k}\ R1 \right) \right)\right)\right)$

```
In[17]:=
    D1 = 0.142;
    SigmaS2 = 0.33596429;
    AConcrete = 21.4435818;
    D2 = 1 / (3 * SigmaS2 * (1 - 2 / (3 * AConcrete)));
    sigmaA1 = 0.068795;
    sigmaA2 = 0.006928606;
    L1 = Sqrt[D1 / sigmaA1];
    L2 = Sqrt[D2 / sigmaA2];
    R1 = 28;
    R2 = 38;
    k = 0.412;
```

In[28]:= **Phi1[r]**

Out[28]= $-\dfrac{1}{r} 3.11665\, e^{0.533732\, r}\, \left(0. + 5.71462 \times 10^{-15}\, S\right) + \dfrac{0.560405\, e^{-0.533732\, r}\, S}{r}$

In[29]:= **Phi2[r]**

Out[29]= $\dfrac{1.45877 \times 10^{-6}\, e^{-0.0822568\, r}\, S}{r} - \dfrac{1.96404 \times 10^{-9}\, e^{0.0822568\, r}\, S}{r}$

In[30]:= **Phi2[31]**

Out[30]= $2.86307 \times 10^{-9}\, S$

In[31]:= **Phi2''[28]**

Out[31]= $7.66889 \times 10^{-11}\, S$

In[32]:= **Phi2''[38]**

Out[32]= $1.65354 \times 10^{-11}\, S$

# APPENDIX B. MATLAB SYNTAX TO SOLVE TRANSIENT EQUATIONS IN REGION I AND II

A MATLAB code is developed to solve the transient equations in region I and region II. We use point kinetics to evaluate the transient behavior of neutrons at $r = 0$ in region I and the transient behavior of neutrons in region II is given by eq. 4.11c. The external neutron source is a pulsed neutron source. At the completion of the pulse, the delayed neutron precursors produce additional fission neutrons. Before the start of the next pulse, there are already some neutrons (coming from the delayed precursors) present in the system. Therefore, when the next pulse arrives, there is a new elevated external source term, which is, DD source neutrons plus the neutrons produced by the delayed neutron precursor concentration from the preceding pulse. This built-up of the external source term due to delayed neutron precursors is accounted for in the transient calculations.

## A. Input parameters

```
function
[t,ton,non,dton,toff,noff,dtoff,tcycle,number,t_concrete,ton_concrete,n
on_concrete,dton_concrete,toff_concrete,noff_concrete,dtoff_concrete,tc
ycle_concrete,number_concrete,S,L,B,rho,l1,l2,l3,l4,l5,l6,B1,B2,B3,B4,B
5,B6,SigmaS2,A_concrete,D2,SigmaA2,v_average] = InputParameters()

%%% Input Parameters %%%
%%% Region I %%%
t=0.01; %%% operation time in seconds %%%
ton=0.0002; %%% source on time in seconds %%%
non=50; %%% mesh points for source on time %%%
dton=ton/non;
toff=0.0098; %%% source off time in seconds %%%
noff=50; %%% mesh points for source off time %%%
dtoff=toff/noff;
tcycle=ton+toff;
number=t/tcycle;
S=1e+8; %%% external neutron source %%%
L=2.01e-04;
B=7.144e-03;
rho=-1.427;
l1=0.01295;
l2=0.0319;
l3=0.127;
l4=0.3345;
l5=1.405;
l6=3.945;
B1=0.0002093;
B2=0.0014653;
B3=0.0013561;
```

```
B4=0.0027985;
B5=0.0009332;
B6=0.0003351;
%%% Region II %%%
t_concrete = 0.01; %%% operation time in seconds %%%
ton_concrete = 0.0002; %%% source on time in seconds %%%
non_concrete = 50; %%% mesh points for source on time %%%
dton_concrete = ton_concrete/non_concrete;
toff_concrete = 0.0098; %%% source off time in seconds %%%
noff_concrete = 50; %%% mesh points for source off time %%%
dtoff_concrete = toff_concrete/noff_concrete;
tcycle_concrete = ton_concrete+toff_concrete;
number_concrete = t_concrete/tcycle_concrete;
SigmaS2 = 0.33596429; %%% Macroscopic scattering cross-section in
concrete (cm^-1) %%%
A_concrete = 21.4435818; %%% Atomic mass of concrete (amu) %%%
D2 = 1/(3*SigmaS2*(1-(2/(3*A_concrete)))); %%% Diffusion coefficient of
neutrons in concrete (cm) %%%
SigmaA2 = 0.006928606; %%% Macroscopic absorption cross-section in
concrete (cm^-1) %%%
v_average = 247232.44; %%% Average neutron velocity at 20 degree
celsius %%%
```

## B. Main Syntax

```
close all
clear all
clc

syms n(t) C1(t) C2(t) C3(t) C4(t) C5(t) C6(t)

[t,ton,non,dton,toff,noff,dtoff,tcycle,number,t_concrete,ton_concrete,n
on_concrete,dton_concrete,toff_concrete,noff_concrete,dtoff_concrete,tc
ycle_concrete,number_concrete,S,L,B,rho,l1,l2,l3,l4,l5,l6,B1,B2,B3,B4,B
5,B6,SigmaS2,A_concrete,D2,SigmaA2,v_average] = InputParameters();

%%% Defining the matrices and setting the ODE %%%
%%% Matrix Psi %%%
%Psi = [n(t); C1(t); C2(t); C3(t); C4(t); C5(t); C6(t)];
%%% Matrix A %%%
a = [(rho-B)/L l1 l2; B1/L -l1 0; B2/L 0 -l2];
b = [l3 l4 l5; 0 0 0; 0 0 0];
c = [l6; 0; 0];
d = [B3/L 0 0; B4/L 0 0; B5/L 0 0];
e = [-l3 0 0; 0 -l4 0; 0 0 -l5];
f = transpose([0 0 0]);
g = [B6/L 0 0 0 0 0 -l6];
A = [a b c; d e f; g];

%%% Initial Condition %%%
I = zeros(7,1);
stependtime = 0; %%% Defining the end time of the zeroth step to be
zero%%%
stependtime_concrete = 0; %%% Defining the end time of the zeroth step
to be zero%%%
```

```matlab
NewS = S; %%%Initial source term for the spatial ditribution of
neutrons %%%
Psinew = [];
timenew = [];
PsinewConcrete = [];
timenew_concrete = [];

for i = 1:number
        [AA,SpatialNeutronPopulation,I_concrete] =
ConcreteNeutronTransient(NewS,D2,SigmaA2);

        [Psi_concrete,I_concrete,timeon_concrete,SP] =
ConcretePulseOn(ton_concrete,non_concrete,dton_concrete,SpatialNeutronP
opulation,I_concrete,stependtime_concrete);
        Temp_concrete = Psi_concrete;
        Temptime_concrete = timeon_concrete;
        PsinewConcrete = vertcat(PsinewConcrete,Temp_concrete);
        timenew_concrete = vertcat(timenew_concrete,Temptime_concrete);
        sizetimenew_concrete = size(timenew_concrete,1);
        stependtime_concrete = timenew_concrete(sizetimenew_concrete);

        [Psi_concrete,I_concrete,timeoff_concrete] =
ConcretePulseOff(toff_concrete,noff_concrete,dtoff_concrete,SpatialNeut
ronPopulation,I_concrete,stependtime_concrete,v_average,AA);
        Temp_concrete = Psi_concrete;
        Temptime_concrete = timeoff_concrete;
        PsinewConcrete = vertcat(PsinewConcrete,Temp_concrete);
        timenew_concrete = vertcat(timenew_concrete,Temptime_concrete);
        sizetimenew_concrete = size(timenew_concrete,1);
        stependtime_concrete = timenew_concrete(sizetimenew_concrete);

        [Psi,I,timeon] =
PulseOn(ton,non,dton,S,L,B,rho,l1,l2,l3,l4,l5,l6,B1,B2,B3,B4,B5,B6,a,b,
c,d,e,f,g,A,I,stependtime);
        Temp = Psi;
        Temptime = timeon;
        Psinew = vertcat(Psinew,Temp);
        timenew = vertcat(timenew,Temptime);
        sizetimenew = size(timenew,1);
        stependtime = timenew(sizetimenew);

        [Psi,I,timeoff] =
PulseOff(toff,noff,dtoff,S,L,B,rho,l1,l2,l3,l4,l5,l6,B1,B2,B3,B4,B5,B6,
a,b,c,d,e,f,g,A,I,stependtime);
        Temp = Psi;
        Temptime = timeoff;
        Psinew = vertcat(Psinew,Temp);
        timenew = vertcat(timenew,Temptime);
        sizetimenew = size(timenew,1);
        stependtime = timenew(sizetimenew);
        DelayedSource = (I(2,1)*l1) + (I(3,1)*l2) + (I(4,1)*l3) +
(I(5,1)*l4) + (I(6,1)*l5) + (I(7,1)*l6);
        NewS = S + DelayedSource;   %%% New source term with delayed
neutrons for the spatial distribtuion of neutrons %%%
end
```

```matlab
m = size(Psinew,1)/7;
neutrons = zeros(m,1);
for i=0:m-1
    neutrons(i+1) = Psinew(((7*i)+1),1);
end


plot(timenew,neutrons,'r')
set(gca, 'YScale', 'log')
title('Neutron Transient at r = 0 in region I')
xlabel('Time (seconds)')
ylabel('neutron population at time t, n(t)')
grid on
grid minor

figure;
plot(timenew_concrete,PsinewConcrete,'b')
set(gca, 'YScale', 'log')
title('Neutron Transient at detectors location in region II')
xlabel('Time (seconds)')
ylabel('neutron population at time t, n(t)')
grid on
grid minor

save PsinewConcrete.mat

%%% To obtain the average predicted pulse %%%
Total = zeros(100,1);

for i = 1:100
    Total(i) = Total(i) + PsinewConcrete(i);
end

for j = 1:(number-1)
    for i =1:100
        Total(i) = Total(i) + PsinewConcrete(100*j + i);
    end
end

Average = Total/number;
for i = 1:100
    time(i,1) = timenew_concrete(i);
end

save Average.mat
```

## C. Pulse ON in region I

```matlab
function [Psi,I,timeon] =
PulseOn(ton,non,dton,S,L,B,rho,l1,l2,l3,l4,l5,l6,B1,B2,B3,B4,B5,B6,a,b,
c,d,e,f,g,A,I,stependtime)


%%% Setting time axis %%%
timeon = zeros(non,1);
```

```matlab
for i = 1:non
    timeon(i) = stependtime + dton*(i);
end



%%% Defining the external source and the initial condition %%%
S = (-dton)*[S/L; 0; 0; 0; 0; 0; 0];
for i = 1:non
    if i == 1
        T = I;
    elseif i==2
        T = vertcat(T,S);
    else
        T = vertcat(T,S);
    end
end
Sext=T;



%%% Setting the ODE d(Psi)/dt = (A*Psi)+Sext using backward Euler
difference %%%

A1 = eye(7); %%%7x7 identity matrix%%%
A2 = (A*dton)-A1;
for i = 1:non-1
    if i == 1
        M = [A1 A2 zeros(7,7*(non-2))];
    else
        t = [zeros(7,7*(i-1)) A1 A2 zeros(7,7*(non-2-i+1))];
        M = [M;t];
    end
end
N = [A1 zeros(7,7*(non-1))];
P = [N; M];



%%% Solving for Psi %%%
Psi = (P)\(Sext);

%%% Setting initial condition for next calculations %%%%
sizePsi = size(Psi,1);
for k=1:7
    I(k) = Psi(sizePsi-7+k);
end

end
```

## D. Pulse OFF in region II

```matlab
function [Psi,I,timeoff] =
PulseOff(toff,noff,dtoff,S,L,B,rho,l1,l2,l3,l4,l5,l6,B1,B2,B3,B4,B5,B6,
a,b,c,d,e,f,g,A,I,stependtime)
```

```matlab
%%% Setting time axis %%%
timeoff = zeros(noff,1);
for i = 1:noff
    timeoff(i) = stependtime + dtoff*(i);
end


%%% Defining initial condition %%%
II = zeros(7*noff,1);
for j = 1:7
    II(j) = I(j);
end


%%% Setting the ODE d(Psi)/dt = (A*Psi)+Sext using backward Euler
difference %%%

A1 = eye(7); %%%7x7 identity matrix%%%
A2 = (A*dtoff)-A1;
for i = 1:noff-1
    if i == 1
        M = [A1 A2 zeros(7,7*(noff-2))];
    else
    t = [zeros(7,7*(i-1)) A1 A2 zeros(7,7*(noff-2-i+1))];
    M = [M;t];
    end
end
N = [A1 zeros(7,7*(noff-1))];
P = [N; M];

%%% Solving for Psi %%%
Psi = inv(P)*II;

%%% Setting initial condition for next calculations %%%%
sizePsi = size(Psi,1);
for k=1:7
    I(k) = Psi(sizePsi-7+k);
end
end
```

## E. Initial conditions for transient calculations in region II

```matlab
function [AA,SpatialNeutronPopulation,I_concrete] =
ConcreteNeutronTransient(NewS,D2,SigmaA2)


SpatialNeutronPopulation = 2.86307 * 10^-9 * NewS;
aa = 1.65354 * 10^-11 * NewS; %%% (Del)^2 Phi[r] evaluated at R2 %%%
bb = 7.66889 * 10^-11 * NewS; %%% (Del)^2 Phi[r] evaluated at R1 %%%
AA = (((D2*aa)/(2*SpatialNeutronPopulation)) -
((D2*bb)/(2*SpatialNeutronPopulation)) - SigmaA2);

%%% Initial Conditions %%%
```

```matlab
I_concrete = SpatialNeutronPopulation;

End
```

## F. Pulse ON in region II

```matlab
function [Psi_concrete,I_concrete,timeon_concrete,SP] =
ConcretePulseOn(ton_concrete,non_concrete,dton_concrete,SpatialNeutronP
opulation,I_concrete,stependtime_concrete)

%%% Setting time axis %%%
timeon_concrete = zeros(non_concrete,1);
for i = 1:non_concrete
    timeon_concrete(i) = stependtime_concrete + dton_concrete*(i);
end

%%% Pulse On %%%
for i = 1:size(timeon_concrete,1)
    if timeon_concrete(i) == 0
        Psi_concrete(i,1) = 0;
    else
        Psi_concrete(i,1) = I_concrete;
    end
end

%%% Setting initial condition for next calculations %%%
sizePsi = size(Psi_concrete,1);
I_concrete = Psi_concrete(sizePsi);
SP = timeon_concrete(size(timeon_concrete,1));
end
```

## G. Pulse OFF in region II

```matlab
function [Psi_concrete,I_concrete,timeoff_concrete] =
ConcretePulseOff(toff_concrete,noff_concrete,dtoff_concrete,SpatialNeut
ronPopulation,I_concrete,stependtime_concrete,v_average,AA)

%%% Setting time axis %%%
timeoff_concrete = zeros(noff_concrete,1);
for i = 1:noff_concrete
    timeoff_concrete(i) = stependtime_concrete + dtoff_concrete*(i);
end

%%% Defining initial condition %%%
II = [I_concrete;zeros((noff_concrete-1),1)];

%%% Pulse off %%%
for i = 1:(noff_concrete-1)
    if i == 1;
        TempAA = [1 ((dtoff_concrete*v_average*AA)-1)
zeros(1,noff_concrete-2)];
    else
        T = [zeros(1,(i-1)) 1 ((dtoff_concrete*v_average*AA)-1)
zeros(1,(noff_concrete-2-i+1))];
        TempAA = [TempAA;T];
```

```matlab
    end
end
N = [1 zeros(1,(noff_concrete-1))];
AAA = [N;TempAA];

%%% Setting for Psi %%%
Psi_concrete = pinv(AAA)*II;


end
```

# REFERENCES

[1]  R. C. Runkle, D. L. Chichester, and S. J. Thompson, "Rattling nucleons: New developments in active interrogation of special nuclear material," *Nuclear Instruments and Methods in Physics Research, Section A: Accelerators, Spectrometers, Detectors and Associated Equipment*. 2012.

[2]  S. Fetter, V. A. Frolov, M. Miller, R. Mozley, O. F. Prilutsky, S. N. Rodionov, and R. Z. Sagdeev, "Detecting nuclear warheads," *Sci. Glob. Secur.*, vol. 1, no. 3–4, pp. 225–253, Jan. 1990.

[3]  S. Board and T. Force, "Preventing and Defending Against Clandestine Nuclear Attack," *Defense*, no. June, 2004.

[4]  B. D. Sowerby and J. R. Tickner, "Recent advances in fast neutron radiography for cargo inspection," *Nucl. Instruments Methods Phys. Res. Sect. A Accel. Spectrometers, Detect. Assoc. Equip.*, vol. 580, no. 1 SPEC. ISS., pp. 799–802, 2007.

[5]  T. Gozani, "Active Nondestructive Assay of Nuclear Materials," *Nureg*, vol. CR--0602, p. 417, 1981.

[6]  The Royal Society, "Detecting nuclear and radiological materials," no. December 2007, 2008.

[7]  J. M. H. Pi, B. Rusnak, and P. J. Fitsos, "High-Energy Neutron Imaging Development at LLNL," no. May, 2007.

[8]  P. A. Hausladen, P. R. Bingham, J. S. Neal, J. A. Mullens, and J. T. Mihalczo, "Portable fast-neutron radiography with the nuclear materials identification system for fissile material transfers," *Nucl. Instruments Methods Phys. Res. Sect. B Beam Interact. with Mater. Atoms*, vol. 261, no. 1–2 SPEC. ISS., pp. 387–390, 2007.

[9]  T. Gozani, T. Shaw, and M. King, "Intense photoneutron sources for nuclear material detection," *AIP Conf. Proc.*, vol. 1336, pp. 696–699, 2011.

[10]  P. Kerr, M. Rowland, D. Dietrich, W. Stoeffl, B. Wheeler, L. Nakae, D. Howard, C. Hagmann, J. Newby, and R. Porter, "Active detection of small quantities of shielded highly-enriched uranium using low-dose 60-kev neutron interrogation," *Nucl. Instruments Methods Phys. Res. Sect. B Beam Interact. with Mater. Atoms*, vol. 261, no. 1–2 SPEC. ISS., pp. 347–350, 2007.

[11]  J. E. Eberhardt, S. Rainey, R. J. Stevens, B. D. Sowerby, and J. R. Tickner, "Fast neutron radiography scanner for the detection of contraband in air cargo containers," *Appl. Radiat. Isot.*, vol. 63, no. 2, pp. 179–188, 2005.

[12]  G. Chen and R. C. Lanza, "Fast neutron resonance radiography for elemental imaging: Theory and applications," *IEEE Trans. Nucl. Sci.*, vol. 49 I, no. 4, pp. 1919–1924, 2002.

[13]  R. C. Runkle, A. Bernstein, and P. E. Vanier, "Securing special nuclear material: Recent advances in neutron detection and their role in nonproliferation," *J. Appl. Phys.*, vol. 108, no. 11, 2010.

[14]  M. Mayer, J. Nattress, and I. Jovanovic, "Detection of special nuclear material from delayed neutron emission induced by a dual-particle monoenergetic source," *Appl. Phys. Lett.*, vol. 108, no. 26, 2016.

[15]  B. Archambault, A. Hagen, K. Masuda, N. Yamakawa, and R. P. Taleyarkhan, "Threshold Rejection Mode Active Interrogation of SNMs Using Continuous Beam DD Neutrons With Centrifugal and Acoustic Tensioned Metastable Fluid Detectors," *IEEE Trans. Nucl. Sci.*, vol. 64, no. 7, pp. 1781–1788, 2017.

[16]  J. R. Lapinskas, S. M. Zielinski, J. A. Webster, R. P. Taleyarkhan, S. M. McDeavitt, and Y. Xu, "Tension metastable fluid detection systems for special nuclear material detection and monitoring," *Nucl. Eng. Des.*, vol. 240, no. 10, pp. 2866–2871, 2010.

[17]  IAEA, "IAEA Nuclear Energy Series Non-HEU Production Technologies for Molybdenum-99 and," *IAEA Nucl. Energy Ser.*, pp. 1–75, 2013.

[18]  M. Fujiwara, K. Nakai, N. Takahashi, T. Hayakawa, T. Shizuma, S. Miyamoto, G. T. Fan, A. Takemoto, M. Yamaguchi, and M. Nishimura, "Production of medical 99m Tc isotope via photonuclear reaction," *Phys. Part. Nucl.*, vol. 48, no. 1, pp. 124–133, 2017.

[19]  B. Y. Hatsukawa, Y. Nagai, T. Kin, M. Segawa, H. Harada, O. Iwamoto, N. Iwamoto, K. Ochiai, K. Takakura, C. Konno, and M. Hashimoto, "Isotope production for medical usage using fast neutron reactions," vol. 329, pp. 327–329, 2011.

[20] A. J. Youker, S. D. Chemerisov, P. Tkac, M. Kalensky, T. A. Heltemes, D. A. Rotsch, G. F. Vandegrift, J. F. Krebs, V. Makarashvili, and D. C. Stepinski, "Fission-Produced $^{99}$Mo Without a Nuclear Reactor," *J. Nucl. Med.*, vol. 58, no. 3, pp. 514–517, 2017.

[21] A. Jalilian, H. Targholizadeh, G. Raisali, H. Zandi, and M. Kamali Dehgan, "Direct Technetium radiopharmaceuticals production using a 30MeV Cyclotron.," *Daru*, vol. 19, no. 3, pp. 187–92, 2011.

[22] G. F. Knoll, *Radiation Detection and Measurement*, Third Edit. Hoboken: John Wiley & Sons, Inc., 2000.

[23] J. R. Lamarsh, *Introduction to Nuclear Reactor Theory*. Addison-Wesley Publishing Company, 1966.

[24] R. D. Evans, *The Atomic Nucleus*. New York: McGraw-Hill, 1955.

[25] N. Tsoulfanidis, *Measurement and Detection of Radiation*, Second Edi. Washington, DC: Taylor & Francis, 1995.

[26] Silverside Detectors Inc., "Technical Reports-Silverside Neutron Detector Performance." [Online]. Available: https://sside.co/technical-resources/. [Accessed: 29-Jan-2018].

[27] K. A. Jordan, T. Gozani, and J. Vujic, "Differential die-away analysis system response modeling and detector design," *Nucl. Instruments Methods Phys. Res. Sect. A Accel. Spectrometers, Detect. Assoc. Equip.*, vol. 589, no. 3, pp. 436–444, 2008.

[28] D. L. Chichester and E. H. Seabury, "Using electronic neutron generators in active interrogation to detect shielded fissionable material," *IEEE Nucl. Sci. Symp. Conf. Rec.*, pp. 3361–3367, 2008.

[29] K. A. Jordan and T. Gozani, "Detection of 235U in hydrogenous cargo with Differential Die-Away Analysis and optimized neutron detectors," *Nucl. Instruments Methods Phys. Res. Sect. A Accel. Spectrometers, Detect. Assoc. Equip.*, vol. 579, no. 1, pp. 388–390, 2007.

[30] K. A. Jordan and T. Gozani, "Pulsed neutron differential die away analysis for detection of nuclear materials," *Nucl. Instruments Methods Phys. Res. Sect. B Beam Interact. with Mater. Atoms*, vol. 261, no. 1–2 SPEC. ISS., pp. 365–368, 2007.

[31] E. . Lewis, *Fundamentals of Nuclear Reactor Physics*. Burlington, 2008.

[32]  K. O. Ott and R. J. Neuhold, *Introductory Nuclear Reactor Dynamics*. La Grange Park: American Nuclear Society, 1985.

[33]  R. . McConn, C. . Gesh, R. . Pagh, R. . Rucker, and R. . Williams III, "Compendium of Material Composition Data for Radiation Transport Modelling," Richland, Washington 99352, 2011.

[34]  J. . Taylor, *An Introduction to Error Analysis: The Study of Uncertainties in Physical Measurements*. Mill Valley: University Science Books, 1982.